IMN MacroNano ®
Fakultät für Maschinenbau
Fachgebiet Technische Optik

Dissertation

System design of optical trapping setups

A dissertation submitted in partial fulfillment of the requirements
for the degree of Doktor-Ingenieur (Dr.-Ing.)

to the Faculty of Mechanical Engineering
of the Technische Universität Ilmenau

by: Dipl.-Ing. Andreas Oeder

1st Reviewer: Prof. Dr. rer. nat. habil. Stefan Sinzinger
2nd Reviewer: Prof. Dr. rer. nat. habil. Cornelia Denz
3rd Reviewer: Prof. Dr.-Ing. habil. Andreas Ostendorf

urn:nbn:de:gbv:ilm1-2013000271

Abstract

The objective of this thesis is the introduction and verification of a holistic design process for optimized optical systems for optical trapping. In this process the principles from classical optics design are used and combined with a force calculation module. Hence, it becomes possible to identify optimum overall systems configurations.
This new perspective on optical trapping systems enables the extension of the current fields of application and the development of optical manipulation technology towards a cost effective tool in the industrial environment.
Consistency between simulation and actual application is achieved by using optics design software to model the system behavior and calculating the influence of the system on the optical forces based on this model. Since most of the leading optics design software and their optimization routines use ray optics, we opted to use ray tracing for the calculation of optical forces as well. Upcoming technologies for the fabrication of optical free form surfaces enable the production of unconventional optical components. This leads to new design freedom which leads to novel system configurations. We demonstrate the idea of system optimization using three examples. First the potentials for improving the performance of conventional microscope objectives are shown. The central achievement on the experimental side is the successful design and test of a compact trapping system with a record working distance of 650 µm. This experiment proves the potential of the design process. As an outlook we present concepts for specialized optics for trapping in air.
Generally, the demonstration of the functionality of the design concept qualifies it as a basis for the development of specialized optics for trapping.

Zusammenfassung

Ziel dieser Dissertation ist die Einführung und Verifikation eines Entwurfsprozesses für optimierte optische Pinzettensysteme. In diesem Prozess werden die Prinzipien aus dem klassischen Optikdesign verwendet und mit einem Modul zur Berechnung optischer Kräfte kombiniert. Dadurch wird es möglich, optimal angepasste Gesamtsysteme zu entwerfen.
Diese Sichtweise auf optische Systeme für die Mikromanipulation ermöglicht ferner die Erweiterung des Anwendungsspektrums und die Entwicklung dieser Technologie hin zum kostengünstigen Einsatz im industriellen Umfeld. Die Nähe zur realen Anwendung wird erreicht, indem vorhandene Optikdesignsoftware zur Berechnung des Systemverhaltens genutzt wird und dessen Einflüsse auf die Kraftwirkungen in der optischen Falle auf dieser Grundlage bestimmt werden. Da gängige Optikdesignsoftware und deren Optimierungsverfahren mehrheitlich mit strahlenoptischen Modellen arbeiten, wird in dieser Arbeit die Kraftsimulation ebenfalls nach dem strahlenoptischen Ansatz berechnet. Aufkommende Technologien zur Herstellung optischer Freiformflächen gestatten es, auch unkonventionelle Bauelemente zu fertigen. Daraus ergeben sich im Design neue Freiheitsgrade, die zu neuen Systemkonfigurationen führen.
Der Gedanke der Systemoptimierung wird in dieser Arbeit anhand von drei Beispielen dargestellt. Zunächst werden die Optimierungspotentiale eines konventionellen Mikroskopobjektivs aufgezeigt. Mit dem Design und erfolgreichen Test eines kompakten Pinzettensystems mit einem Arbeitsabstand von 650 µm wird die Leistungsfähigkeit des Konzeptes experimentell demonstriert. Ausblickend werden Konzepte für eine spezialisierte Optik für optische Fallen in Luft präsentiert.
Durch den erbrachten Nachweis der Funktionalität kann das vorgestellte Entwurfskonzept als allgemeine Grundlage für die Entwicklung spezialisierter Optiken für optische Fallen betrachtet werden.

Contents

List of Figures

List of Tables

Glossary

Abbreviations

AFA beam	Apertured Foucsed Aberrated Beam
AOM	Acousto optical modulator
AR	Anti-reflection
AU	Arbitrary units
ARROW	Anti-Resonant Reflecting Optical Waveguide
BPP	beam parameter product
CA	California
CAD	Computer Aided Design
CAM	Computer Aided Manufacturing
CGH	Computer Generated Hologram
CNC	
DOE	Diffractive Optical Element
GLMT	Generalized Lorentz Mie Theory
GPC	Generalized Phase Contrast
GUI	Graphic User Interface
IFTA	Iterative Fourier transform Algorithm
IGES	Initial Graphics Exchange Specification
HOT	Holographic Optical Trap
Hz	Hertz
NA	Numerical Aperture
NIR	Near infrared
NPM(Machine)	Nano Positioning and Measuring (Machine)
PDMS	Polydimethylsiloxane
PFM	Photonic Force Microscopy
PIFSO	Planar Integrated Free-Space Optics
PMMA	Polymethylmethacrylate
PS	Polystyrene
SLM	Spatial Light Modulator

TEM mode	Transverse Electro Magnetic mode
TIR	Total Internal Reflection
TIRF	Total Internal Reflection Flourescence
UP	Ultraprecision
VCSEL	Vertical-Cavity Surface-Emitting Lasers

Variables and Constants

E	electric field strength
F	force
FWHM	Full Width half maximum
$\hbar$	Planck's constant
$\vec{k}$	K-vector, wave vector
λ	wavelengths
M	position vector of the center of the sphere
M^2	M^2-factor
MgO_2	Magensiumdioxide
N	number of photons interacting with a particle
n_0, n_1 n_0	refractive indices
ω_0	divergence angle
P	power
Q	trapping efficiency
R	radius of particle
Rz	surface roughness
S	position vector of the intersection of a ray and the surface of a particle
T	transmission coefficient
θ	divergence angle
X	position vector of the particle

Trademarks

1 Introduction

Optical forces are a fascinating phenomenon that has been employed for various applications for more than 40 years. Over all these years, optical trapping has become a subject of basic research as well as a field of applied experimental work. In basic research, optical traps are examined by physicists and mathematicians. The development of applications is predominantly driven by microbiologists and physicists that use the equipment that is already available on the market. Until now, the design of specialized optical systems has not been part of the consideration. We want to close the gap between theory and application by introducing a design process which links the requirements of a given application with mathematical models that describe optical traps. By doing so, a paradigm shift is suggested which draws the attention from the performance of the actual trap to the performance of the entire system. This idea is supported by the concept of using specialized optical elements in order to reduce complexity in the setups, which is enabled by functional integration of optical tasks in freeform optical elements. A second objective of this approach is the implementation of new functionalities of optical traps.

1.1 Motivation and research questions

The research on optical manipulation in Ilmenau mainly originated in two projects which required highly specialized optical manipulation optics. The search for existing trapping setups which could provide the required functions did not lead to satisfying solutions. Thus it became necessary to develop own designs.

The first project was in cooperation with the Institute for Bioprocessing and Analytical Measurement Techniques (IBA), Bad Heiligenstadt. Here, we had to integrate an optical micromanipulation system with an existing microfluidic chip [1]. The challenge was to implement an optical trap with a working distance of more than 500 µm. Simultaneously, the periphery of the microfluidics imposed extensive restrictions of the available space in the experimental setup.

The second major project is the design of an optical nanotool for the use in the nanopositioning machines that are developed in the Collaborative Research

Centre SFB 622 "Nanopositioning and Nanomeasuring Machines". Currently, these nanomachines are able to position with a repeatability of one nm. The resolution specification is 0.1 nm. However, for a real nanofabrication the range of available tools is limited. At the nano scale, intermolecular forces exceed gravity. Hence, as soon as particles get in contact with surfaces, they stick to them and cannot be released any more. The key advantage of optical tweezers in this application is the ability to release the particles in a reliable way. Therefore, optical manipulation in this application is intended to provide an additive tool, which allows the precise deposition of nanoscopic particles.

The Ilmenau optics group has a strong background in traditional lens design [2]. Since 2002, various topics in microoptics, integrated optics and ultrapecision machining were added to this research portfolio. The combination of these fields allows us to look at optical trapping from another perspective. Instead of asking: "Can the trapping task be realized with the available components?" we can ask: "Which components are needed to realize the task?".
Hence, the central research questions for this thesis are:

1. Can classical lens design contribute to the improvement of optical trapping setups?

2. Is it possible to realize new trapping tasks by combining the knowledge from classic lens design and optical trapping?

1.2 History of optical micromanipulation

A brief look into the history of optical forces reads as a "Who is Who" of researchers of the last centuries. The fascinating phenomena which are caused by radiation pressure have been observed for a long time.
Optical forces were first predicted by Kepler [3] in 1619. He described radiation pressure as the cause for the fact that comet tails are always pointing away from the sun. Today, this prediction is accepted as correct. In the 17th and 18th century, however, astronomers preferred to stick to Newton's theory and discarded Kepler's assumption which did not quite fit into the picture. The next famous researcher who supported the thought of radiation pressure was Euler in 1746 [4]. Euler believed that light waves cause pressure on bodies that they fall on. Once again, this hypothesis did not become accepted due to criticism by the peers. Over a century further on, the idea of radiation pressure finally gained momentum when a number of notable scientists picked up the topic

again and developed a more differentiated understanding of the phenomenon. Maxwell and Thompson published the book "A treatise on electricity and magnetism" [5] in 1873, in which they predicted a ponderomotive force caused by radiation. They already calculated the pressure that the sun's radiation exerts on the earth's surface. The authors further suggest that a more concentrated electric light source could deliver more energy for optical forces. Of course, all this is published almost a century before the discovery of the laser and without any experimental verification. While Maxwell only spoke of thermal radiation, Bartoli generalized the occurrence of radiation pressure to all kinds of radiation in 1876 [6]. After these two initial publications, a whole series of researchers such as Boltzmann and Heaviside worked on the theoretical aspects of the topic [3].

Along with the theory, some elaborate experiments were proposed to actually measure the magnitude of radiation pressure. A main challenge in all the early experiments was the elimination of forces due to thermal effects. For instance, in Crooke's Radiometer (also known as the light mill) the forces measured are four orders of magnitude higher than can be expected from Maxwell's considerations [7]. Later, it was shown that the rotation of the vanes in the radiometer is a result of thermal heating. These forces have been named radiometric forces. In the early 20th century, a number of researchers tried to improve Crooke's experiment and to eliminate any parasitic effects in order to really measure the radiation pressure. Peter Lebedev [7] published an article entitled "Untersuchungen über die Druckkräfte des Lichtes" (Examinations of the pressure forces of light).

The physical models that are still used for the calculation of optical forces date from the first decade of the 20th century as well. Gustav Mie published his paper on scattering of light by small colloidal particles in 1908 [8]. One year later, Debye discussed the radiation pressure on spheres of arbitrary material [9].

Another physical effect that should be mentioned is photophoresis. This term has been introduced by Ehrenhaft in 1918 [10, 11] and denotes the movement of small particles when irradiated. Here, we have to distinguish between direct photophoresis (pure radiation pressure) and indirect photophoresis (radiometric forces). Indirect photophoresis has its origin in a thermal gradient in the particles which results from absorption of radiation. It strongly depends on the properties of the particle and the surrounding medium.

In the following decades, there was little debate on the influence of radiation pressure. One of the few exceptions is a paper by Frisch in 1933 [12] describing an experiment which proves Einstein's postulate of radiation recoil.

Eventually, it was the invention of lasers that prepared the way for major progress in optical manipulation. Due to the high degree of spatial coherence, laser beams can be focused much tightlyer than thermal light sources. Now, the experimental proof of Maxwell's prediction for forces due to radiation pressure in highly concentrated light could be produced. The laser trap started its success story in 1970 when Arthur Ashkin published his first work on optical manipulation and trapping [13]. He could confirm that the dominating effect in his trapping experiment is in fact radiation pressure. The proof of principle was soon followed by numerous experiments which added to the understanding and versatility of optical trapping as a tool for trapping of atoms as well as nano- and microscopic particles (e. g. [14, 15, 16, 17, 18]). The latest fundamental progress to be mentioned was Ashkin's demonstration of a single beam gradient trap in 1986 [19]. This experiment, which has been dubbed optical tweezers is the concept that allowed the integration of optical traps in standard microscopes. Starting from these pioneering works, a large number of theoretical models (overview in 2.1) and experimental variations have been presented (overview in 3.1).

1.3 Applications

The main fields of application for optical micromanipulation are found in biotechnology, medicine, microscopy and atom cooling.
The feature of contact-free confinement of living samples makes optical trapping an ideal tool e. g. for investigation of single cells [20, 21, 22, 23, 24]. Based on the functionality of holding a cell with optical forces, more complex setups have been demonstrated. Optical cell sorters are used to separate different cell types. The sorting can be realized by actively controlled single traps [25, 26] or by a passive potential landscape which causes particles in a flow to change the direction of their movement [27, 28].
A prominent example for medical applications is the so-called optical cell stretcher [29, 30, 31]. This device is capable of distinguishing various cell types by measuring the deformation of the cell caused by optical forces. This method is highly selective, which allows e. g. the differentiation of healthy and cancerous cells. One goal of the development is a precise cancer diagnosis within minutes. In combination with laser scalpels, optical tweezers have been successfully tested for in vitro fertilization [32].
Optical traps do not have hard walls which define the trapping area. In fact, optical traps are mechanically very soft. Trap stiffnesses range from 0 to 100 pN/µm [33]. Thus, a trapped particle is not located at one precise point but

in a trapping volume. In this volume, the particle moves randomly as a result of Brownian motion. Due to the softness of the trap, very small forces change the motion pattern of the trapped particle. These changes can be detected and used for measurements of small forces in the order of pN and fN Such forces are exerted by molecular motors, when strains of DNA are elongated and retracting the pseudopodia ("legs") of macrophages [34].

A less precise but easier to realize way of measuring trapping forces is the determination of the escape force in an optical trap. To this end, a fluid flow is generated in the trapping chamber. A trapped particle is now pushed out of the equilibrium of the trap by Stokes friction forces. When the velocity of the flow is increased gradually until the trapped bead escapes the trap, the force can be calculated as $F = 6v\nu r\pi$.

The property of soft trapping is also used for microscopy. In Photonic Force Microscopy (PFM) [35, 36] nanoparticles are trapped and moved in the proximity of a surface. The interaction of the surface and the particle causes the center of the particle's movement in the trap to shift. This variation can be used to calculate a 3D height profile of the measured surface. For precise measurements, the setups are calibrated [37, 38, 39]

The first application of optical manipulation is trapping and cooling atom clouds [40]. The 1997 Nobel Prize in Physics has been awarded to the pioneers in optical trapping Steven Chu, Claude N. Cohen-Tannoudji and William D. Phillips. Under their supervision, optical traps [41, 42] and magneto-optical traps [43, 44] have been developed. These systems enable cool clouds of neutral atoms to temperatures of only a few µK.

Optical manipulation has been successfully used for the manipulation and assembly of microscopic polymer structures, that were generated by two-photon polymerization [45, 46, 47]. These works present optical trapping as an opportunity for micro and nano fabrication.

In addition to optical forces on single particles it has been shown that electromagnetic fields generate inter-particle forces. This effect is called optical binding and results in a self-organization of particles [48, 49, 50]. A NASA study investigated the feasibility of laser trapped mirrors for space telescopes. While the researchers come to the conclusion that such mirrors seem to be feasible, demonstration experiments are still to be provided [51].

As this overview of applications confirms, the users of optical trapping are predominantly physicists and biologists. The engineering and optics design side of optical trapping setups have not been in the main focus of research so far.

1.4 Synopsis

This thesis is structured as follows.
Chapter 2 provides an overview of the theoretical background of optical manipulation and optical trapping focusing on the ray optics approach which is later used for the calculation of forces during the presented design process.
In the following chapter (Chapter 3), the state of the art in the instrumentation of optical traps is described. Optical trapping systems will be categorized by their main features: 2D vs. 3D trapping, intensity patterns, the number of simultaneous traps and dynamics. The state of the art in integrating optical systems and optical trapping setups concludes this section.
In Chapter 4, the design process for optimized trapping systems is introduced. The goal of this self-contained/holistic design concept is the integration of a classic lens design with a force calculation. Following these general considerations, the software that we use for the assessment of optical forces and optical trap shapes is presented. The actual beam shapes of the laser source and the limitations of fabrications and assembly are taken into account.
In order to verify the presented method, three examples that show the possibilities of integrated designs are presented in chapter 5 and 6. After the evaluation and optimization of a traditional microscope objective, a new design for a single beam gradient trap with a large working distance is described. The fabrication and successful experimental characterization provide the validation of the proposed design process. As an outlook, a design study for a specialized optical system for trapping in air is presented in chapter 6.
As a conclusion, chapter 7 provides an overview and an evaluation of the results and includes an outlook to further research topics.

2 Physical basics and Force simulation

The aim of this chapter is to provide a basic understanding of optical trapping fundamentals. It starts with the question of the general existence of stable optical traps and introduces the electromagnetic and ray optical theories. In the second part, the mathematical state of the art in modeling trapping forces is depicted.

2.1 Physics of optical micromanipulation

As described in section 1.2, the effect of forces due to radiation pressure has been predicted and discussed as early as in the 19th century. The fundamental physical theories that are still used today dates from the early years of the 20th century. The goal of this section is to provide a general understanding of the physical basics of optical trapping. Since this thesis mainly focuses on developing a process for designing new optical systems for optical trapping, the rather complex theories of optical forces are not discussed in detail. Most of these complex theories are based on the fundamentals presented in this section. Where appropriate, reference to further readings is provided.
Generally speaking, the forces transferred to microscopic particles are the result of the interaction of radiation and matter. During the interaction, the incident field is altered which means a change of momentum. The law of conservation of momentum is preserved by transferring the difference in momentum to the particle.
For the actual calculation of this effect, a variety of theoretical models have been presented.
Fig. 2.1 shows the ranges of validity for different particle sizes. These ranges are documented, among others, in publications by Wright and co-workers [52, 53]. For particles much smaller than the wavelength, the Rayleigh approximation of the Lorenz-Mie theory is considered a valid approach for the description and calculation of optical forces. On the other end of the scale (for particles larger than approx. 17 times the wavelength), it has been shown that the problem

can be treated with a ray optics approach. In the community, the particles which are too large for the Rayleigh approximation are often referred to as "Mie particles". For these particles, more rigorous methods such as the Generalized Lorenz-Mie theory are applied.

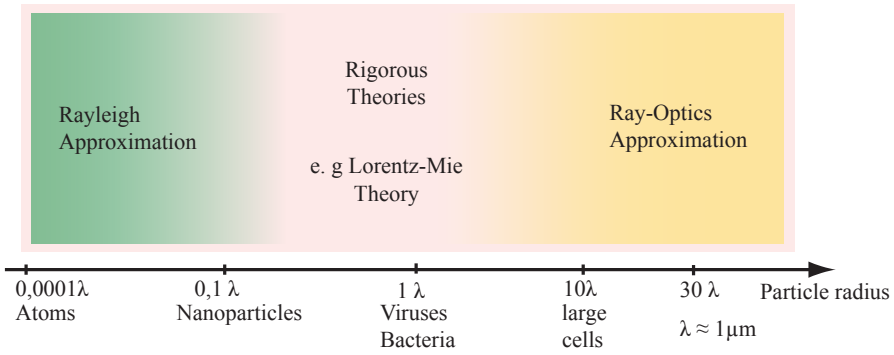

fig. 2.1: Validity of theoretical explanations of optical forces

In atom trapping, optical forces result from coherent and incoherent momentum exchange [41]. The coherent effect is the redistribution or lensing of the incident field by the particle. Incoherent momentum transfer occurs as a result of absorption and reemission of photons. The two kinds of forces thus reflect the interaction of the light with the real part and the imaginary part of the index of reflection respectively.

2.1.1 Stability of optical traps

In general, In order to trap "large" particles, i. e. particles larger than the wavelength, two main conditions have to be met. Firstly, the imaginary part of the particle's index of refraction has to be low - in other words, the particles need to be transparent at the trapping wavelength (see. 2.1.1). Secondly, the refractive index of the particle has to be higher than the index of the surrounding media.

Before the discovery of 3D optical trapping, the forces on small particles that are exerted by radiation pressures could only be confirmed by observation. As a fundamental issue it had to be established, that stable optical trapping in three dimensions is possible at all. Furthermore, the physical prerequisites for such traps had to be defined. The repulsive forces that are generated by radiation pressure have been observed and described in many publications, starting with Kepler. The mathematical description of a stable equilibrium is the existence

of a minimum in a potential function. In [54] the authors show analogies to the Earnshaw theorem which describes the existence and conditions for stable electromagnetic potentials. It is shown that stable trapping can only be realized if the non-conservative scattering force is compensated with a second force. This conservative second force has been named gradient force, since it is caused by field gradients in the trapping beam. Ashkin also states that the scattering force has to be kept at a low level in order to achieve stable trapping. Therefore, the majority of experiments are carried out with dielectric particles that have low absorption coefficients. In fact, according to Roosen et al. [55], a stable equilibrium in a TEM_{00} laser beam is only possible for solid dielectric particles. In this paper and several other publications [56, 57] it is also shown that metallic particles and hollow dielectric spheres can be trapped in a TEM_{01} (Laguerre-Gaussian) beam.
The gradient force is also responsible for particles being drawn on the axis of a beam once they get inside the beam. In loosely focused beams, the particle is accelerated in the direction of propagation simultaneously. Optical trapping, in this case, can be achieved by pushing the particle against a glass surface or an interface between two media.

The creation of a stable equilibrium in three dimensions i. e. the confinement of microscopic particles in space can be achieved by three main approaches (fig. 2.2):

1. Optical forces in combination with another force (e. g. gravitation, magnetic field, surface tension)

2. Counterpropagating beams. The beams push the particles towards each other and an equilibrium is generated in the middle.

3. One highly focused beam. The axial gradient force exceeds the scattering force and particles are pulled towards the focus of the beam.

As an additional condition for stable trapping, the trapping potential well needs to be deeper than the thermal energy of the particle [19]. Otherwise, the Brownian motion would cause the particle to escape the trap over time. The smaller the particles get, the higher is the influence of thermal energy.
In conclusion, the stability, shape, stiffness and depth of the trapping potential depend on the material properties and shape of the particle as well as on the wavefront of the trapping beam. An established measure for the quality of an optical trap is the so-called trapping efficiency Q. The trapping efficiency

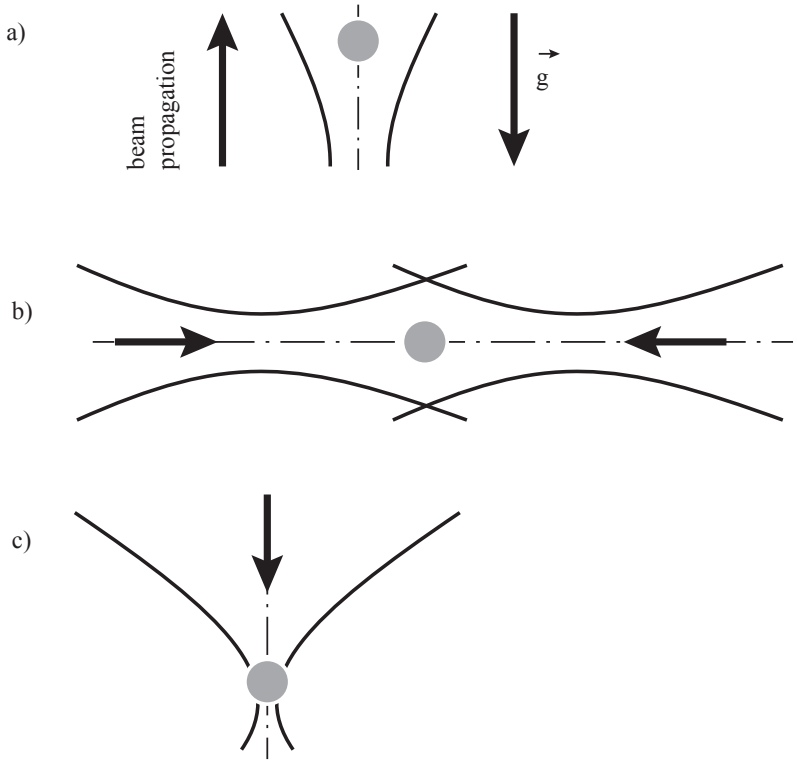

fig. 2.2: Basic configuration for 3D optical trapping. a) optical levitation b)counterpropagating c) single beam gradient trap (optical tweezers)

establishes a linear relationship between the trapping force $\vec{F}$ and the laser power P that reaches the particle.

$$\vec{F} = \frac{1}{c} P \cdot \vec{Q} \tag{2.1}$$

2.1.2 Coherence

The requirement of coherence in optical trapping is rarely discussed. As stated before, Maxwell already assumed that highly concentrated light will lead to higher ponderomotive forces. As described in more detail in 3.1.2, the possible concentration and coherence are directly connected. For almost all theoretical models of optical traps, it is assumed that the beams are coherent. However, also partially coherent laser sources such as semiconductor laser diodes have been tested in optical trapping.
Overall, it is known that especially spatial coherence is crucial for optical manipulation. Only two papers could be retrieved that explicitly discuss the influence of coherence on trapping forces and stiffness [58, 59]. Both publications are

focused on Rayleigh particles i. e. particles much smaller than the wavelength. Temporal coherence is a criterion that is of interest for the case of supercontinuum lasers and thermal light sources. The spectrum of these sources is wide and therefore temporal coherence is small. However, it has been shown, that particles can be stably trapped [60, 61] in light emitted by these sources.

2.1.3 Ray Optics Approach

The most accessible physical model for optical forces is based on ray optics (RO). The physics of the RO approach can be understood by using a vectorial representation of individual rays. Snell's law, the Fresnel equations and the law of conservation of momentum suffice to determine the forces and their directions. Using this model, the interaction of particles with radiation can be visualized in an intuitive way. Fig. 2.3 shows representations for the the retractive axial forces as well as for the lateral forces that draw particles onto the optical axis of a laser beam.

The first detailed studies on the forces in a tightly focused laser beam was

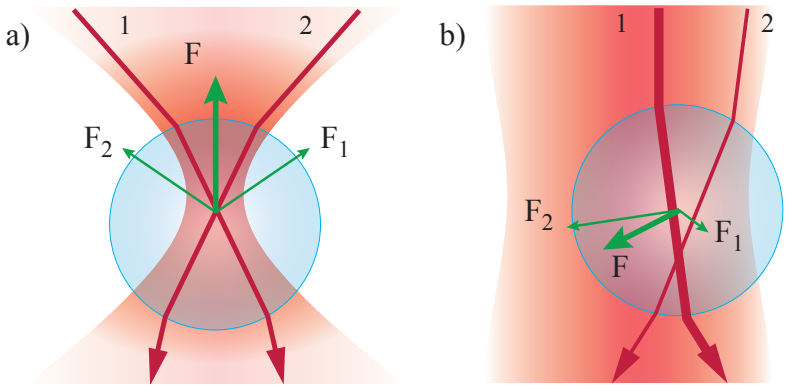

fig. 2.3: Ray optics explanation for the generation of forces due to radiation pressure a) generation of retracting axial forces b) generation of lateral forces

presented by Gussgard et al. in 1992 [62, 63]. The authors mention that earlier works on the ray optics model (e. g. by Roosen and co-workers [55]) only describe the forces in a weakly focused laser beam.
Following this publication, several other groups have contributed to the analytical and numerical refinement of the ray optics model [64].
As written earlier in this chapter, the ray optics approach is correct if the particles are larger than 17 times the wavelength of the laser. Below this threshold, the ray optics calculations overestimate the actual forces. However, Gussgard et al. state that the errors for smaller particles such as living cells (1 to 10 µm

are small enough to achieve useful results [63]. A second source of errors is the nature of Gaussian beams, especially strongly focused Gaussian beams. The exact wave optical behavior in the focus cannot be considered in the geometric optics regime [22].
Since the mathematics behind the RO approach are used in the development of our force calculation tool, a more detailed description is provided in section 4.3.

2.1.4 Electromagnetic Approach

Since the particles that we handle in biological applications can be treated with a ray optics approach, this section gives just a brief overview over the existing theories. For more background information, references to the literature are given.
The fundamentals of the electromagnetic theory date back to the beginning of the 20th century.

To illustrate the general idea of electromagnetic descriptions of optical forces, the formulae of the Rayleigh approximation are very well suited [19]. Equation 2.2 describes the forces that arise due to scattering. Equation 2.3 explains the forces that are generated by gradients in the field.

$$F_{scat} = \frac{I_0}{c}\frac{128\pi^5 r^6}{3\lambda^3}\left(\frac{m^2-1}{m^2+2}\right)^2 n_b \tag{2.2}$$

$$F_{grad} = -\frac{n_b}{2}\alpha grad E^2 = -\frac{n_b^3 r^3}{2}\left(\frac{m^2-1}{m^2-2}\right) grad E^2 \tag{2.3}$$

n_b is the refractive index of the surrounding media, m is the effective index and α is the polarizability of the trapped particle. It can be derived from these formulae that the gradient force gets the more dominant the smaller the particles get. The gradient force is proportional to the polarizability of the particle.
Following the first EM models, the scientific community has added a number of more exact models for the description of a Gaussian beam and a microscopic particle. An overview over the evolution of theoretical models of optical traps is given in [39].
The Lorenz-Mie theory and the Rayleigh approximation respectively do not include representations of Gaussian beams. A more comprehensive approach is provided by the Generalized Lorenz Mie Theory (GLMT) [65, 66].
Examples for further EM models and their improvements for more precise calculations of optical forces are mentioned in the following section.

2.2 System Modeling and Simulation

Starting from the first publications of optical manipulation, much attention has been paid to the refinement of the physical and mathematical descriptions of optical traps. The goal is the best possible representation of the reality and the exact calculation of forces. The parts of the system that need to be taken into account are visualized in fig. 2.4. The interaction of the particle and the beam depends on the modulation that occurs to the beam in the optical system

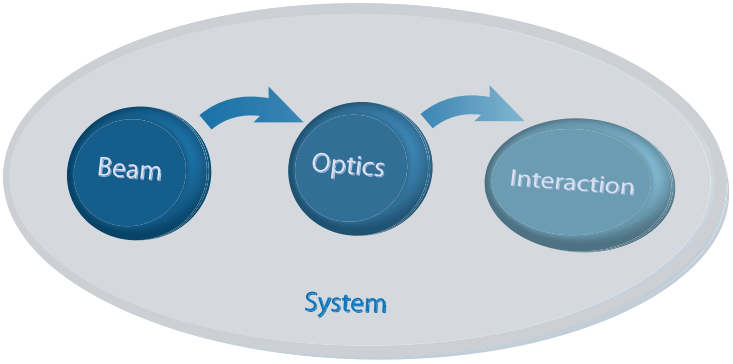

fig. 2.4: Block diagram of the main aspects of modeling optical trapping systems

The simulation of optical trapping is composed of several aspects: the representation of the beam, the influence of the optical system, the actual interaction of the particle and the beam. On the one side, the accuracy of the model is defined by the theories that form the basis for the simulation. On the other side, the connection between theory and reality is the optical system that forms the beam into the trap and its real world behavior. While fig. 2.4 suggests a simple structure of the model, the precise representation of the reality often requires high mathematical effort to be modeled and calculated. This is also the case for optical traps where mathematical approximations are used to prepare the theoretical descriptions for numerical algorithms.
In this thesis, we aim to set up a seamless process for simulating optical traps on the system level. To this end, a simulation sequence has to be chosen which satisfies the needs of optics designers and simultaneously provides the necessary accuracy in the calculation of the optical forces.
This section follows the system simulation from the source to the trap and describes the current methods for simulation approaches that are based on electromagnetic and ray optics theory. This introduction is followed by an overview of models for the optical system itself and a summary of how fabrication and alignment errors are currently treated in the literature.

2.2.1 Modeling the beam

Precise models for the light-matter interaction in optical traps have been introduced in the previous section. In order to receive exact results the inputs for the calculation need to be detailed representations of the real trapping beam. The common shape of the employed beams is a Gaussian profile. The early calculations of trapping forces did not take the nature of the Gaussian beam and its focusing behavior into account.
This is true for the Lorenz-Mie theory which dates back to the beginning of the 20th century. It was the first EM model used as a description of optical forces. The GLMT enables the consideration of Gaussian beams [67]. Ganic narrows this statement down and states that this theory is only correct for loosely focused beams [68]. The vectorial diffraction theory, introduced by Török et al. [69], will yield more precise results for annular and doughnut beams.
In order to simulate a Gaussian beam in a ray optics simulation, the wavefront of the beam has to be sampled along its propagation. A single set of straight rays cannot express the variation of the curvature of the wavefront in a Gaussian beam. This is especially true for positions close to the beam waist. Nemeto et al. present a RO approximation of a Gaussian focus [70].
The dependence of optical forces on the polarization of the trapping beam has also been discussed [71, 72]. In [71] Dutra states that the differences between circularly and linearly polarized beams are not very high, but may induce asymmetry in the trap. Using similar theoretical models, also trapping forces in azimuthally and radially polarized beams can be simulated [73, 74]. Since polarization plays an important role in higher order beams, this is an important effect to be included in the modeling of the beam.

2.2.2 Modeling the optics

Most established tools in optics design are based on ray-tracing algorithms. Therefore ray-tracing for us is the preferred method, when a link between the laser source and trapping forces has to be made. The early simulations assumed ideal behavior of the system which can be analytically described. It is known that microscope objectives are commonly designed to obey the sine condition [75, 76].

$$\frac{n \sin \sigma}{n' \sin \sigma'} = \beta' \tag{2.4}$$

The above condition implies that such an objective ideally converts a plane wave into a converging spherical wave. For simulations, this condition is a

commonly used assumption (e. g. [77, 33]). A rarely mentioned property of microscope objectives is the radially varying transmittance. In fact, the only publication that elaborates on this issue in detail has been written by Viana et al. [78]. The authors suggest that the reflections at all interfaces in the trapping setup lead to a drop of the transmittance from the optical axis to the edge of the objective's entrance pupil. The total transmission of microscope objectives in the near infrared is described and measured more often (e. g. [79]).

In most optical trapping setups the laser propagates in several different media before it reaches the focal plane which leads to spherical aberrations. In microscopy superior resolution is realized, when the optical system before the image plane is kept within fine tolerances. Minimal spherical aberrations can be maintained by using standardized cover glasses, defined immersion media and the location of the image plane at the surface of the cover glass. In optical trapping, however, the trap location (the image plane) is set several microns behind the cover glass. By shifting the focus behind the designed image plane, spherical aberrations are introduced. The influence of spherical aberrations is also the error that is discussed most thoroughly in optical trapping [80, 65, 81, 82, 83]. Since optical traps are often located on the optical axis, they are the dominating geometric aberration. If the trap location is off-axis, aberrations that depend on the image field come into play as well. Higher order aberration terms and their correction are predominantly discussed in the context of holographic optical traps [84, 85, 86, 77]. In these cases, the main approach is not the simulation of forces in order to improve the accuracy of the model. Instead, the wavefront at the trap location is detected and corrected with a spatial light modulator. The authors present the decomposition of the actual wavefront into the well-known Zernike polynomials as a method to describe the performance of their setups.

A common practice in optical trapping is to overfill the entrance pupil of the focusing optics. This improves the trapping efficiency Q but leads to a truncation of the Gaussian beam. Consequently, the truncation has been considered as an additional influence on trapping forces [39, 76]. Section 4.1 includes an overview of overfilling as a measure to improve traps.

Concerning the modeling of the trapping system, Rohrbach enlists the sources of variations and their potential magnitude [33]. In summary, he states that the remaining uncertainty of the calculation results is about 100%.

While the descriptions of the optics for optical manipulation include a variety of details, no publication using a representation of the actual optics for the simulation of optical forces could be retrieved. In fact, actually only few authors present a precise description of the setup that is used in the experiment [33] or provide reasons for the selection of the used components.

In his 2004 review paper, Neuman [79] points out the complexity of high NA objectives as multi-element systems, and suggests that internal effects such as reflections should not be underestimated. Furthermore, it is noted that the trapping wavelength may differ from the design wavelength. Hence, the performance deteriorates significantly. So far, the systems are modeled by selecting analytic assumptions about the real system. Lock et al. describe the real trapping beam as an apertured, focused and aberrated beam (AFA beam) to take this fact into account [87].

2.2.3 Modeling the particles

The most common model for particles in optical trapping are homogenous, dielectric, microscopic spheres. Similar to the descriptions for the beam and the optics, the representations of the trapped particles have become more and more specific over the years. In analogy to the previously mentioned range of validity of the theories for the light matter interaction, the modeling of the trapped particles depends on their size. In small particles, the geometry does not dominate the trapping forces. Instead, the dipole character and the scattering cross-section define the trapping behavior.
Gustav Mie assumed spherical particles [8]. Therefore, his theory is limited to homogenous spherical particles [88].
The actual shape and structure of the specimen is important for large particles. Consequently, the variety of models for Mie particles is considerably larger than for Rayleigh particles.
In microbiology, usually, living cells such as bacteria and viruses have to be trapped. Chang et al. propose a more detailed model for living cells [89, 90]. In these publications the authors describe cells as multilayer bodies that are composed of nested spheres with varying refractive index.
However, many cells are not spherical. Gauthier has presented geometric optical considerations for trapping forces upon rod shaped [91], ring shaped [92] and cubic [93] microparticles. For particles with low symmetry, not only a force acts on the particle, but also a torque. The equilibrium state for non-spherical particles depends on the location and the rotation of the particle in the beam [94, 24]. It has been shown that anisotropic particles show an effective torque which causes a permanent rotation [95]. In [93] Gauthier also proposes a method of modeling more complex bodies such as red blood cells. A good description of red blood cells in optical traps is essential for applications such as cell stretchers [96]. Several groups have demonstrated optical trapping of Rayleigh particles with complex index of refraction such as metallic particles (e. g. [97]). For the

representation of such particles no special model is necessary. In this range of sizes, the polarizability of the particle dominates the trapping forces. This effect makes the trapping of metallic nanoparticles possible

2.2.4 Handles for Tolerancing and Fabrication

Adding details to the analytical models increases the accuracy. However, the manual selection of parameters and suitable coefficients is still required. Parametric studies have been presented which analyze the influence of e. g. spherical aberrations in optical traps [53]. Currently, there are no systematic procedures for the simulation of the forces when alignment errors and non-ideal optical components are present. In setups that use adaptive optics, aberrations introduced by the system can be eliminated by a closed-loop optimization of the focus [85]. In this thesis, a way of implicitly modeling trapping optics is proposed. By directly entering the system geometry, any deviations from the ideal geometry can be taken into account without having to know analytic descriptions of the effect. This allows the optics designers and engineers to work with trapping optics more intuitively.
Additional parameters of the system can be included in the system models. Commercial optics design software is capable of simulating the influence of dispersion and anti-reflection coatings (AR-coatings). For later fabrication, an easy to use implementation of parameter studies can be considered.

2.3 Summary

Optical forces are a result of the interaction of light and matter. The incident light is scattered by the particle, which results in a transfer of momentum to the particle. Radiation pressure has been identified as the origin of forces in optical traps. Stable optical traps were predicted theoretically and demonstrated experimentally in the 1970s. The dominating property for trapping small particles in a beam of light is a strong gradient of the incident field. Suitable physical and mathematical models are selected according to the size of the trapped particles. For the description of the beam, the optics and the interaction between light and the matter, a large diversity of models is available. This system modeling is widely based on analytic assumptions. The influences of deviations from the ideal system are known, but not comprehensively included in simulations. The correction of aberrations is implemented by closed loop optimization in adaptive setups.

3 Instrumentation - State of the Art

Due to the large variety of trapping setups, an unambiguous categorization of the different setups is almost impossible. Also, theory and experiments are strongly linked, which makes it difficult to separate the previous chapter from this chapter. This is a conclusion that even the "father" of optical trapping, Arthur Ashkin, had to make in his 2006 book [98]. Hence, it is inevitable that some aspects that were already presented in the theory chapter will be picked up again. In the first section of the chapter a number of key features of trapping setups are used to describe the main function of each system and the instrumentation used to realize the individual function.
In the following sections the system components that can be added to the optical system as periphery and the range of available commercial products are presented. Again, some ambiguity remains as some elements fulfil more than one function in a setup.

3.1 Overview of optical trapping setups

The summary of the state of the art included in this section follows the segmentation proposed in fig. 3.1. The four chosen key elements are the dimensionality of the trap (2D and 3D), the optics that is employed to generate the necessary field gradients, the beam shaping elements that create more complex trap geometries and technologies to achieve multiple trapping and dynamic traps.

3.1.1 2D and 3D traps

A fundamental distinction to be made is the fact that traps can be two dimensional (2D) and three dimensional (3D). As the name suggests, 2D traps are optical traps which confine a particle in two directions while the confinement in the third direction is provided by other physical effects. This type of trapping or manipulation was the first to be observed by Ashkin [98]. He described that a particle that crosses a laser beam is instantly drawn into the middle of the beam and is pushed in the direction of the beam propagation. Common implementations are optical traps at an interface of two media (oil water, water glass). The lateral trapping of particles in a slightly focused beam can be achieved with low

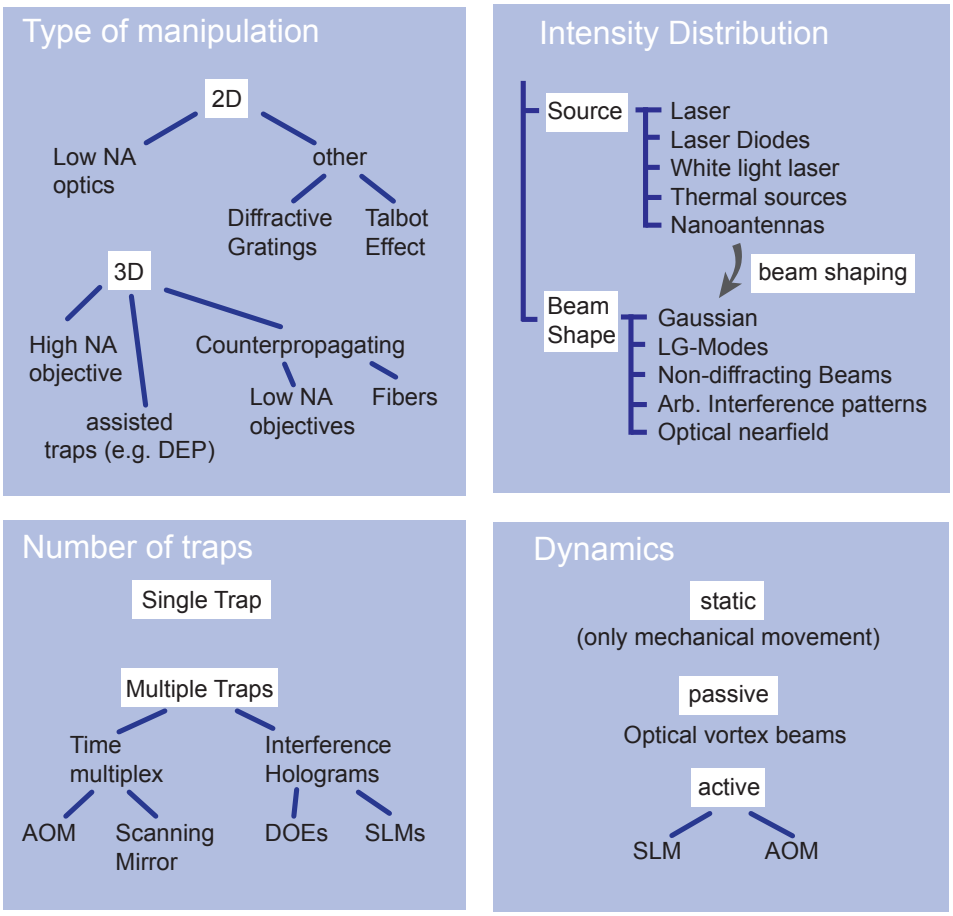

fig. 3.1: Overview of optical trapping setups

NA objectives. In Ilmenau we successfully trapped particles in 2D with an NA of 0.2. This NA is comparable to the one of the optical fibers which are used in optical manipulation [99].

The earliest method of creating a stable 3D trap is the so-called optical levitation [14, 100, 101]. Here, a stable 3D trap is the result of optical forces and gravity acting on the trapped particle (see fig. 2.2).

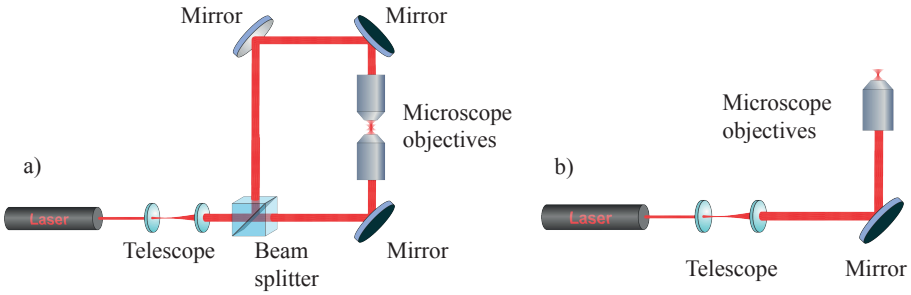

fig. 3.2: Basic configurations of optical trapping systems; a) counterpropagating trap b) optical tweezers, single beam gradient trap

Setups using the counterpropagating beams principle (fig. 3.2a) were the first experiments demonstrating trapping by optical means only [13]. Here, the NA is not that critical since lateral forces are generally quite strong in comparison to the retracting axial forces. In our preliminary experiment mentioned above, we demonstrated 3D optical trapping with low NA focusing in a microfluidic chip with thick channel walls. A setup with two Nikon 10x SLWD objectives was used. The working distance of these objectives is 20.3 mm which results in a total distance of both optics of more than 40 mm (fig. 3.3a). The large distance between the objectives was necessary because the fluid connectors shown in fig. 3.3b) had to fit in the working space. The critical issue in counterpropagating setups is the alignment of both optics. The axes of both laser beams need to coincide, which requires precise lateral and angular alignment.

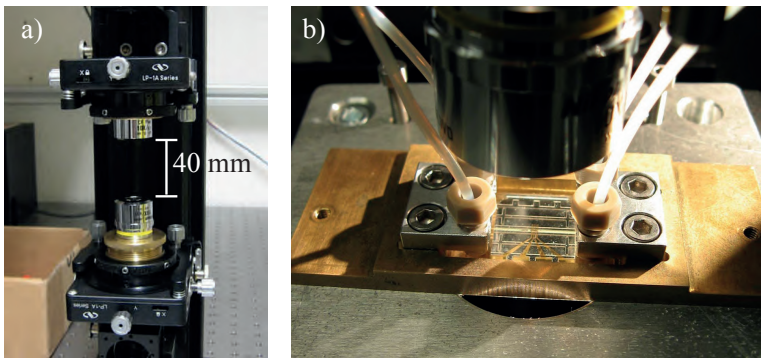

fig. 3.3: Experimental setup for counterpropagating trapping; a) the two microscope objectives which are seperated over 40mm b) microfluidic chip with fluid connections

From the optics perspective, stable optical trapping with a single focusing optics can be seen as the most challenging task. The setups for these so-called optical tweezers are less complex than counterpropagating traps (fig. 3.2b).

But the requirements to be met for focusing are high which can be concluded from the large number of publications which discuss the strong influence of geometric aberrations in optical tweezers [80, 83, 82, 84, 65]. The generation of a high axial field gradient is essential for the realization of optical tweezers. The axial gradient forces have to over-compensate the scattering force. The off-the-shelf optics that are capable of focusing light tightly enough are microscope objectives with a high numerical aperture (NA). In his early work on optical tweezers Ashkin observes that trapping of glass particles in water is possible with a NA of 0.5 (convergence of input beam = 29°) [62]. However, this configuration produces only weak axial trapping forces and reasonable axial forces can only be generated with immersion objectives. This class of optics has become the standard in optical tweezers. Many groups utilize sophisticated microscopes as a platform for their trapping experiments. Since this approach is very convenient for research not focused on trapping technology itself, most commercial setups are based on standard microscopes which are equipped with a laser source (see 3.4).
In a publication by Merenda et al. high NA focusing mirrors are used for focusing and trapping [102]
While the setup for the classical optical tweezers stayed comparatively similar for the last 30 years, many groups have demonstrated other ways of realizing optical manipulation and trapping.

- Fiber traps represent a large group of setups. The laser is coupled into optical fibers and usually the ends of the fibers are placed into a water reservoir. Fibers with flat endfaces emit divergent beams with numerical apertures of up to 0.28. Thus, the common setups for fiber traps are counterpropagating configurations [99, 103, 104]. Several groups have demonstrated 3D trapping with single fibers, as well. The fiber tips in these setups have been modified applying microtechnological processes in order to produce high field gradients in the near field of the fiber tip. Published experiments include lensed fiber probes [105, 106], tapered fibers [107, 108], axicon shaped fibers [109] and fibers which produce annular light distributions [110].
  A group of researchers at the University of Pavia demonstrated a reflection based optical fiber trap which consists of a bundle of fibers [111, 112].

- Apart from purely optical traps, several experiments use other physical effects to improve the trapping properties. Typical examples are magneto-optical traps. Here, a weak magnetic field is superimposed with the optical field. Another method of stabilizing an optical trap is the generation of ul-

trasound standing waves in the trapping volume [113]. The standing waves of the acoustic field concentrate particles in planes where the effective forces due to acoustic pressure. This pre-alignment assists the manipulation with optical forces and helps to realize robust 3D trapping. Optically controlled trapping or optoelectronic trapping [114] are combinations of optically addressed crystals and dielectrophoretic forces. A locally varying index of refraction can be written into an optically active material [115]. When a voltage is applied to the crystal, a locally varying electric field arises. As a result, particles can be trapped by dielectrophoretic forces.

- A variety of recent experiments focus on near field optical trapping. In these setups near field effects such as evanescent fields are used to manipulate particles. The setups use microscope objectives with extremely high NA which are mainly applied in total internal reflection fluorescence (TIRF) microscopy [24, 116, 117]. The researchers selectively illuminated the experimental chamber with the light which is total internally reflected, thus creating an evanescent field. The gradient of this exponentially decaying field suffices for optical trapping. A group at the university of Brno introduced the term optical conveyor belt [118]. They demonstrated a near field trap in an optical standing wave by using two counterpropagating beams. The phase of one beam is varied, which produces a travelling standing wave. The force on particles is highly sensitive to the particle diameter which allows the separation of particles that differ only a few nanometers in size [119].

- In integrated optofluidic systems (see. 3.3.2) optical manipulation can be implemented by coupling laser light into a liquid filled hollow core fiber. In these so-called ARROWs (anti-resonant reflecting optical waveguide) the losses are relatively high. The setup demonstrated at the university of Santa Cruz (CA) relies on this behavior instead of gradients due to beam divergence [120]. The farther the light travels in the ARROW, the weaker it becomes. One field of application of opposing beams is the efficient manipulation of fluorescent particles on an optofluidic chip [121].

- A new method of optical manipulation are plasmonic optical traps. In these traps the extremely high field gradient between two metallic nanostructures is used [122, 123, 124]. These nanoantennas usually have the shape of two opposing triangles. They are illuminated by a laser beam with a frequency that matches the resonance of the nanoantenna. The electromagnetic field is concentrated in the gap between the two nanoan-

tennas, thus generating the mentioned field gradient.

3.1.2 The trapping beam

The second major prerequisite for efficient optical manipulation is the working media itself, i. e. the beam. The following section describes the main characteristics of beams that are used in practice.

Radiation Sources

Another name of optical traps is laser traps. This is because the discovery of the laser is the most important technological milestone that led to the development of optical trapping. Before the discovery of these radiation sources, it was not possible to focus light strongly enough to create sufficiently high trapping forces. The focusability depends on the spatial coherence of a beam. As shown in fig. 3.4a), the image height is the limit of concentration in extended light source. The spatial coherence can be increased by filtering the source with a pinhole or by increasing the distance between the source and the optics. However, neither of these options will increase the gradients in the focus. Laser beams behave differently and emit spatially coherent radiation. While this leads to a much higher focusability, there is a theoretical limit for the size of a laser focus. The smallest possible foci can be reached with in the Gaussian TEM_{00} mode 3.4b).

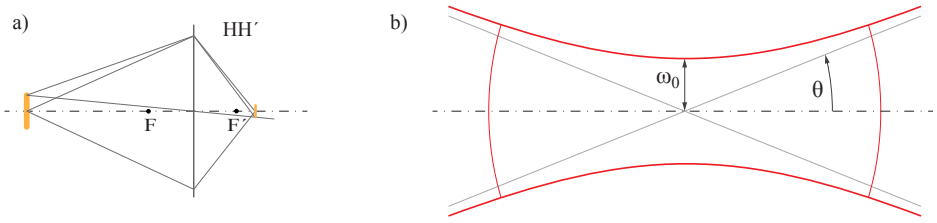

fig. 3.4: Cross-section of a Gaussian beam with a beam waist ω_0 and divergence θ

The theoretical beam waist ω_0 of a this beam is defined by

$$\omega_0 = \frac{2\pi}{\theta} \tag{3.1}$$

In practice, most lasers do not emit an ideal Gaussian TEM_{00} mode but also higher modes. The spatial coherence is decreased and, as a result, the focus is larger than the theoretical value mentioned above. Consequently, the field gradients and the gradient forces are lower. In laser technology the quality of a

laser is specified by the M^2 [125] factor or the beam parameter product (BPP) [126].

$$BPP = \omega_0 \cdot \theta = M^2 \frac{\lambda}{\pi} \tag{3.2}$$

Typical values for M^2 are between ≈1 (gas lasers) and 1000 (semiconductor laser bars) Usually, lasers with wavelengths in the near infrared (NIR) are used as radiation sources for optical trapping. This preference originates from the main application of optical tweezers in microbiology where heating of the specimen has to be avoided. The absorption of radiation in living cells strongly depends on the wavelength and is low for NIR [127].

The strong wavelength dependence is used in micro dissection. For optical scalpels wavelengths are chosen at which cells show high absorption. Thus, lasers can be used to cut tissue and cell membranes.

Edge emitting semiconductor laser diodes have also been successfully used in optical trapping. These lasers commonly exhibit an astigmatic beam profile which results in a decreased focusability. For the application in optical trapping the beams have to be shaped into a symmetric beam [128, 129].

Vertical-cavity surface-emitting lasers (VCSELs) have been employed in a series of experiments [130, 131, 132]. Since VCSELs can be fabricated with planar chip technologies, they allow for an easy combination with microfluidic chips. Furthermore, the beam profiles are better than the ones of edge emitting laser diodes.

Today, supercontinuum lasers [133, 134, 60, 135, 136] and high pressure gas lamps are still rather exotic sources used for optical manipulation.

Supercontinuum lasers or white light lasers consist of a pulsed laser which is coupled into an optical fiber. The combination of several nonlinear effects in the material of the fiber leads to a very broad spectrum at the output [137]. When this beam is focused, the focus is elongated according to the axial chromatic aberration of the focusing optics. It has been shown that particles of different sizes are trapped at different positions in this focus.

High pressure gas lamps are extended thermal light sources of thermal light and therefore do not provide the above-mentioned coherence that is necessary for tight focusing. By strong spatial filtering the effective area of the light source can be reduced and optical manipulation becomes possible [61]. In the cited experiment at the university of Monterrey, Mexico the authors use a 300 W Xe lamp and couple about 12% of the radiation power into a single mode fiber. To demonstrate optical guiding, the beam was shaped into an elongated focused

Bessel beam in which the guiding of particles could be observed.

Beam shaping

Generally, the term beam shaping is understood as any deliberate variation of a beam. By this definition, the classical focusing would also be considered as beam shaping. However, in this chapter the focusing has a special position and is excluded from this section. Beam shaping in this context is understood as all measures for the filtering and improvement of laser beam profiles. It is used for several purposes in optical trapping. The most common applications are the improvement of the trapping efficiency Q of a single trap by spatial filtering, the correction of aberrations introduced by the optical system and the generation of multiple traps.

As described in the previous section, real laser sources commonly do not emit ideal Gaussian beams. The beam is filtered by placing a pinhole in an intermediate focal plane in the optical system. The diameter is matched to the diameter of the airy disk and is blocking the spatial frequencies that originate from the higher modes of the laser beam. In addition to the filtering, the beam is usually expanded to a diameter that is larger than the entrance pupil of the microscope objective. As a result of this so-called overfilling, the Gaussian beam is truncated. The effects of truncation on the focal spot size is discussed in [138]. The trapping efficiency can also be increased by blocking the middle of the beam with a circular disk. With this simple measure, the forces in the direction of the beam are reduced.

In various experiments beam shaping is used to correct the aberrations introduced by the system [86, 139, 84]. Especially the spherical aberration has been shown to have major influence on the trapping forces [140]. In holographic optical tweezers, spatial light modulators (SLM) provide the option for correction as a built-in feature [85, 141]. Due to their flexibility SLMs are the most common devices in wavefront correction. In [139] deformable mirrors are proposed for this purpose.

The basic theoretical models of optical traps commonly assume a Gaussian beam profile and spherical particles in the trap. During the last decades of optical manipulation a series of other beam profiles have been successfully used to achieve 2D or 3D optical trapping. Starting from the first years after the demonstration of single beam gradient traps, a series of alternative beam profiles have been used in optical trapping experiments. Annular beams and Laguerre-Gaussian beams (doughnut beams) have been presented [62, 142, 143]. Initially, the generation of donut beams was achieved by intra-cavity beam shaping. Starting in the 1990s Laguerre-Gauss modes in optical trapping are now predominantly

generated by diffractive elements [144, 145].
Trapping with the other classes of beam profiles has been demonstrated as well. Meyrath et al. show manipulation of atoms in Hermite-Gaussian beams [146]. Woerdemann et al. realize trapping with Ince-Gaussian beams [147]. Several groups have demonstrated 2D optical manipulation in Bessel beams [148, 149]. In this type of non-diffracting beams [150] it is possible to trap several particles along the extended focal line typical for Bessel beams. Other non-diffracting beams have been successfully used for optical trapping as well. Examples are Mathieu beams [151, 152] and Airy beams [153].
Optical gradient forces also arise in interference patterns. Rohner et al. have demonstrated trapping in high gradient interference fringes [154].

3.1.3 Multiple trapping and Dynamic traps

Simple optical traps have become standard setups today. A next step towards an effective tool was the ability to trap more than one particle and to move those particles with respect to each other. This lead to the development of multiple traps as well as to dynamic features in the setups. A basic setup used in dynamic traps is shown in fig. 3.5.

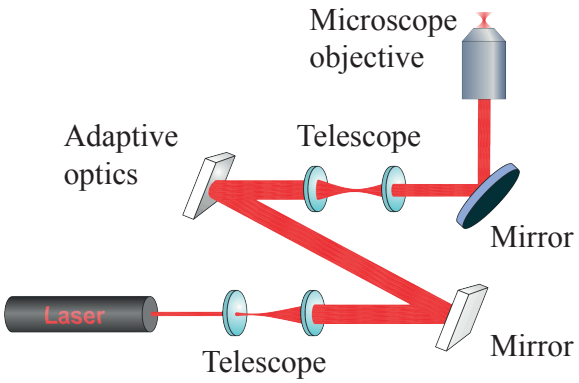

fig. 3.5: Basic configuration of a dynamic optical trapping system

Multiple trapping

A straight forward method of realizing multiple traps in one setup is the use of more than one laser. Multiple sources can be found in setups that use VCSEL arrays [130, 132]. Combining several conventional laser sources would result in a rather complex optical system. As an alternative to multiple sources, beam splitters are used to generate multiple beams. An example is shown in [140]

where a polarizing beam splitting cube is applied to split up a single source in two beams which can be used independently.
Diffractive optical elements allow for the integration of more complex patterns in the trapping setup [155, 77]. To this end computer generated holograms (CGH) are calculated with iterative algorithms. Trapping experiments that use CGHs are called holographic optical tweezers (HOT).
The desired intensity pattern in the image plane is selected and the corresponding phase information in the Fourier plane is stored in the CGH. The collimated beam hits the modulator and the desired phase is imprinted on the beam. The focusing optics acts as a Fourier transformer and reproduces the desired intensity pattern in the sample chamber. As an alternative to SLMs the diffractive phase element can be structured into a glass substrate or replicated into a polymer layer. An example of a multiple trap we generated using a diffractive 4 x 4 beam splitter is shown in fig. 3.6.

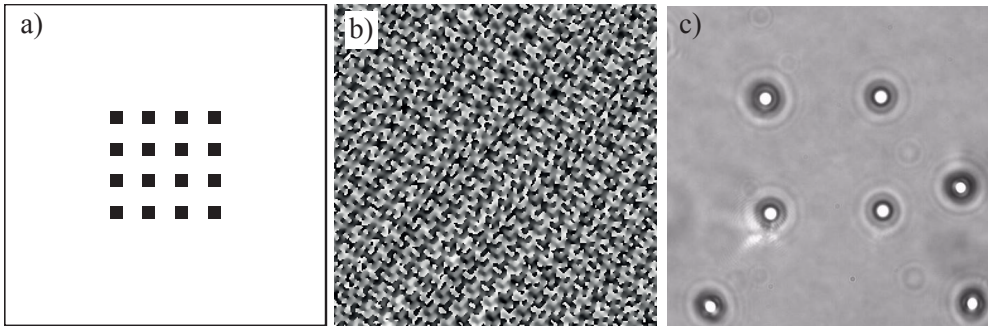

fig. 3.6: Multiple trapping by using computer generated diffractive phase elements a) desired intensity pattern in the image plane b)diffractive phase structure for a 4 by 4 beam splitter calculated by an IFTA algorithm, phase information is coded in the greyscale c) trapping of 4 beads in the 4 center spots simultaneously in a microfluidic channel

Massively parallel manipulation can be realized by using the Talbot effect [156, 157]. The Talbot effect describes the self-imaging of periodic microstructures such as diffractive gratings. The diffraction orders interfere behind the grating in such way that the original pattern is reproduced at selected distances (Talbot distances).Thus, a 3D intensity pattern can be generated and used for optical trapping. To demonstrate the effect, the Ilmenau optics group has fabricated silicon masters of checkerboard like gratings with feature sizes between 2 and 9 microns. These diffractive structures were replicated in transparent polymers (Polydimethylsiloxane, PDMS) [158] thus producing diffractive phase elements.

As shown in 3.7, a regular spot pattern could be generated in a fluidic channel. Particles in the channel were drawn onto this periodic grid and pushed against the opposing channel wall.

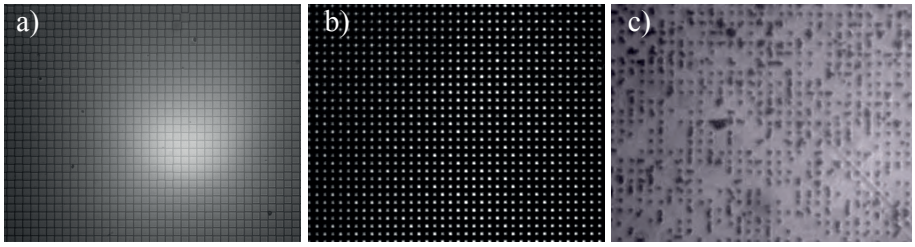

fig. 3.7: Optical manipulation with Talbot patterns generated with a chessboard pattern phase element. a) image of the diffractive structure (feature size 6 microns) in PDMS b) image of intensity pattern in a Talbot plane c) grating of 3 micron silica spheres generated by manipulation in the Talbot pattern

So-called time-multiplexing or time-sharing is a further option for multiple trapping. This method typically uses acousto-optical modulators [159, 160] and scanning mirrors [161, 140]. Typical switching frequencies are in the order of several kHz [162].
The laser beam is steered across the observation plane and only visits each trap for a fraction of the time. In the time between visits Brownian motion causes the particle to move out of the trap. For stable trapping the time-averaged effective potential has to exceed the kinetic energy of the particles [163, 164]. Therefore, the maximum number of traps in this class of setups is limited by the switching frequency.
When optical traps are generated off-axis, the imaging properties and the forces vary from position to position. The issue of uniformity has been addressed e. g. in [165].

Dynamics

The two most common options for the realization of dynamic optical traps have already been presented for their application in multiple trapping. The use of SLMs and active optical elements enables dynamic altering of the beam profile during operation. This improves the flexibility of an optical trapping setup significantly.
The realizations of dynamic traps can be divided in two main groups: Setups that use spatial light modulators and setups that use beam steering elements.
The first group has been described in their application for multiple trapping.

Modern phase modulators have refresh rates of 60 Hz [166] which allows smooth movement in the trap. In the second approach using beam steering elements, the trap is moved directly when the laser is deflected. In both cases, multiple individual traps can be independently steered.
So far, the presented dynamic trapping systems are actively controlled. Some beam profiles possess an inherent dynamic behavior which can be used for passive dynamic traps. The most widespread example are optical vortex beams (Laguerre-Gaussian beams). These beams have a rotating helical phase. This so-called optical charge can be observed on trapped particles in these vortices. The momentum along the ring focus causes a circular transport of the particles. An elaborate experiment that employs the dynamics of helical beams is an optical pump that has been published by Ladavac and Grier [167]. Six optical vortices with opposing direction of rotation create a flow which is capable of pumping on a microscopic scale.

3.2 Periphery

"Proof of principle" experiments under controlled laboratory conditions are the first step in the development of commercial products. Users of optical tweezing systems do not want to worry about alignment of optical components and expect a robust and reliable tool. This demand has been adopted by numerous research groups and several companies. To meet this expectation, a variety of convenient functions have been developed and easy to use systems are commercially available 3.4. The two main features of these systems are presented in this section.

3.2.1 Imaging/Position Detection

In the key applications of microbiology the trapped particle needs to be observed in the trap. Since many setups use microscopes as the platform for optical traps, the imaging of the workspace can be realized by the same objective that is used for focusing the trapping laser. An additional advantage of this procedure is that the focal plane and the trap location coincide. In laboratory experiments the observation often is realized by a second objective. In some cases the observation optics is placed in a 90 degree angle w. r. t. the optical axis. Examples for this approach can be found in the early work by Ashkin [19] and in the general phase contrast (GPC) based setups of the Programmable Phase Optics group at the Technical University of Denmark [168].

Particles in optical traps scatter the incident light. The scattered light is used to detect the presence of a particle in the trap and to study the movement of the

particle in the trap. In photonic force microscopy (PFM) quadrant photodiodes provide precise signals of the location of trapped beads. In the literature the resolution of the position tracking is a fraction of the detection wavelength (1/4 to 3/4 of the wavelength) [36, 169].
Fluorescence detection is a rare feature in optical trapping, since the trapping lasers commonly have wavelengths in the near infrared. In this spectral range hardly any flourophores can be excited. By using an excitation beam with a shorter wavelength, fluorescence detection can be included. An example is presented in [170].

3.2.2 User interfaces

The user of an optical trap needs a convenient interface to control the manipulation in the system. The simplest interface is a visual inspection through the trapping microscope. In a next step, the human eye is replaced by a digital camera for observation. Using a handle to steer the beam or moving the trapping chamber, the user can control the trap location in real-time on a computer screen. Today, users expect an intuitive user interface. An example is dragging and dropping items on the computer screen instead of manually varying the parameters of a stage or active optical element. GPC based tweezers have been among the first to be programmed with the option of activating a trap by clicking on the desired spot in the image on the screen [171].
Almost all commercial systems offer the feature of multiple traps and a drag and drop concept for intuitive control of the traps (compare fig. pict:uebercomsys)

3.3 From optical traps to optical trapping systems

Many of the typical trapping applications can be realized with the commercial trapping solutions and other experimental setups that were described in the previous chapter. However, the parameters of the traps are defined and limited by the components used in these systems. More compact and potentially cheaper realizations can lead to a multitude of other applications. To this end it is necessary to view the optical trapping system as a self-contained unit. This approach can be found in integrated optics. The following section outlines the principles of integrating optical systems and depicts the published work on integrated optical trapping systems.

3.3.1 Optical system integration

Miniaturization and integration are two main topics in modern consumer optics. These trends can be found in applications that already are in everyday use. Most modern mobile phones have built-in cameras which are highly compact optical systems. Currently high end phones offer cameras with resolutions up to eight megapixels. To achieve this miniaturized imaging systems the optics had to transition from the conventional spherical lens based cameras to specialized freeform optical modules. Modern fabrication techniques allow the economic production of highly aspherical lenses which provide advanced possibilities to the designer.

Functional integration in optical systems means the combination of two or more optical functions in a single element with no additional mounting parts being required. A prominent example for this approach are camera lenses such as the Canon EF 400 mm 1:4.0 DO IS USM which use lenses that are combined with diffractive optical elements. In this way, the function of color correction is integrated with a focusing element.

Following the above definition of functional integration, a camera lens which is mounted on a camera body does not fall in the category of integrated optics. The assembly forms a unit but a mount for the lens is needed.

Both trends are also found in the field of integrated optics [172].

Within the class of integrated optics, one can distinguish integrated waveguides from integrated free-space optics. In both cases, planar fabrication technologies are the enabling factor to the feasibility of these optics. It is possible to implement diffractive (e. g. gratings) and refractive (e. g. reflow lenses) elements.

Integrated waveguides share the functional principle with optical fibers. The index difference or gradient that is needed to fulfill the conditions for guiding light is generated in various ways. Technological details can be found in textbooks for integrated optics [172, 173]. As the term integrated free-space optics suggests, these classes of optics do not rely on wave guiding. For this class of systems the acronym PIFSO (planar integrated free-space optics) has been introduced. As shown in fig. 3.8, the optical elements are integrated into the surface of a planar substrate.

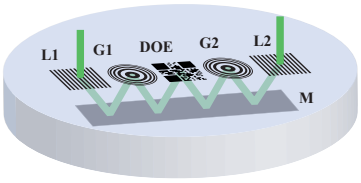

fig. 3.8: Example of a PIFSO system; G1,G2: coupling grating; L1, L2: diffractive lens; DOE: diffractive optical element; M: mirror

The optical path is folded into the substrate. Further examples for such integrated free space optical systems are described in [172, 174, 175].
Integrating optical systems offers a number of advantages. Integrated setups are robust in terms of misalignments. This is especially true for monolithically integrated systems which represent the highest possible degree of integration. In these systems the optical surfaces or components share the same physical body and they cannot be moved relative to each other. Furthermore, contamination of the optics from external sources is excluded.
Combinations (stacks) of several planar optical systems have been presented in [176] and [177].
Along with the benefits, there are also technological challenges that come along with the integration. Since it is not possible to realign the components in the system, a high positioning accuracy has to be maintained during fabrication [178]. Furthermore, it is impossible to include additional functions into the system, once it is fabricated. Last but not least, the diffraction efficiency of integrated systems is a topic of ongoing research. As the optical path is folded into the substrate, the optical elements need to be designed for the oblique incidence of the light. The resulting surfaces are freeform surfaces which are not available as standard elements. The rotational symmetry that is required for turning and polishing optical surfaces does not exist. Diffractive optical elements (DOEs) are not bound to symmetry and offer an attractive solution for planar integrated optics. However, the efficiency of diffractive optical systems may decrease if binary structures are used. The diffraction efficiency of a single binary phase element is approx. 40%. The system efficiency declines exponentially with the number of DOEs. Multilevel DOEs reduce this flaw but increase fabrication costs and effort. Integrated optics using analog phase elements or hybrid elements may be a solution to the efficiency issues [178, 179, 180].

3.3.2 Previous works of integrating optical trapping optics

In general, designing and fabricating customized optics is not an option for researchers and end users. Hence, most optical tweezing setups are assembled using off-the-shelf optical elements. Especially the selection of the focusing unit is highly limited. Consequently, only few publications address the integration and simplification of conventional optical tweezing systems. On the contrary, in the decades after the discovery of optical trapping, the setups became more and more complex. Additional active optics such as spatial light modulators were added to optimize the trapping forces and to include dynamic features in the setups. However, for educative purposes there is a demand for simple, robust and low-cost systems. Smith describes an inexpensive setup, which can be used as a lab experiment enabling students to get a first-hand experience of optical trapping [181]. In order to reduce the costs, he discusses which components can be used to demonstrate the effect as clearly as possible. While in this approach the minimum optical requirements are explored, the basic structure of microscope-based optical tweezers remains preserved. Appleyard presents a trapping experiment for undergraduates, which follows a similar philosophy [182]. He also uses the classic optical scheme to achieve tweezing but realizes the trap without the use of a microscope.

A real integration, i. e. a reduction of elements compared to a conventional system is presented by Sery [183]. In this publication a module is introduced, which can be used to convert an unchanged microscope into optical tweezers. This module contains the entire laser illumination and is put in between the microscope tube and the objective.

Even though the authors of [184] do not describe functional integration, another interesting benefit of system integration is addressed. The authors demonstrate an optical trap with a diode laser as a radiation source. This reduces the required space for the entire setup as well as the costs.

So far, all of the described experiments are based on conventional imaging systems. In the last years, the possibilities for miniaturizing and integrating refractive optical elements have been extended by modern fabrication methods. In addition to the planar processes that are adopted from the computer chip industry, an upcoming technology is ultraprecision machining [185].

The most accessible way for system integration is the modification of the fluidic system that is used in most experiments. In [158] Amberg describes a fluidic system made from PDMS which allows the integration of diffractive optical phase gratings in the wall of the chip. 3D optical traps with a low NA focusing objective were presented by Schonbrun and co-workers in [186, 187]. Here, a

Fresnel zone plate has been integrated into the chip by evaporating gold rings onto the chip's surface. This amplitude grating acts as an additional lens.
These approaches can be attributed to the wide field of lab on a chip systems. With the same field of applications in mind, Merenda et al. showed an array of miniaturized high NA-mirrors [102]. The mirrors were fabricated by embossing a commercial hexagonal microlens array into an UV-curing resist. The authors show a parallel trapping of over 100 fluorescent beads.
An even higher degree of integration can be achieved, if the optics do not have to fulfill focusing tasks. This kind of non-imaging optical trapping systems is mainly found in the field of optofluidics [188, 189, 190, 191]. Here, the light for trapping is supplied by optical fibers which are directly integrated in the fluidic chip. The fibers generate an intensity gradient in the fluidic channel which is sufficiently high to manipulate particles in the channel. Since the fibers produce diverging beams, it is generally necessary to use counterpropagating setups in order to achieve 3D trapping. A well-known application of optofluidic systems is the optical cell stretcher [29] that has already been mentioned in chapter 2. As the name suggests, in this device optical forces are employed to deform cells with optical forces. Since this deformation is characteristic to each cell type, it is possible to precisely identify different cells.
Other optofluidic applications are optical traps in liquid waveguides. Coupling light into a liquid filled fiber generates a counterpropagating trap [192]. An optofluidic chip with the laser source integrated directly on the chip is presented in [193, 194].
Fiber based traps that realize optical trapping with a single fiber have been suggested in [107, 106] and [110]. In these papers the tips of the fibers have been prepared specifically to generate a high field gradient behind the fiber.
For the generation of high gradients for optical trapping, nanoantennas have been successfully employed. These devices typically consist of two opposing metallic triangles which are deposited onto a planar substrate. The tips of both triangles are separated by a nanometer sized gap. When the antennas are illuminated with a laser beam, a high field electric field is generated in the gap as a resonance effect.
When speaking of system integration, not only the optics and mechanics, but also the necessary electronics and data processing need to be considered. As mentioned earlier in this chapter, electronic integration has already been demonstrated in the fluidic chips with built-in laser sources [194] and the use of compact laser diodes [128].

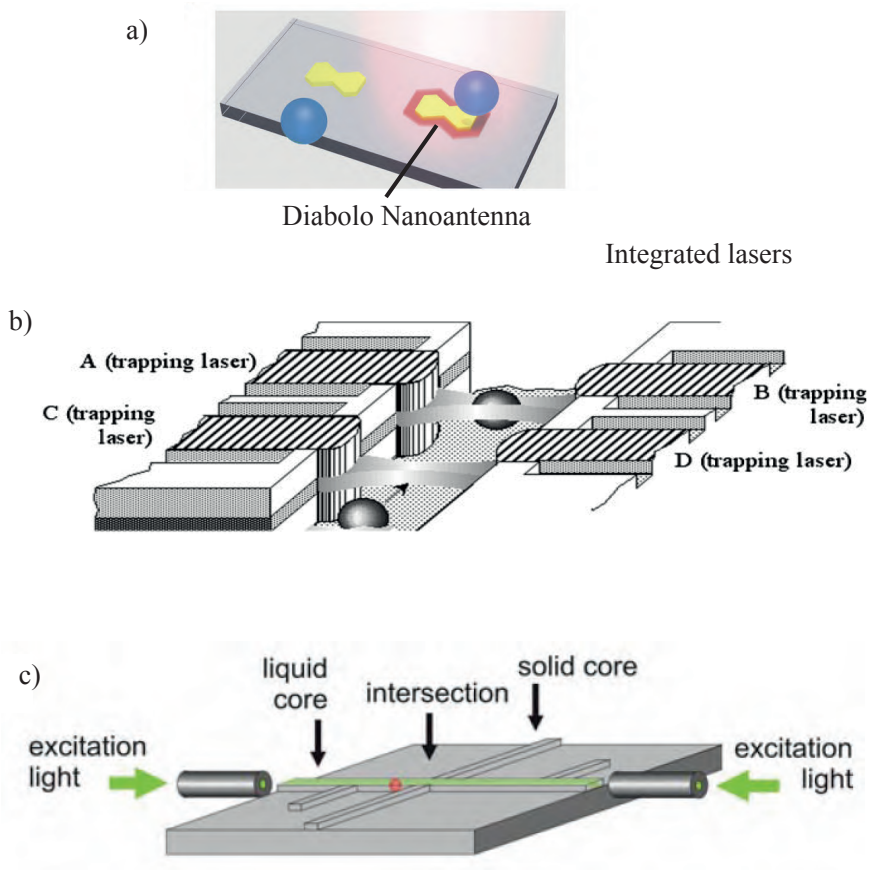

fig. 3.9: Examples of optofluidic and near field trapping systems. a) diabolo nanoantennas (from [124]) b) integrated laser (from [194]) c) hollow core optical fiber trap (from [120])

Setups that provide a PC-based user interfaces or measuring features are commonly equipped with detection, control and data processing components [195, 196, 36]. While in these setups several functions are incorporated, they do not represent integrated optical systems according to the definition stated at the beginning of this chapter.

3.4 Commercial systems

The main topic of this thesis is the optimization and integration of optical trapping systems and its goal is the development of new applications, which offer new, improved or more specific features to the user. To get an impression of the features that are available in commercial setups, the systems that are currently on the market have been compared in fig. 3.10. The table has been filled with the information that the suppliers present on their websites. Even

though the alternatives differ in several aspects, the general setups are similar. The inverted microscope is the standard platform. Most systems offer multiple trapping and force measurement.

In Industrial applications, e. g. for microfabrication, the optical trap becomes a tool in a process chain rather than a stand-alone device. This implies that the design of the trapping system has to take the restrictions imposed by the machine environments into account.

3.5 Summary

This chapter includes a broad overview over the variety of setups for optical trapping. As a knowledge base, these setups form a basis for the search for new trap concepts. As shown, there is a large number and variety of publications in the field. In this chapter we categorize optical trapping setups according to four criteria: dimensionality of the trap, the intensity pattern, the number of parallel traps and dynamics of the trap. The vast majority of trapping experiments that have been proposed were tested under controlled laboratory conditions. Here, the experimental setup can be adapted freely in order to demonstrate the desired effects.
The variety of commercially available systems is small, compared to the experiments found in the literature. Generally speaking, they are based on standard inverted microscopes with an additional laser source. Typically, the price for such products exceeds EUR 100,000. Multiple trapping and a user friendly software interface are state of the art in commercial optical tweezers. Without exemption, these systems are composed of standard optical components.
To extend the range of application, optical trapping systems need to become more flexible in terms of system costs and setup. The methods of integrated optics present opportunities to achieve this goal. The utilization of custom made components and application oriented design enables new options for designing novel trapping systems.

Supplier	Arryx	MMI Molecular Machines & Industries	Palm (Zeiss)	Thorlabs	JPK Instruments	Elliot Scientific	In development by the PPO group at Denmark Tech. Univ
Product name	**Bioryx 200**	**mmi CellManipulator Plus**	**PALM Series**	**Optical tweezer kit**	**NanoTracker**		**BioPhotonics Workstation**
Platform	Nikon TE2000	Inverted microscopes (Nikon or Olympus)	Inverted microscope (Zeiss)	Thorlabs components (optical setup comparable to inverted micoscope) Nikon 100x Objektiv	Inverted microscopes (Zeiss, Nikon or Olympus)	Inverted microscopes Various models (Licence from University of St. Andrews)	Custom platform, GPC based counterpropagating trap
Wavelength	532 nm or 1064 nm	1064 nm	1064 nm	980 nm	1064 nm	685nm,785nm or 1070 nm	NIR
Power	2 W	8 W	3W	330 mW	3 W (others available)		
Particle sizes		0,1 – 200µm	0,1-100				1-100 µm
Trap force		up to 800 pN	0,1-200 pN				
Functions	Holding, aligning manipulating, assembly of 3D structures	Holding, moving, rotating, combining, separating, stretching			Simultaneous fluorescence measurement		Trapping, rotating
Number of individual traps	up to 200 (HOT)	10 parallel traps (scanning mirror)	1	1	2 by using two independent polarizations and scanning mirror; more traps possible with time multiplexing	1 – Multiple (AOM)	100 (in a workspace of 250 µm)
Price			>150.000 €	16.400 $ (2012)			
Optional features	Micro dissection	Force measurement Zellsortierung Micro dissection; 10 additional traps	Force measurement Micro dissection RoboMover	Force measurement	Force measurement with fN sensitivity	PFM Force measurement	Spectroscopy

fig. 3.10: Comparison of commercial trapping systems

4 Design process

The optics design of an optical trapping system is for the most part identical to any optics design for imaging. The desired system performance is specified and numerically optimized according to a merit function. The geometry of the individual optical surfaces then results from an optimization loop. In the case of optical traps, the actual performance of the optics i. e. the optical forces cannot be assessed by only using the spot diagrams and intensity patterns that suffice for conventional imaging optics. The forces and shape of the trap depend on the overall geometry and intensity distribution of the beam as well as the diameter of the trapped bead. This three-dimensional information is not contained in the spot image in an individual plane.
Thus, a force simulation module needs to be included into the design process. In this experiment, this is realized using the interfaces between commercial optics design software and loading the data into a self-written ray tracing tool in MATLAB.
At the beginning of this chapter, we discuss the practicability and benefit of an efficiency criterion that reflects the efficiency of the entire trapping system. This chapter also includes an overview of the simulation tools and the workflow that are used during the design of the systems presented in this thesis.

4.1 System efficiency of optical trapping systems

Obvisously, when planning a new trapping application, the designer wants to choose the most appropriate setup. So far, the dominating design criterion is the trapping efficiency Q, i. e. the magnitude of trapping force that is exerted by one unit of power that hits the particle. If the radiation exposure at the sample needs to be minimized and the power efficiency of the whole system is not an issue,then the trapping efficiency is an excellent measure. If other restrictions like limited space, laser power or budget come into play, the efficiency of the trap and the efficiency of the entire system are two different perspectives to look at the possible solutions. A design requirement can be the use of a low-cost laser diode to reduce the costs for the setup. The task for the designer now, is to find an optical system which provides the best trapping performance (i. e.

the highest force per unit of power from the laser source under this boundary condition).

A value which describes the system efficiency of different trapping systems and alternatives can be a useful tool in the design process. It enables the comparison of different trapping setups even for designers who are not experienced in both classic lens design and the physics of optical trapping.

This section proposes guidelines for the selection of systems with the highest possible system efficiency.

To this end, the main sources of influence on the force that occur in the system are discussed. Following this overview, a specific setup will be evaluated.

The types of influences and their sources are enlisted in table 4.1 and 4.2. The shape and depth of the optical trapping potential depend on the wavefront and the intensity pattern of the radiation. These two properties are a result of the beam's various interactions with optical components in the system. Many publications document and discuss the role of influences such as geometric aberrations. However, the actual optical properties of real components (in general) are not explicitly taken into account.

It would be ideal if the system efficiency could be described by a single factor which enables the comparison of different setups. In analogy to the trap efficiency Q, a System Efficiency Q_{sys} could be defined by $F = Q_{sys} \cdot P$. This requires the combination of the parameters that determine the performance of the trap into one single formula.

In terms of power efficiency, the relation is straight forward. Every component can be assigned an efficiency η. The system power efficiency η_{sys}, i. e. the fraction of power that actually reaches the trapped particle, can be written as the product of all individual efficiencies (eq. 4.1). This is a valid approach because the efficiency of one component does not influence the efficiency of the following elements.

$$\eta_{sys} = \eta_1 \cdot \eta_2 \cdot \cdot \eta_n = \prod \eta_i; \eta_a \neq f(\eta_b) \tag{4.1}$$

The effects that influence the focusing properties are more difficult to describe. The interdependence of the contributions of single elements to the total beam shape is more pronounced than the power efficiency.

As described in chapter 2, the trapping properties are a function of the particle diameter and shape, the refractive indices, the location of the particle in the beam and the shape of the beam. This number of parameters leads to a high complexity of the link between the source and force. The beam shape is particularly hard to describe analytically.

Table 4.1: Influences on the power efficiency in optical trapping setups

Effect	**Introduced by**	**Minimizedy by**
Absorption	Material property, aperture stops in the beam	Selection of materials that do not absorb at the working wavelength
Fresnel Losses	Reflections at interfaces between media	Reduction of elements; AR-Coatings
Reflection	Mirror coatings do not reflect 100% of the light AR-Coatings do not reduce the reflectivity to 0%	AR- Coatings designed for trapping wavelength
Diffraction losses,	Diffractive Elements	Increased number of phase levels
Stray light	Rough surfaces, machining marks, material impurities	Increased surface quality

The uncertainty in the system description starts with the radiation source. Generally, the profile of a real laser beam is not an ideal Gaussian profile. The common measure of the beam quality is the M^2 factor. M^2 contains information about the center of gravity of the beam and standard deviation from the ideal mono-modal beam. Each component in the beam varies the phase (and amplitude) profiles of the beam. Different to the efficiencies η the contributions of the individual elements on M^2 are inseparable. A good example for this behavior are two plano convex lenses that form a telescope. The first lens introduces spherical aberrations which are partly compensated by the second lens. This principle of aberration compensation is a common tool in classic lens design but makes simple analyses impossible.
The final effect of each variation on the trapping forces and an individual contribution to the system efficiency cannot be determined discretely. This overall complexity prevents a simple analytic connection between the system geometry and the trapping force. The major sources of influence on the trap/ beam shape are listed in table 4.2.

An example for influences that cancel each other out is increasing the beam quality from the source by inserting a pinhole in the beam. This spatial filtering removes higher modes from the beam which results in a better focusability of the beam. While the trapping efficiency can thus be improved, the remaining power in the beam is significantly reduced behind the pinhole.
Truncation is a further example in this context. The entrance pupil is overfilled with the laser beam in order to improve the ratio between the power in the

Table 4.2: Influences on the trap shape

Effect	**Introduced by**	**Minimizedy by**
Real beam shape	Real laser source	Spatial filtering, beam shaping
Astigmatism	E. g. edge emitting laser diodes	Correction elements
Higher order Aberrations	Fabrication Errors, Design, Misalignment	Design, higher alignment effort, higher quality optics
Dispersion	Material property	Design, Material selection
Angular spectrum in the beam	DOEs, truncation, diffraction	Refractive beam shaping, higher number of phase levels
Spherical aberration	Lenses, Different media	Design, Water immersion

center of the trapping beam and the power at the edge. While this actually improves the trapping efficiency Q, the maximum trapping force is not necessarily increased. In fig. 4.1 the ideal overfilling from a system point of view is depicted. The variable a is the ratio between the $1/e^2$ value of the beam and the diameter of the entrance pupil. It can be seen, that overfilling (a>1) in fact does not increase the total trapping force. The improved trapping efficiency Q is canceled out by the amount of energy that is lost at the entrance pupil.

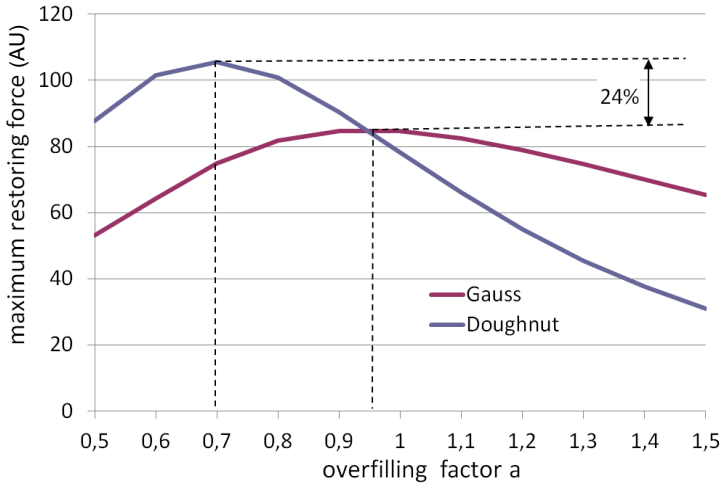

fig. 4.1: Influence of different factors of overfilling; with an increasing overfilling factor a the power that is blocked by the entrance pupil exceeds the benefits that are gained by improved trapping efficiencies

Correction of spherical aberrations with an SLM and conversion of the TEM_{00}

into a Laguerre-Gaussian beam can be treated in a similar way. The focus quality has been shown to be improved which results in a higher trapping efficiency Q. The costs of this transformation are the reflection losses and the limited diffraction efficiency of the SLM. More exotic setups such as near field optical traps and optofluidic traps can also be evaluated using the criteria of tables 4.1 and 4.2. However, these setups differ strongly from conventional trapping setups so that the pre-selection according to the boundary conditions dominates.
The choice of the best trapping setup for an application is further reduced by boundary conditions as listed in 4.3. The task of selecting the best suited alternative for the given application remains.

Table 4.3: Boundary conditions in optical trapping setups

Restricted factor	**Implication for the design**
Weight	Limitation of the system weight by using lightweight material and reduction of optical elements
Space	Construction of compact setups and integrated systems
Working Distance	Selection of a suitable focusing optics or design a custom focusing unit
System cost	Selection of budget components and reduction of system features
Availability	Application of state of the art system and off-the-shelf components
Compatibility	Use of a setup which is compatible with the platform technology

As an example, a setup based on an inverted microscope (fig. 4.2 is analyzed (see table 4.4). To this day, these setups represent a standard and can be considered as benchmark systems for other system configurations. This standard setup will be taken as a reference for the new design presented in chapter 5.2. Inverted microscopes are the standard platform for optical manipulation in microbiology i. e. the trapping of living cells. Here, a key issue is photo-damage in the trapped cells which depends on the dose of radiation that hits the particle [197, 198]. Thus, the major requirement in the design of the setup is the trapping efficiency Q. The power efficiency in this example is of minor concern and the goal is to maximize the force per unit of power at the trapping location.

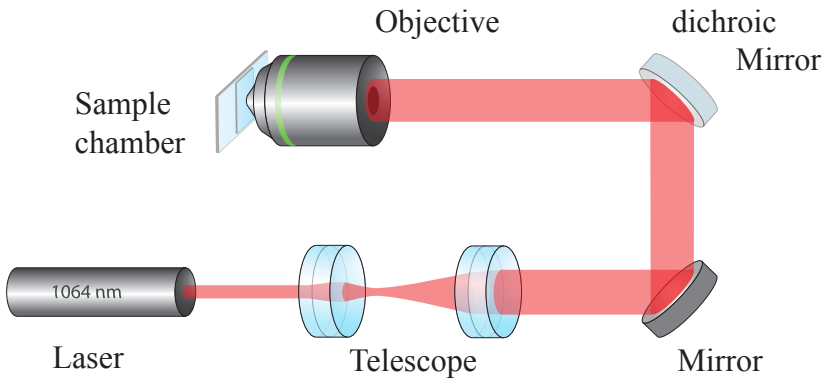

fig. 4.2: Example system for the estimation of the system efficiency

As a result of the analysis, it can be stated that only one third of the initial power actually reaches the trapping chamber. The beam quality in this setup is high. If oil immersion is used, the trapping force will depend on the depth of the trap in the fluidic channel. Since the flexibility of the setup is restricted, the opportunities for optimizations are limited as well. The user can vary the overfilling or correct aberrations with an active optical device.

Table 4.4: System performance of a trapping setup based on an inverted microscope

Element	**Efficiency (Power)**	**Beam shape**
Laser source	100%	$M^2 = 1.02$
Telescope (2 Achromats)	96% · 96%	SA, Coma
Mirror (silver coating)	92%	—
Mirror (dichroic)	99%	—
Entrance Pupil (Overfilling, Truncation)	80%	truncated Gaussian
Objective	50%	SA, Errors due to Dispersion, radially varying transmission
Immersion fluid	96%	SA (in most cases)
Cover glass	96%	
Parasitic reflections, Scattering, Diffraction		
Sum	34%	SA, Coma, Truncation

4.2 Design Workflow for optical trapping systems

In this section, we present a holistic design process for new optical trapping systems. The structure of this process is outlined in 4.3. Similar to classical lens design, the generation of trapping systems is not a linear process. Instead, the design is an iterative process that usually requires several loops of optimization.

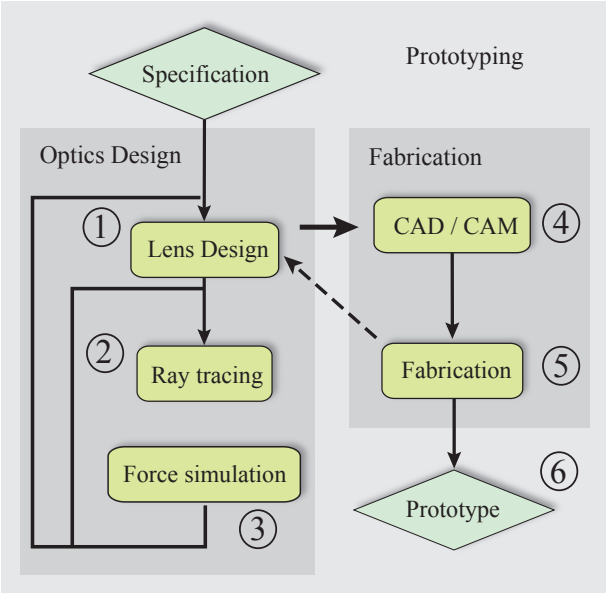

fig. 4.3: Flow chart of the design process

1) Lens Design

The starting point of the process is the system specification where the functionality of the setup is defined. An initial system configuration is chosen and optimized using ZEMAX (Version 110711). For this design software large libraries of sample systems are available. The strength of ZEMAX in this application is fast and precise optimization of geometric optical models. The merit functions for the optimization can be modified to match the actual specifications of the setup. The optical system is defined as a set of parameters that describe the optical surfaces. At this early stage it is advisable to account for the boundary conditions that are imposed by the fabrication.

2) Ray tracing

In the presented workflow we use ASAP (2009 V2R2) for the physical behavior of the system. Other groups have shown the modeling of optical traps using ZEMAX and a force calculation only [77]. However, the connection between the geometrical model and the force simulation is smoother, when ASAP is used for the simulation of the more detailed systems. The result of the first step is

a geometric model of the trapping system which is imported into ASAP. Alternatively, the systems can be manually transferred into ASAP code.
The light source can be either described by a set of beam parameters or by measured data from the real laser beam. Thus, the very laser that will be used in the experiment can be included in the simulation.
The optics is represented in a parametric model. The physical properties (radii, spacings, etc.) can be directly accessed and varied. This enables easy parameter studies and tolerance considerations. Within this thesis, the tolerancing has been performed manually, but an automated routine can be programmed in later works.
In order to get the simulation as realistic as possible, the ASAP wave optics mode [199] is used. In this mode a Gaussian beam is represented by a set of rays (base rays, waist rays, divergence rays). More complex wavefronts are decomposed into a series of Gaussian beams which can be traced through the optical system. The result is the superposition of the beams while taking the different optical path lengths (= phase differences) to the neighboring rays into account. With this approach, ASAP is able to calculate interference patterns that occur in coherent radiation. An example is shown in fig. 4.4. The interference pattern due to increasing spherical aberrations is visible in b) and c).
In the wave optics mode Fresnel reflection losses and multilayer anti reflection

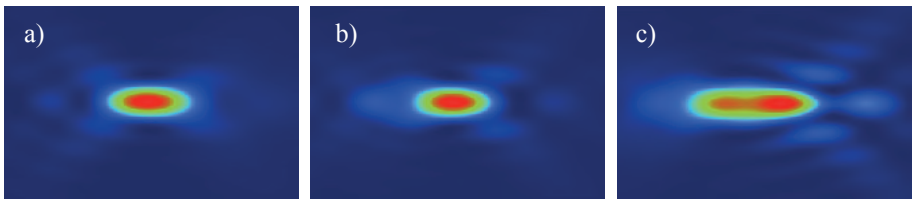

fig. 4.4: Cross-section of foci in ASAP; representation of spherical aberrations in varying depths in water

coatings can be included in the simulation.
The subsequent force simulation requires the data from the ray trace. In ASAP the export interface of ray data from the optics simulation generates an easy to read text file which contains the vector data as well as the power carried by each ray. This enables an easy inspection of this data before the force calculation. In ZEMAX the simulation data is exported in the IGES format which does not support the export of the information on the power.

3) Force calculation

The calculation of optical forces in MATLAB is based on the photon stream

method by Gauthier [100]. This procedure has already been tested and verified for the numerical calculation of optical forces. Essentially, the method is a ray tracing approach which interprets the total optical forces as the sum of the contributions of each photon. The power that is assigned to a ray of the illumination beam is directly proportional to the number of photons that interact with the particle per unit of time. By the calculation of the individual forces exerted by single rays, the contribution to the total force can be determined and favorable beam shapes can be chosen.
Parameter studies of the system performance are run as a loop between step 2 and 3. This loop is repeated while changing the figures of interest in the model description. If no system configuration fulfills the requirements, the iterative loop has to go another step back and, where necessary, the optical start system has to be modified.
When the performance of the system is satisfactory, the geometry data can be prepared for the fabrication.

4) CAD / CAM

This step is especially important, when specialized optical elements for the trapping system have to be fabricated. A CAD/CAM model is generated which allows the final selection of appropriate tools and machining strategy. As mentioned in step 1, the capabilities of the fabrication ought to be taken into account at the first stage of the design process. The conversion of the parametric description of an optical element into CAD data is a crucial issue in the fabrication of precision optics. Approximations of the optical surfaces will influence the performance of the system. The description of curved surfaces using splines and interpolation is a common measure to reduce the amount of data in the CAD file. In our design described in 5.2 the geometric data was transferred manually into the machine code, to avoid the loss of precision by approximations. The surfaces were programmed as the actual polynomials from the simulation and the machine control computes the necessary 3D coordinates on the fly. The remaining limiting factor is the positioning accuracy of the machine.

5) Fabrication

One main goal of this work is to introduce and validate a process that serves as a basis for the prototyping of novel optical systems for optical trapping. Therefore, the fabrication is a necessary step of the prototyping process in order to provide a proof of concept. The accuracy in machine tools depends on the mechanical stiffness, the tool quality and the machine environment. As the performance of optics deteriorates when surface qualities are decreased, machines

for the direct fabrication of optics need to work with precision tools (diamond or carbide) under controlled conditions (e. g. temperature stabilization or stable supply of pressurized air). The available tool geometries limit the variety of possible shapes. The same is true for the overall dimensions of the optical components. Another important issue that needs to be kept in mind is the assembly of the individual optical elements in the final setup. The tolerances for spacings between two lenses, or tilts and shifts of components are defined during design and have to be realized during fabrication or assembly respectively.

6) Prototype
The assembled prototype allows the assessment of the performance of the system. The quality of the system model and simulations can be evaluated by comparing the calculated trapping forces with the measured values. The characterization of the system and its components also delivers information about the quality of the fabrication. The findings of the experiments can be used to improve the design or to adjust the fabrication process.

4.3 Force estimation tool

Numerous groups have written their own software and user interfaces in order to calculate and visualize optical forces (e. g. [200]). The force calculation used in this work is a variation of the ray optics approach [201]. It is based on the photon stream concept presented by Gauthier [100] which interprets the illumination beam as a stream of photons which is altered by the interaction with the particle. This representation of the incident field is convenient since it offers a straight forward interface to the optics design software used to generate the rays to be traced. As mentioned in the description of the workflow, a set of rays is incapable of representing interference effects. However, the Gaussian profile and aberrations can be found in the ray data exported from ASAP. The interference pattern can be seen in the local densities of the rays in the focal area.
The force simulation tool can import the ray data directly from ASAP via an import filter. The vector information, as well as the power that is assigned to each ray, is transferred without loss of information.

4.3.1 Model and Algorithms

Ray tracing in general and the photon stream method in particular have been chosen for the following reasons:

- smooth integration with available commercial optics design and simulation software
- compatibility to ray-tracing design and simulation (no in-depth knowledge of the physics of optical traps necessary)
- verified calculation method which is valid for large particles
- ability to extend the model in order to include polarization and non-spherical objects.

The intensity pattern is represented as a stream of photons travelling along the rays. The algorithm behind our calculation is explained in the following paragraphs.
The basic geometric scenario consists of a sphere and a ray which hits the sphere (see fig. 4.5).

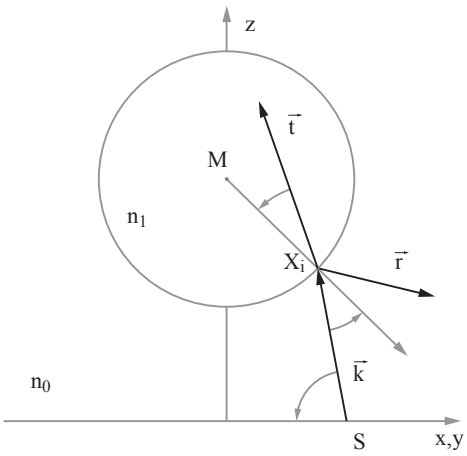

fig. 4.5: Vector diagram of a ray that originates from S in the direction $\vec{k}$; At the location X_i the ray intersects with the surface of the sphere with center M. The photon stream that is represented by the ray is split into a reflected part $\vec{r}$ and a transmitted part $\vec{t}$; n_0 and n_1 are the refractive indices of the surrounding medium and the particle respectively

The representation of the incident ray in cartesian coordinates can be written as

$$\begin{aligned} x(t) &= S_x + k_x d \\ y(t) &= S_y + k_y d \\ z(t) &= S_z + k_z d \end{aligned} \tag{4.2}$$

S is the position vector of the starting point of the ray. The vector $\vec{k} = k_x, k_y, k_z$ in this case is a direction vector with unit length. d is a control variable.

The surface of the sphere with radius R is defined by

$$R^2_{sphere} = x(d)^2 + y(d)^2 + z(d)^2 \tag{4.3}$$

The intersection X_i of the ray and the sphere can be found when equations for the coordinates 4.2 are inserted in equation 4.3. If no values for d fulfil the condition, then the program concludes that the ray misses the sphere.
The normal vector is defined by the local vectors of the center of the sphere $\vec{M}$ and $\vec{X}_i$. When the equation of normal vector is written as $\vec{n} = \vec{M} - \vec{X}_i$ then the normal vector points outwards. The normal vector and $\vec{k}$ determine a plane. The refracted ray $\vec{k}$ and the reflected ray $\vec{k}$ lie in the same plane. The calculation of the vectors was taken from [92]. For the subsequent interactions with the particle's surface the vector of the refracted ray is used as the incident ray.
The previous considerations define the geometrical paths of the rays (application of Snell's law). In combination with the following equations the model for the transfer of momentum to the particle is completed.

According to de Broglie, a photon of the wavelength λ carries a momentum $\vec{p}$.

$$\vec{p} = \hbar\vec{k} = \frac{h}{2\pi}\frac{2\pi}{\lambda}(k_x\vec{e}_x + k_y\vec{e}_y + k_z\vec{e}_z) \tag{4.4}$$

where Planck's constant $\hbar = \frac{h}{2\pi}$. During the interaction at the particle's surface each photon can either be refracted into the particle or reflected from the surface. In both cases, the momentum of the photon is changed. These changes obey the law of conservation of momentum. Hence, the change of momentum for a reflected photon is

$$\Delta\vec{p}_r = \frac{\hbar n_0}{\lambda_0}(\vec{k} - \vec{r}) \tag{4.5}$$

n_0 is the refractive index of the surrounding media. Likewise, the equation for the refracted (transmitted) photon is written as:

$$\Delta\vec{p_t} = \frac{\hbar n_0}{\lambda_0}(\vec{k} - n_{rel}\vec{t}) \tag{4.6}$$

here n_{rel} equals $\frac{n_1}{n_0}$ where n_1 is the refractive index of the particle. λ_0 is the vacuum wavelength. For further interactions of the refracted beam with the surface, n_0 and n_1 have to be swapped in equation 4.6.

The actual number of photons on a ray per unit of time can be calculated as [92]:

$$N_i = \frac{I(x,y,y)\lambda_0 dA}{\hbar c} \tag{4.7}$$

The number of photons depends on the energy of each photon, the value of the intensity at the origin of the ray $I(x,y,z)$ and the area dA that is determined by the lateral sampling of the intensity pattern.

The probability for a photon to be refracted or reflected can be derived from the Fresnel coefficients. It is assumed that the laser beam is not polarized. Therefore, the mean value of both coefficients can be used to determine the required ratio (as given in eq. 4.8).

$$R(\theta_1,\theta_2) = \frac{1}{2}\left[\frac{sin^2(\theta_2-\theta_1)}{sin^2(\theta_2+\theta_1)} + \frac{tan^2(\theta_2-\theta_1)}{tan^2(\theta_2+\theta_1)}\right] \tag{4.8}$$

In this formula for the reflectivity R, θ_1 and θ_2 are the angles between the incident ray and the refracted ray w. r. t. the normal of the surface. For this calculation only non-absorbing particles are considered. So far, the changes of momentum have been written down in eqns. 4.5 and 4.6. The force that causes this change of direction of the photon is the time derivative of the momentum.

$$\vec{F} = \frac{d\vec{p}}{dt} \tag{4.9}$$

The calculation of the entire force of a photon stream is based on the number of photons per unit of time. The possible paths of the photons and their probabilities are shown in fig. 4.6.

Due to the symmetry in the sphere, the angles at each interaction of the ray with the particle remain the same. Hence, the Fresnel coefficients for the ray have to be calculated only once.

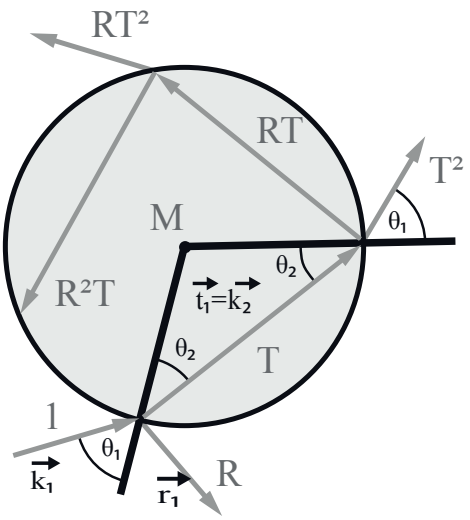

fig. 4.6: Ray tracing in spherical particle; T=transmission coefficient R Reflection coefficient M center of sphere $\theta_{1,2}$ angles of incidence $\vec{k}$, $\vec{t}$, $\vec{r}$ directions of incident, transmitted and reflected rays

The total force vector is the sum of the individual forces upon each interaction.

$$\vec{F}_{ray} = \sum_{i=1}^{m} \vec{F}_i \tag{4.10}$$

The power of the refracted ray drops exponentially with each further interaction with the particle's surface. For instance, if the transmittance of the particle is 0.96, the major part of the force arises due to refraction. In the software a threshold is programmed which limits the number of interactions which need to be evaluated. The calculation is stopped when the power drops to 0.1% of the initial power of the beam. Typically, this occurs after two to three interactions. The contribution of further reflections in the particle are neglected.

The force of one interaction can be split up into two components. The force for the first interaction of the i-th ray thus becomes

$$\vec{F}_1 = N_i \left[R\Delta\vec{p}_{r,1} + T\Delta\vec{p}_{t,1} \right] \tag{4.11}$$

T is the transmittance coefficient. The first part of the sum in the squared brackets stands for the force due to reflection, the second part stands for the force due to refraction. In the algorithm for the calculation it needs to be taken into account that the ray originates from the surrounding medium (refractive index n_0 in the first interaction). In the following interactions the ray originates from the medium inside the sphere n_1 and carries the fraction T as the initial

power. Thus every further partial force $\vec{F}_j; j \geq 2$ is written as:

$$\vec{F}_j = N_i \left[TR^{j-1} \Delta \vec{p}_{r,j} + T^2 R^{j-2} \Delta \vec{p}_{t,j} \right] \tag{4.12}$$

Using the above formalism, the optical forces can be calculated. In order to compare the expressions with those of other publications, the formulae can be re-arranged. A common notation of optical forces puts the input power in relation to the generated force

$$\vec{F} = \frac{1}{c} P \cdot \vec{Q} \tag{4.13}$$

Where P is the input power and $\vec{Q}$ is the efficiency factor. As a control for the mathematical correctness of this formalism one can get to a similar notation when eqns. 4.6, 4.5 and 4.7 are put into eqns. 4.11 and 4.12

$$\vec{F}_1 = \frac{I(x,y,y)\lambda_0 dA}{\hbar c} \left[R \frac{\hbar n_0}{\lambda_0} (\vec{k}_1 - \vec{r}_1) + T \frac{\hbar n_0}{\lambda_0} (\vec{k}_1 - n_{rel} \vec{t}_1) \right] \tag{4.14}$$

The transmitted ray $\vec{t}_1$ of the first interaction becomes the new k-vector for the second interaction $\vec{k}_2$. In further interactions the reflected ray $\vec{r}_{j-1}$ becomes the new k-vector $\vec{k}_j$.

$$\vec{F}_j = \frac{I(x,y,y)\lambda_0 dA}{\hbar c} \left[TR^{j-1} \frac{\hbar n_0}{\lambda_0} (\vec{k}_j - \vec{r}_j) + T^2 R^{j-2} \frac{\hbar n_0}{\lambda_0} (\vec{k}_j - \frac{1}{n_{rel}} \vec{t}_j) \right] \tag{4.15}$$

The vacuum wavelength λ_0 and Planck's constant can be eliminated. Using $P = I \cdot A$ 4.14 and4.15 become:

$$\vec{F}_1 = \frac{P}{c} \left[R n_0 (\vec{k}_1 - \vec{r}_1) + T n_0 (\vec{k}_1 - \frac{1}{n_{rel}} \vec{t}_1) \right] \tag{4.16}$$

$$\vec{F}_j = \frac{P}{c} \left[TR^{j-1} n_1 (\vec{k}_j - \vec{r}_j) + T^2 R^{j-2} n_1 (\vec{k}_j - \frac{1}{n_{rel}} \vec{t}_j) \right] \tag{4.17}$$

The efficiencies of the first interaction $\vec{q}_1$ and the following interactions $\vec{q}_j$ equal the expressions in the squared brackets.

$$\vec{q}_1 = R n_0 (\vec{k}_1 - \vec{r}_1) + T n_0 (\vec{k}_1 - \frac{1}{n_{rel}} \vec{t}_1) \tag{4.18}$$

$$\vec{q}_j = TR^{j-1} n_1 (\vec{k}_j - \vec{r}_j) + T^2 R^{j-2} n_1 (\vec{k}_j - \frac{1}{n_{rel}} \vec{t}_j) \tag{4.19}$$

The total efficiency of one ray is

$$\begin{aligned}\vec{q}_{Ray} = &\left[Rn_0(\vec{k}_1 - \vec{r}_1) + Tn_0(\vec{k}_1 - \frac{1}{n_{rel}}\vec{t}_1)\right] \\ &+ \sum_{m=2}^{j}\left[TR^{j-1}n_1(\vec{k}_j - \vec{r}_j) + T^2R^{j-2}n_1(\vec{k}_j - \frac{1}{n_{rel}}\vec{t}_j)\right]\end{aligned} \tag{4.20}$$

The total force generated by the ray then can be written as:

$$\vec{F}_{Ray} = \frac{1}{c}I(x,y,z)dA\vec{q}_{Ray} \tag{4.21}$$

The intensity and the area information are input variables for the calculation. Therefore, the major part of numerical effort lies in the determination of the ray efficiency $\vec{q}_{Ray}$.

The sum over all force vectors of the photon streams results in a vector which represents the effective force that the beam generates on a particle at one location within the beam.

$$\vec{F} = \sum_{i=1}^{l}\vec{F}_{ray,i} \tag{4.22}$$

For the display of the forces in axial and lateral direction the projection on the coordinate axes can be obtained by calculating the scalar product of the force vector and the unit vectors.

$$F_z = \vec{F}\vec{e_z} \tag{4.23}$$

$$F_x = \vec{F}\vec{e_x}; F_y = \vec{F}\vec{e_y} \tag{4.24}$$

We have compared the results of our calculations with data from [62] and could confirm the correctness of the algorithm. For the interpretation of the results, the limits of ray tracing calculations need to be kept in mind. For particles about the size of the wavelength or smaller, the ray optics approach cannot be applied. Furthermore, our ray optics representation does not capture the exact nature of the Gaussian beam e. g. the shape of the beam waist.
When simulating idealized light distributions (perfect focus), the ray optics predict forces which are independent of the particle's size. In our simulations, we mostly use real distributions from optics simulations with finite focal areas. In case of particles which are in the order of magnitude of the focus, the optical forces drop.

This effect is shown in fig. 4.7. For smaller particles, the geometry changes and an increasing fraction of the beam misses the sphere.

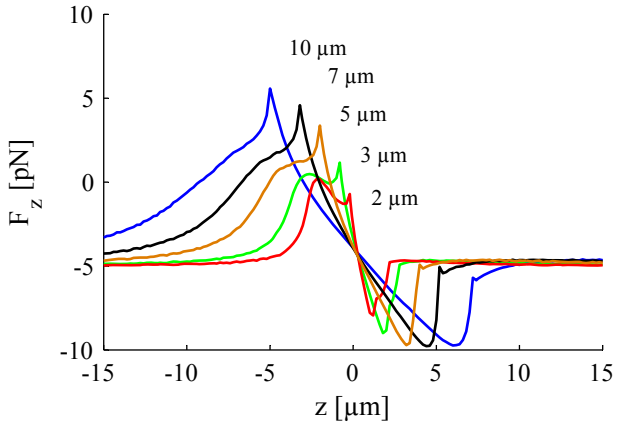

fig. 4.7: Varying axial forces for particles with diameters in the order of magnitude of the focus diameter

It has to be added that this result does not represent the size dependency for Rayleigh particles as shown in the literature [52, 68]. There, the effect results from the rapidly decreasing scattering cross-section of particles smaller than the wavelength.

4.3.2 Program structure

While writing the code of the simulation tool, future additions to the program have been kept in mind. Hence, the software is divided in modules with universal interfaces. The input variables include four matrices loaded into the workspace. These arrays contain the information of the starting points of the rays, their directions, the power assigned to the ray and the areas represented by the ray. The latter depend on the method of sampling the aperture of the optics or the beam. For most cases described here, the beam is sampled as a rectangular grid. Thus, the area for each ray is identical. The refractive indices of the media, the diameter and the location of the particle are defined in the tool.
After loading the input data, the user chooses an analysis in the user interface and sets the additional parameters needed. A scan along the z-axis requires the definition of the starting point, the end point and the increment.

Fig. 4.8 shows the calculation layers used for the determination of the force on a sphere. For each ray, in the input field, the force is calculated and stored separately. At the bottom layer, the ray is geometrically traced through the sphere. The result is the force efficiency of that particular ray which is represented by a vector. This vector is returned to the next higher level where it is multiplied with the power of the ray which results in a force vector for the ray. This routine is repeated for all rays in the input field. The vector sum over all rays is the total force acting on the sphere.
After the calculations, the force information can be displayed in different ways (see. 4.3.4).

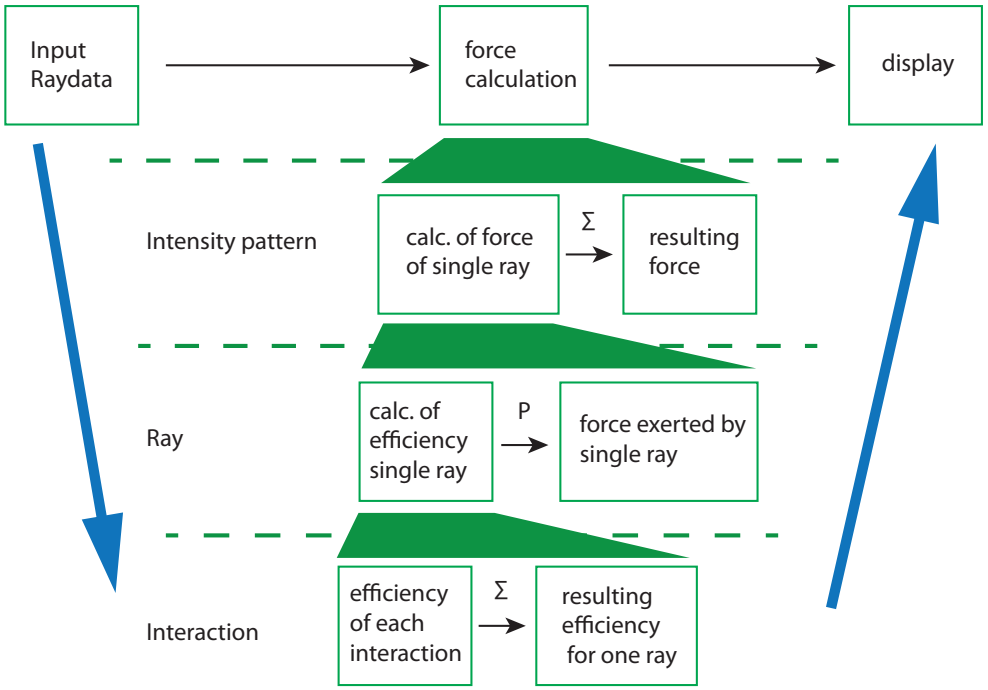

fig. 4.8: Sequence of the force calculation; For each ray, the single actions are determined. The resulting efficiency of the ray is multiplied with the power in the ray. The sum of all rays represents the resulting force

4.3.3 User Interface

For an improved usability, a graphic user interface (GUI) has been programmed. The GUI, as shown in fig. 4.9, allows the user to access all program features of the force calculation. Apart from the force calculation itself, the interface enables the user to import, save and manage the intensity patterns that are examined.

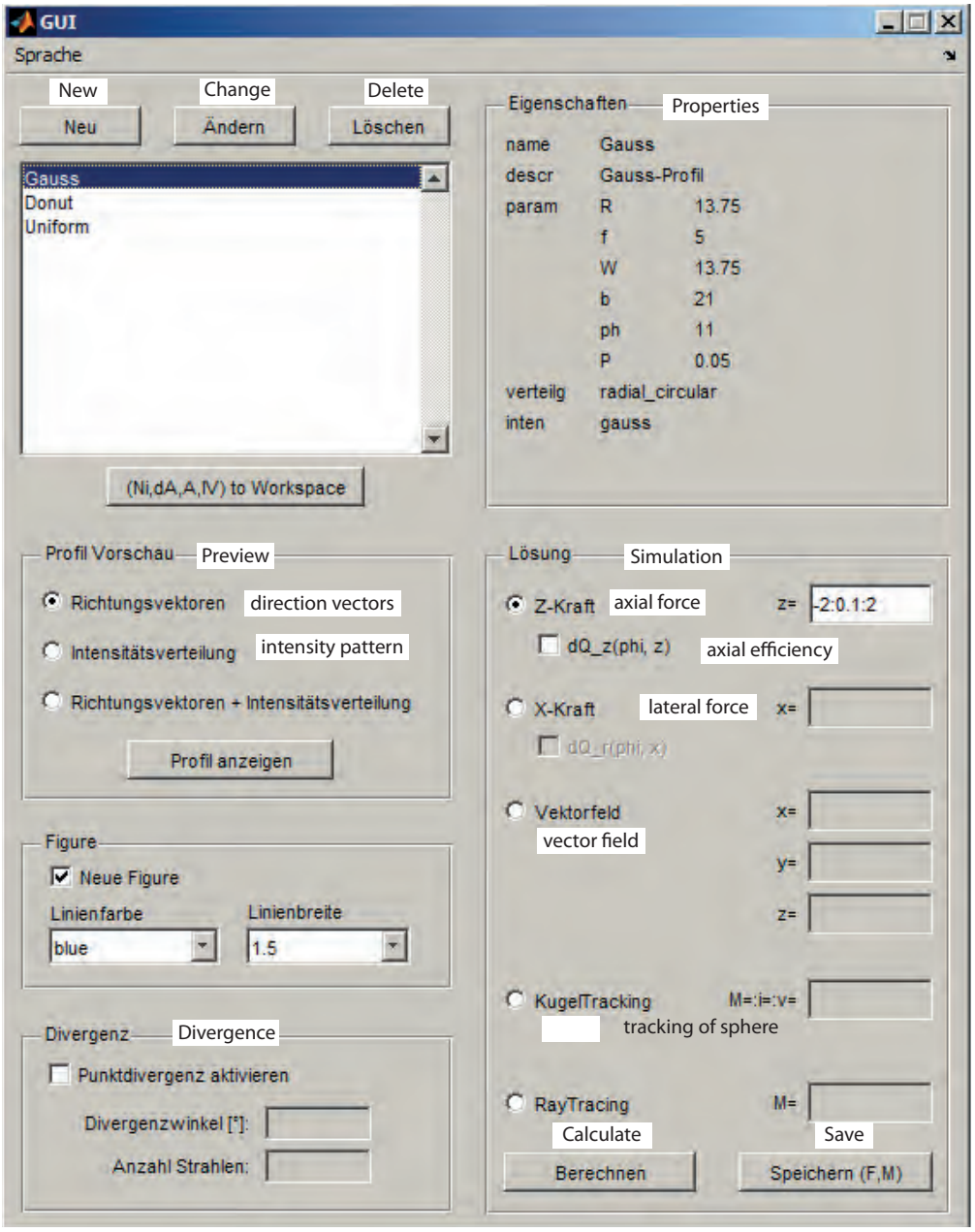

fig. 4.9: Graphic user interface of the force estimation tool

4.3.4 Program Features

The basic task of the software is file management (import, creation and storage of ray files). What is more important, is its visualization routines as the raw data from the ray trace is difficult to interpret. Therefore, the simulation tool offers several options to analyze and display the properties of the trap.

Import into MATLAB

The result from the ray trace in ASAP is a text file which can be converted in the necessary form with a simple routine in MATLAB. Every line in the text file represents one ray that hits the detector in ASAP. The import filter stores the information of positions, directions and power in separate matrices, which are the input for the force calculation.

Library

The input fields can be stored in a library file. This is a convenient feature when the performance of different trap geometries needs to be compared. Previously used intensity patterns can be recalled quickly for further analysis and/ or as reference curves for new designs. Also, the user can generate test patterns in the library. Before the simulation, the user can display a preview of the ray pattern. Optionally, in order to simulate aberrated optics and influences due to diffractions, the user can add divergence in the ray pattern. When this option is enabled, one ray is split up into a number of rays which diverge at a selected angle from the ideal direction. In practice, this option is rarely used.

Test patterns

The potential to use different test patterns has been programmed as one of the first options. The user can select a beam geometry and superimpose an intensity pattern onto that geometry. For instance, an ideally focused beam can be overlaid with a Gaussian, Laguerre-Gaussian or a uniform intensity distribution. The NA of the focusing and the overfilling are defined as well. The calculation results show very good agreement with Ashkin who uses geometric optical calculations for large particles in [62]. The Gaussian beam waist is not modeled in the simple test patterns. The optical forces in this calculation show the size-independent behavior mentioned earlier in this chapter. It is well known that this is not the case in reality [52]. However, within the known limits of force calculation with the geometric optics, the results could be used to verify that the algorithm is working as expected.

Displaying Data

The calculated forces are stored as vectors in 3D and can be displayed in different ways. The views implemented in the simulation tool assist the designer in the assessment of the trap's performance and shape.
The resulting forces are decomposed in Cartesian coordinates where the positive z-axis is the direction of the propagation of the laser. This coordinate representation has also been chosen because it usually coincides with the coordinate systems of the periphery.

Force of individual rays and efficiency The basic function of the algorithm is to track a ray in the particle until the power of the initial ray drops below a defined threshold. This basic process can be displayed and the generated forces at each interaction are depicted by arrows. An example is shown in fig. 4.10a). The total force exerted by the ray is displayed by a second arrow. Commonly, the trapping efficiency is used as a proportionality factor which links the trapping force to the power of the beam.

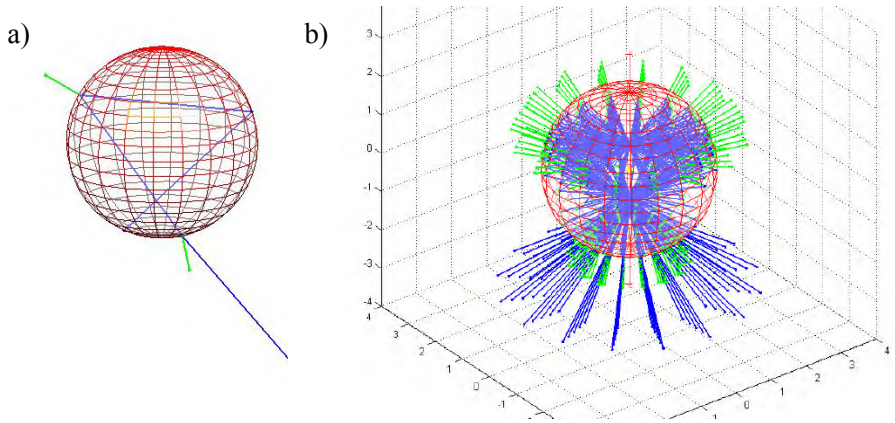

fig. 4.10: Individual rays traced through sphere; a) single ray b) arbitrary set of rays

In the software, the option to display the trapping efficiency of every single ray at one location is implemented. This information helps to get a more detailed understanding of the resulting force which is generated by a ray that hits the sphere under a certain angle. We call this the "ray efficiency" As an example, the ray efficiencies in an ideally focused beam have been plotted (fig. 4.11).

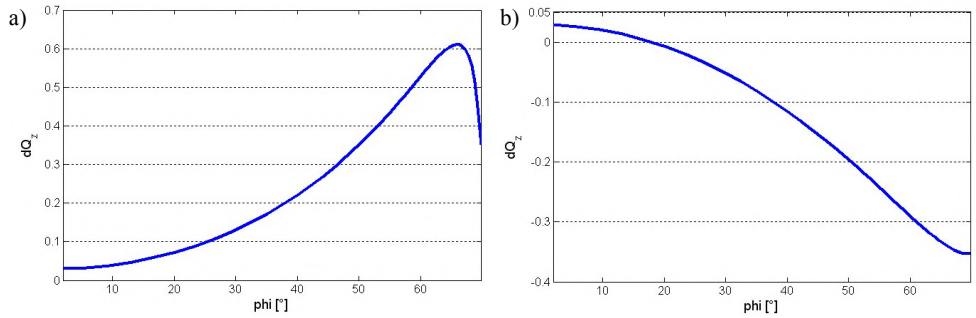

fig. 4.11: Display of local efficiency factors for a converging beam with a cone angle of 70 degree. a) at location of maximum pushing force b) at location of maximum retracting force

The main objective of the visualization of the single ray efficiency is the use in the design process. If the most efficient rays can be identified, then a tailored intensity pattern could be engineered which produces the optimum trap shape. However, the interpretation of the images of the ray efficiencies is difficult. As an example, the two graphs of fig. 4.11 show how the same set of rays produce a different axial efficiency in different positions. In a position in front of the trap location all rays have positive efficiency factors. In a position behind the trap, the rays from angles above 20 degree have negative efficiencies in z. As the force of one ray is a multiplication of the efficiency with the power of the ray, we can conclude that a ray that creates a pushing force in one location, creates a retracting force in another.
Nevertheless, the observations of other authors can be confirmed. When looking at fig. 4.11b) it becomes clear, why obscuring the center of the beam increases the trapping efficiency. The rays that "push" are blocked.
A further visualization which helps to get a feeling for the dependence of optical forces on the geometry of the beam is a 3D plot of single rays (fig. 4.10a)) and sets of rays (fig. 4.10b)).

Axial and lateral force curves The most common way to display optical forces are axial and lateral scans of the trapping force in the propagation direction or perpendicular to the laser beam. Examples for this visualization are shown in fig. 4.12. The user can display several force curves in one plot by un-checking the option for "new figure" in the GUI.

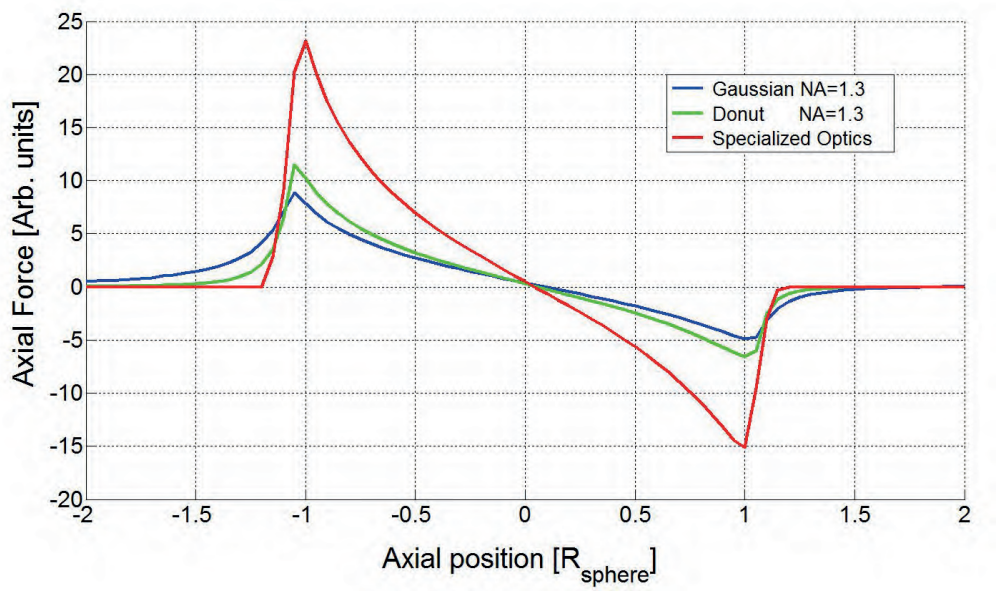

fig. 4.12: Axial force curves of an ideal Gaussian distribution and an ideal Laguerre-Gaussian distribution

Force field and Potential The stable equilibrium of the trap is not necessarily located on the optical axis and the perpendicular plane at the beam waist. In multiple or dynamic optical traps this is an intended feature. If aberrations due to fabrication error and misalignments are present, the shift of the trap location can be a parasitic effect. To find the actual minimum, one has to scan along the coordinates of the trap location. A better impression of the actual shape of an optical trap can be gained with plots of a cross section of the trapping area. In the MATLAB environment, two visualizations have been realized. The option force field calculates the optical forces for a 2D or 3D array of positions. The resulting force vectors are plotted into the observed plane or volume. A stable trapping region can now be identified quite easily by finding an area where all force vectors point towards the same point (see fig. 4.13b).
Plots of cross-sections of the optical potential represent a rarely used visualization of optical traps (e. g. [33]). In this simulation, the optical potential is calculated as the sum of all potential energies from a starting point to the end point.

$$E_{optical} = \sum F_{i,x} \cdot dx + \sum F_{i,y} \cdot dy + \sum F_{i,z} \cdot dz \tag{4.25}$$

As shown in fig. 4.13, the non-conservative nature of the optical trap results in a deformed potential landscape. The reference potential in this example has been set in front of the trap.

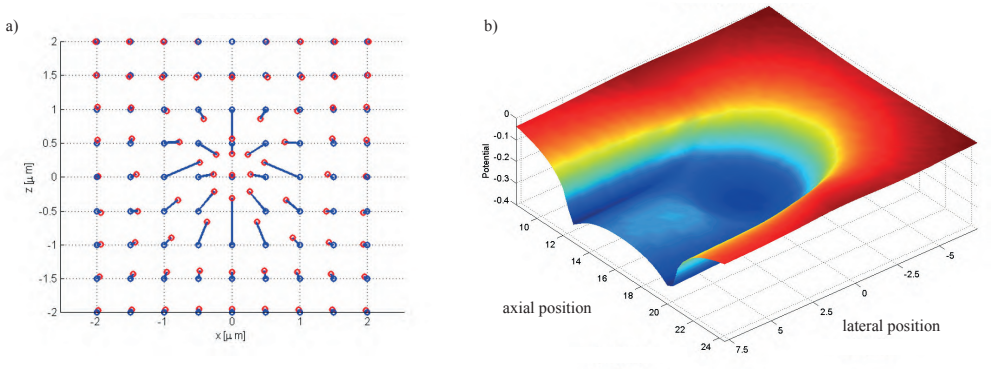

fig. 4.13: 2D Visualizations of the trap; a) vector field b) Potential landscape

Since optical trapping is realized by a combination of the conservative gradient force and the non-conservative scattering force (2.1.1), the strictly mathematical definition for a potential is violated. Thus, the potential well of an optical trap is deformed and the potential behind the focus of the trapping beam is assigned a lower value. This is also reflected in the axial force curves of an optical trap. The integral of the force curve in front of the equilibrium point is larger than the integral behind it.

4.4 Summary

In order to design optical trapping systems, the classical lens design process has to be supplemented by a force simulation. The imaging or focusing properties of the system are no direct measure for the trapping forces. The influences of misalignments and fabrication errors only become obvious when the trapped particle itself is taken into the consideration.
We have proposed a process in which we exploit the strengths of established software and combine it with a force simulation module. Using this combination, it is possible to represent the actual shape of the beam, the optical properties of all individual components and the deviations from the ideal optical system. We verified the software calculating basic beam shapes and comparing the results to values from the literature. The visualizations of the force simulation support the designer selecting of the best trap shape.

5 Verification of the design concept

To explore the capabilities of our design concept and to prove the functionality of the prototyping process presented in the previous chapter, two example systems have been examined. At first, an entire microscope objective was simulated and the influence of AR-Coatings and misalignments in the experiment was determined. We evaluated what would be necessary to optimize the objective for optical trapping. The information gathered from these simulations delivered reference data as a benchmark for further designs. The second test was a run through the entire design and prototyping cycle. As a result, we could we present a specialized and highly integrated trapping system with large working distance [202]. This system has been fabricated and successfully tested.

5.1 Analysis and optimization of a high NA Objective

High NA microscope objectives are the key component of most optical trapping setups. They fulfill the task of focusing the trapping laser very well. However, the limitations of high NA objectives in optical trapping has been discussed in a series of publications (e. g. [79, 203]. The design assumes a very specific experimental setup: the optics is optimized for superior optical resolution over an extended field of view. Objectives are also corrected for a large color spectrum. The best performance is achieved when the sample is located on the surface of a cover slip. In optical tweezing, however, the particle - i. e. the image plane - usually is not located directly on the surface of the cover glass. This results in spherical aberrations and a degradation of the trapping forces (e. g. [81]). Further influences on the trap performance are introduced by truncating the Gaussian beam, dispersion and misalignments in the experimental setup.
The scientific community is well aware of the above issues and has come up with measures to correct the mentioned errors. Common tools to improve the trap are external spatial light modulators [84]. The incident wavefront is recorded and a corrective phase pattern is written on the modulator. Another way of correcting aberration has been presented by Ota et al. who use a deformable mirror as an adaptive optical element [139].

5.1.1 Modeling a microscope objective

As mentioned in 2.2.2, the common models for the focusing optics in optical tweezers are based on analytic assumptions such as the tangens condition or the sine condition respectively. Here, we simulate the performance of an actual system.
Since optics manufacturers do not provide the design data from their current product lines, we chose an objective design which was already available as a ZEMAX model. This setup is similar to a design printed in Laikin's book "Lens Design" [204]. Laikin himself provides references to works by J. Benford which were published in the mid 60s.

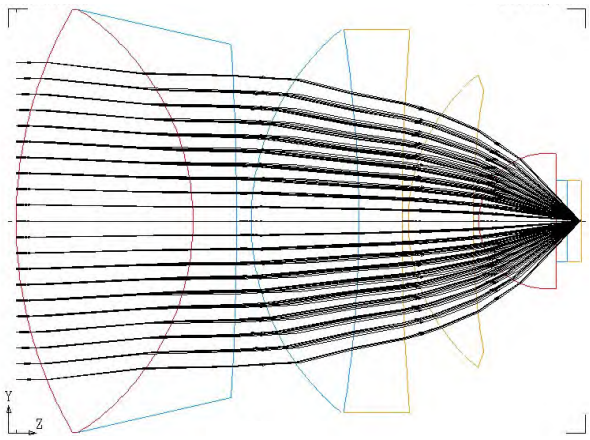

fig. 5.1: ASAP model of an oil immersion microscope objective (98x, NA=1.28) [204]

We transferred this model to ASAP for the physical ray tracing. As source, a Gaussian beam with a beam waist of 2 mm has been used. The beam waist was positioned at the tube length before the objective and the divergence was set to overfill the entrance pupil 1.5 times.
The force simulations have been carried out with spherical particles (10 µm diameter, polystyrene n=1.59 - 1.57). Throughout the simulations presented in this section, the system environment remained unchanged. Since single beam axial trapping is the main challenge, only the axial forces are compared in this study. The absolute values of the forces strongly depend on the chosen parameters. Therefore, only the relative changes between the simulations are considered to indicate the effect of the variations of the system.
The refractive index of water at the working wavelength of 1064 nm is only slightly lower (1.328) in the visible spectrum (1.331 - 1.344) [205].

5.1.2 Performance of microscope objectives in the infrared

In 1990 Parker and Raine [206] first investigated the performance of microscope objectives in the near infrared. They identify the aberrations that may occur and discuss options to reduce spherical aberrations. Also, they state that coma and astigmatism only have minor effects if the object remains on axis.
However, material dispersion is a nonlinear effect. Hence, the influence of dispersion on the focusing quality can also be assumed to be nonlinear.
In 1999, Neuman [197] assessed a number of microscope objectives and characterized them by measuring the overall transmission of each objective. The transmission values of typical high-NA objectives were measured between 40% und 60%. The authors describe the complex structure of modern microscope objectives. Several years earlier, Svoboda et al. address the influence of antireflection (AR) coatings [207]. They state that the low throughput is a consequence of the AR coatings not being designed for the trapping wavelength.
Most publications do not include detailed reasoning regarding the selection of the objectives that are used in the experiments. Only few authors recommend the use of IR-corrected optics [79, 33].
As one of few groups Viana et al. [78] measured the radial variation of the transmittance of a trapping objective. They use the so-called dual-objective method and conclude that the transmission of the objectives is not uniform. According to their measurements, the relative error is about 6% when a uniform transmission is assumed. For the analysis of the example objective a series of equidistant radial sample rays have been traced through the objective. Fresnel losses and the influence of various thin film coatings have been taken into account. The data shown in fig. 5.2 was collected using the objective presented in the previous section and a uniform light source.

After the ray trace in ASAP, each ray is assigned the remaining power and plotted as a function of the relative height in the entrance pupil. As a reference, the transmittance of an uncoated objective was simulated at 550 nm and 1064 nm wavelengths. 550 nm is assumed to be the design wavelength since this choice is common in optics design. Consequently, AR coatings are designed for this wavelength. The solid lines show the improvement of the transmittance for three coatings. The simplest coating is a single layer of MgO_2 with a thickness of $\frac{\lambda}{2}$. Furthermore, a two and a three layer coating were tested. At the design wavelength the overall transmittances of over 90% are reached with all three coatings.

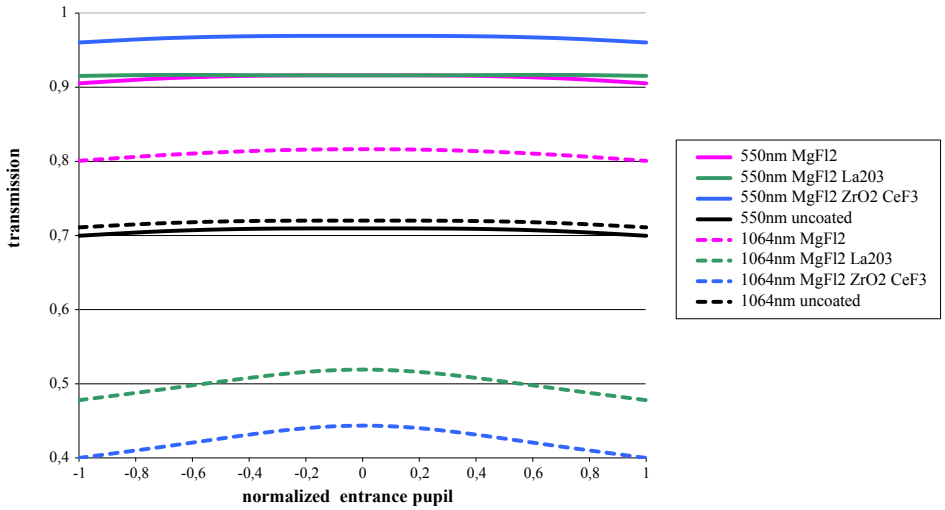

fig. 5.2: Radially varying transmission of a microscope objective for different AR-coatings

The transmittance drops for all coatings, when the wavelength is changed to the "wrong" wavelength of 1064 nm. The more specialized multilayer coatings reduce the overall transmittance to 50% and below. As mentioned above, these values match the values that are found in the literature [79].
The radial variation of the transmission is obvious in the curves of fig. 5.2. The origin of this effect can be found in the angular dependence of the reflection coefficient. The thickness of the coatings has been calculated for perpendicular incidence. The rays that are close to the edge of the entrance pupil see a mean angle of incidence instead of the ideal incidence. The angular dependence is most pronounced for the multilayer coatings that are illuminated with the wrong wavelength. For optical tweezing this means that the rays that potentially generate the highest retracting force are damped above average.
If an AR-reflection is designed in such way that the transmittance is highest, for the trapping wavelength at the mean angle of incidence of the outer rays, the trapping force can be increased without changing the geometry of the objective at all.

5.1.3 Sensitivity to shifts and tilts

When an optical system is set up, the precision of the alignment is limited by the means for positioning and detection of the deviations from the ideal alignment. Within the limits of the alignment accuracy, which can be realized with positioning stages in the laboratory, no significant variations of the trapping forces were found. When larger tilts up to 0.5 degrees were applied, the axial and lateral forces dropped about 14% and 9% respectively (fig. 5.3)

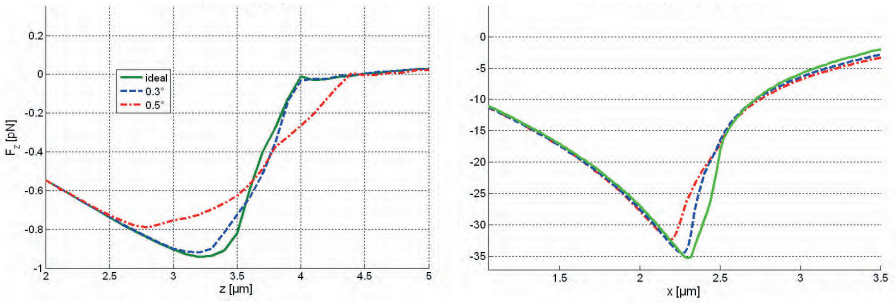

fig. 5.3: Influence of increasing tilts of the objective w.r.t. the trapping beam. a) axial forces b) lateral forces

In these simulations the entrance pupil has been overfilled by a factor of two. The incident Gaussian beam therefore is already flattened and the trapping forces for a shift of the beam w.r.t. the objective of up to 500 µm did not affect the trapping performance The misalignments that we introduced in this example are orders of magnitude higher than the resolution of alignment features in typical optical setups. It can be concluded that the alignment of a microscope objective for optical traps is uncritical.

5.1.4 Optimization of the example objective

The system performance of the initial system (lens data adapted from [204]) is low compared to the diffraction limited resolution of modern objectives. It can be argued that starting from a system with inferior performance naturally leads to easy improvements in the trapping forces. However, spherical aberrations and aberration correction has remained a common topic in optical trapping even in the last years. Therefore, the example provided in this section still allows statements about the potential improvements.
To show, that such improvements can be achieved without having to design an entirely new optical system, only minor changes are investigated.
As a first step of analysis, the performance of the objective in different situations was tested. The overview of all following simulations in this section can be found in fig. 5.4.

1. Simulation at the design wavelength on the surface of the cover glass. The spot radius in the image plane at the design wavelength of 550 nm is 2.23 µm which is 9 times larger than the diffraction limit.

2. Simulation at design wavelength 10 µm into the channel

For the actual optimization the wavelength was changed to 1064 nm. A standard merit function was chosen which minimizes the RMS radius of the spot images. The optimization needs one or more variable parameters. The selection of the starting point and the right parameters decide on the quality of the optimization and, generally, requires experience. Here, three different approaches have been tested.

1. The variation of one spacing between two lenses
2. Aberration correction by making the first surface of the first lens aspheric
3. The variation of the radius of the first lens surface and all spacings of the objective.

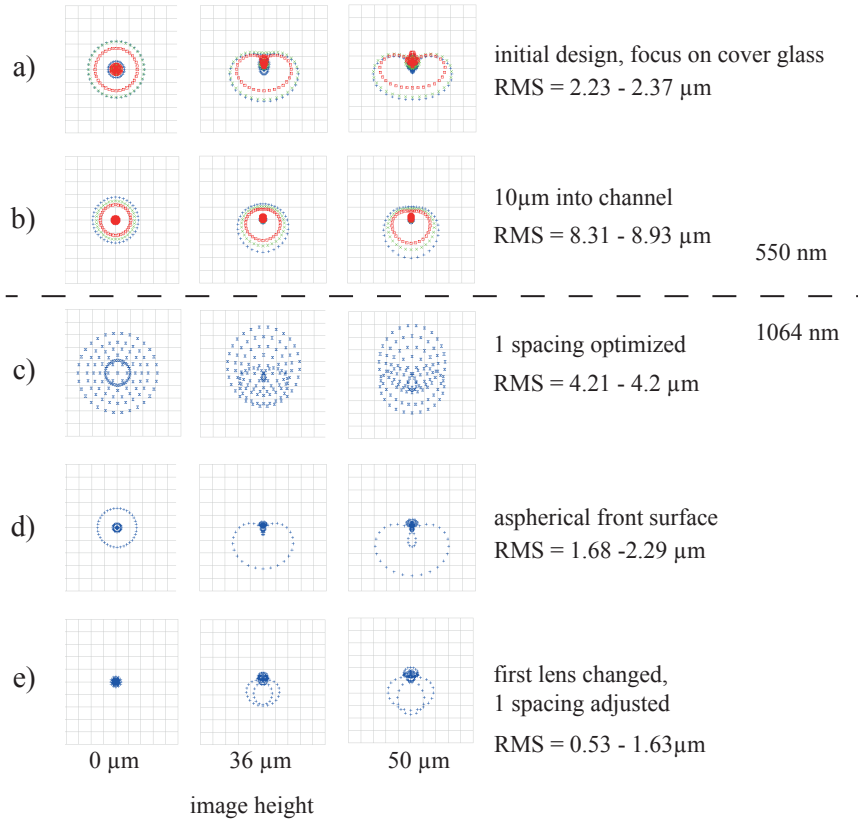

fig. 5.4: Optimization of the microscope objective for trapping in the infrared; the spot diagrams illustrate the shape of the focus on and off axis; Note: the scales of the spot diagrams vary

As can be seen in fig. 5.4 the best result has been achieved with the last of these three options. With the design changes in subfigures d) and e) significant

improvements of the initial performance could be achieved. In the last option the new radius of the first lens surface becomes 4.90 mm instead of 5.35 mm. The overall length of the optics changes from 6.81 mm to 7.03 mm.

The simulation of the axial forces of the initial objective and the two best optimizations is shown in fig. 5.5. In both cases the improvement of the maximum retracting force could be doubled.

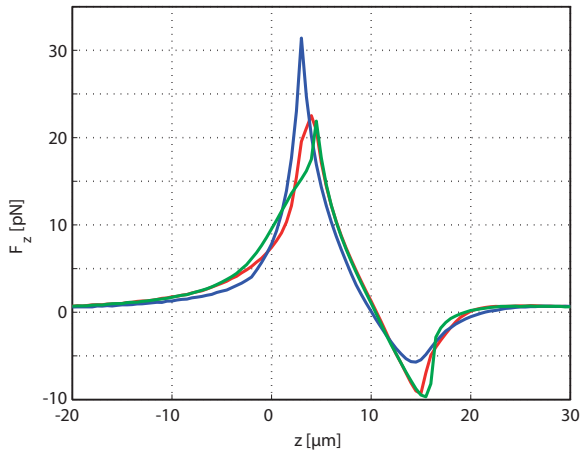

fig. 5.5: Comparison of axial trapping forces of initial objective (blue) and aspheric front surface (red) and an optimized lens 3 (green)

A last simulation with a custom merit function did not lead to a significant change in the force simulation. In this custom function the weighting of the outer areas of the pupil has been increased in order to focus the outer rays more tightly. Since the spot radius before the last step was only a fraction of the particle diameter, the force curves did not show significant improvements for even smaller spot sizes.

An effective method to increase trapping forces is increasing the transmittance of the optics. According to the results shown in 5.1.2 the difference between an uncoated optics and an AR-coated optics can be 20% and more. To investigate the effect on the trap performance, a single layer coating has been applied to the objective and the axial forces were compared to the forces generated with the uncoated lens. The result was the fact that the axial forces scale linearly with the increase of the transmittance. By applying a single layer AR-coating (MgO_2) the predicted increase of the transmittance and maximum retracting force of 25% could be confirmed (see fig. 5.6).

For on-axis trapping spherical aberrations are the most critical. When the trap location is off-axis, higher order aberrations such as coma and astigmatism have to be considered as well. Typically off-axis traps are found in dynamic traps and multiple traps that use spatial light modulators, scanning elements

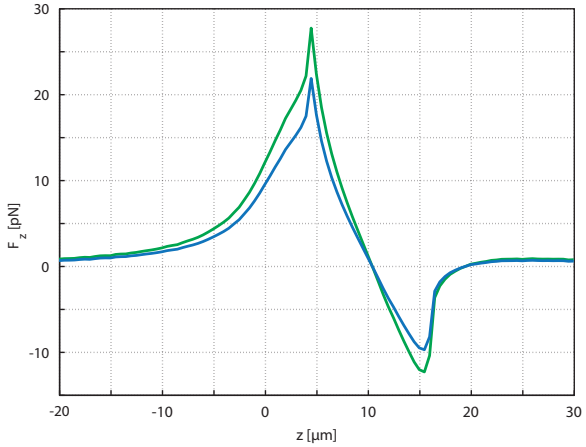

fig. 5.6: Influence of AR Coatings on axial trapping forces; blue line: uncoated, green line: coated with a lambda-half coating of MgO_2

or beam splitters. Uniformity is an issue in these setups [165].
In addition to the on-axis case, two off-axis points have been included in the target function and another optimization step has been run. Fig. 5.7 shows a comparison of the performance of the initial system and objective with the best correction at 36 µm (50% increase in retracting force) and 50 µm (50% increase in retracting force).

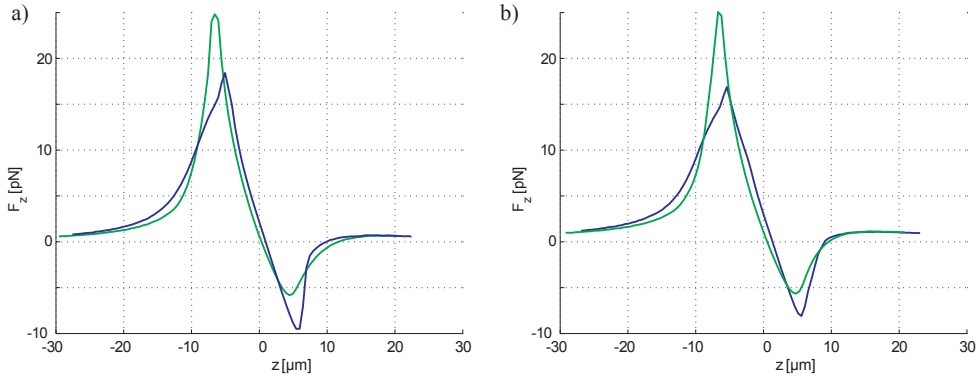

fig. 5.7: Off-axis performance of corrected and uncorrected microscope objective a) 36 µm off axis b) 50 µm off axis

The above results and considerations illustrate the potential of "internal" optimization of the trapping optics. The "external" correction to diffraction limited spots by SLMs has also been demonstrated [85, 86]. If no dynamic trapping is required, our optimizations can be realized with no additional components in the system or increase of laser power.

5.2 Integrated trapping optics for long working distances

As described before, the working distance for conventional high-NA microscope objectives is limited to about 200 µm. Therefore, this is also the limit for optical tweezers. With the system presented in this section this limit is overcome. By designing an optical system specifically for tweezing, one can freely select the needed specifications and omit the features that are not required.
The main goals for the first prototype were derived from the research topics described in the introduction. The complete set of specifications for the optics is listed below.

- 3D optical trapping through a glass substrate with a thickness larger than 0.5 mm
- Realization of a single beam gradient trap, since access to the sample is possible from one side only
- High system efficiency
- Optimum axial force
- Compact integrated system; total system size similar to a microscope objective
- Laser: wavelength of 1070 nm, diameter of 5 mm

Secondary requirements are:

- Manufacturability by ultraprecision machining
- Imaging is not required
- The system efficiency has higher priority than the trapping efficiency Q.

5.2.1 System design

According to the above items, the goal has to be the maximization of trapping force per unit of laser power. To this end, the best compromise between power efficiency and trapping efficiency has to be found.
The selection of the starting system is crucial in optics design. The general structure of the optics is defined at this stage [2].

In practice, the decision for a certain starting configuration is strongly knowledge based and depends on the professional experience of the designer. Apart from the experience of the designer, analytic aberration theory as presented in [208] forms an excellent basis for designing optical systems.
From the theoretical/ analytical considerations it is known that the retracting axial forces are generated by rays that have a large angle w. r. t. the optical axis, i. e. from the outer areas of the illumination cone. The diagram of the axial trapping efficiency q_z of individual rays over the angle of incidence shows, that the sign changes at an angle of approx. 20° 4.11. Thus, the target of maximizing the axial forces can be translated to a trapping beam with a hollow core and a large total NA.
The sum of the requirements and the above physical implications can be visualized in an image, where the system input and the system output are known. At this stage, the system itself is represented by a black box (fig. 5.8).

fig. 5.8: System representation at start of system design

Since an NA of 1.3 is commonly used in optical trapping, we chose to design the optics for this value as well. The working distance was selected to be mbox650 µm ± 50 µm at a glass thickness of 530 µm. The resulting single beam gradient trap significantly extends the working distance possible up to now. Hence, it enables the use of optical manipulation in fluidic chips with thick channel walls at an extended working range.
In the specification the fabrication is addressed as well. It had to be established, if the prototype can be fabricated using the facilities of the IMN MacroNano. The ideal tool for the machining of free-form optical surfaces is an ultraprecision micromilling machine which is available at the institute. Therefore, the geometries of the available milling tools were taken into account. The choice of surfaces is limited by tool parameters such as the minimum tool diameter (here 500 µm).

The optical function can be divided into two separate tasks: beam shaping and focusing.

Beam shaping As described in section 3.1.2, there are a number of methods for shaping the trapping beam into a ring with a dark center.
For our system we choose a conic lens (axicon). This is the most efficient and simple option for the task. Axicons are best known for creating non-diffracting Bessel beams as an interference pattern behind the conic lens. This region has been used for 2D trapping. To avoid confusion, it should be pointed out that we do not use the interference but the ring that forms after this region (compare fig. 5.12).

Focusing For the focusing unit the known available options are standard refractive microscope optics or designs that are used in darkfield microscopy and X-ray telescopes. The combination of axicons and microscope objective has been proposed in [209]. However - as mentioned before - the available working distance of the standard microscope objectives is limited to less than 200 µm, which excludes them for our application.
Focusing light at very large angles of incidence is known from the illumination in dark field microscopes [210]. In 1952, H. Wolter published designs for X-Ray telescopes and used the term "grazing incidence mirror optics" [211, 211].
To take account of the requirement of high system efficiency, the number of optical surfaces was reduced as far as possible thus reducing the Fresnel reflection losses in the system. As the highest degree of integration and simplification we opted for a monolithic realization of the optics. The number of interfaces from the laser beam to the first surface of the glass substrate is reduced to two. This decision implies that only one axicon can be used for generating the ring. The second surface has to fulfill the function of the second axicon and the focusing.

Material selection and definition of the geometry After the structure of the system was determined (fig. 5.9), a ZEMAX model was set up to optimize the optics.

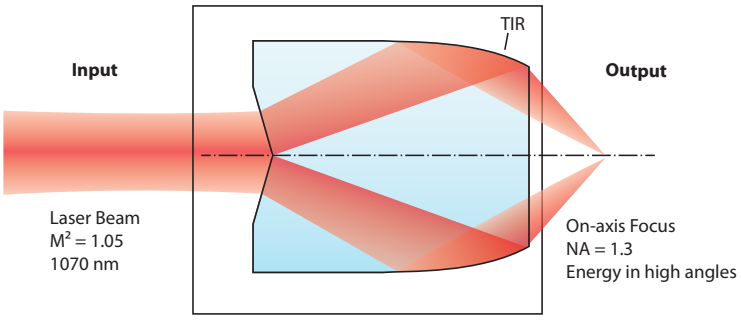

fig. 5.9: Basic structure of the trapping system

The ZEMAX model includes the 530 µm glass substrate and the refractive indices for all materials at the working wavelength of 1070 nm. For reasons of aberration reduction water was selected as an immersion fluid. This configuration is invariant to the relative position of the optics and the fluidic system, because there are aqueous media in front of and behind the glass substrate. The thickness of the immersion layer was set to 50 µm in the optimization. The trap location was positioned 50 µm after the glass substrate.

Figure 5.10 shows a series of cross-sections of different design stages. For

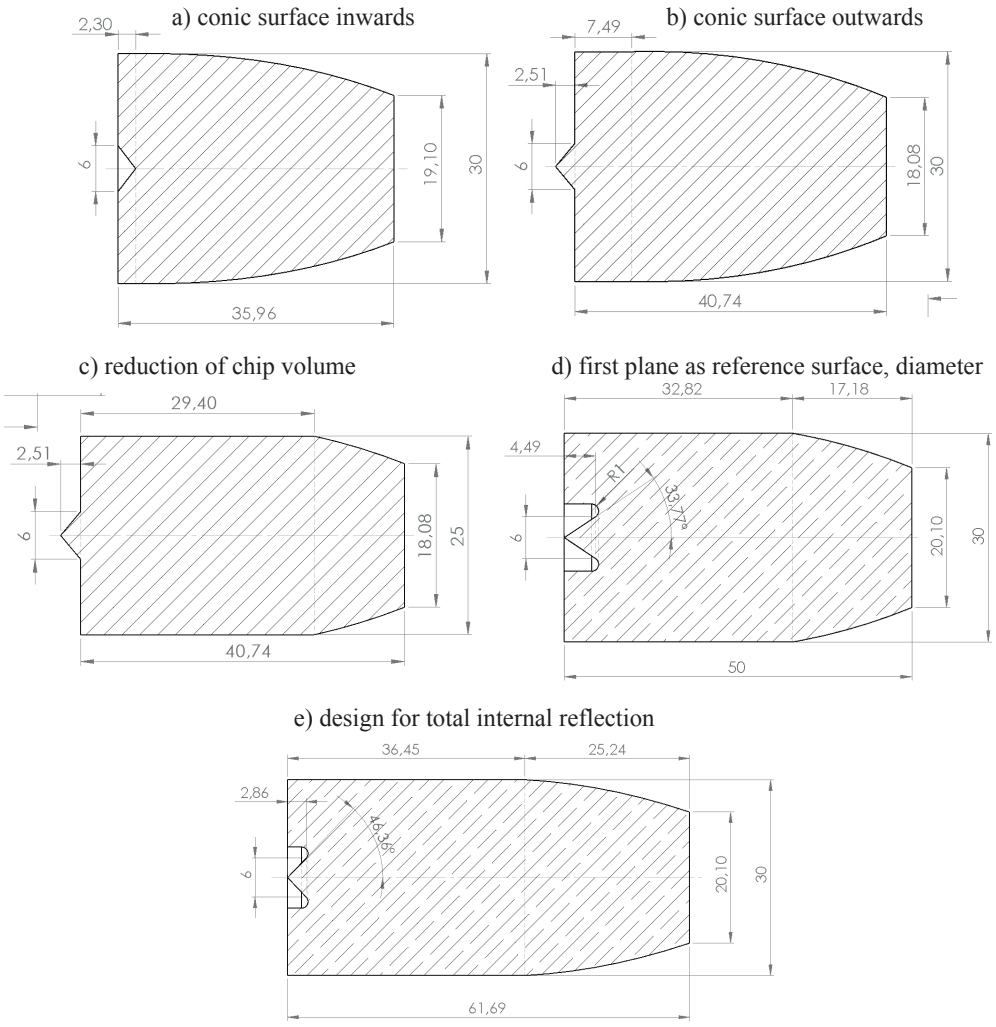

fig. 5.10: Preliminary designs for the trapping optics

the conic lens, there are two possible basic configurations. The design with the axicon pointing inwards (fig. 5.10a) represents the better solution from a lens design point of view. This system would be less sensitive to fabrication errors. In our case, a concession to the fabrication has to be made: It is not

possible to mill the sharp edge at the top of the concave conic surface. Thus, we preferred the configuration with the tip of the cone pointing outwards (fig. 5.10b)). When the optics is replicated from a mold instead of directly milled, the opposite reasoning applies. In order to reduce the fabrication time, the location of the focusing surface is shifted to the end of the cylinder (fig. 5.10c)). To protect the conic surface from damage and to supply a reference surface for the alignment during fabrication, the first surface is shifted inside of the cylinder (fig. 5.10d)). Another structural decision was to keep the angles of incidence upon the focusing surface above the threshold for total internal reflection (TIR). The benefit from this choice is an improved reflectivity and the avoidance of the otherwise necessary mirror coating. This eliminates the coating step as an error source and reduces the total process effort. As a result, the length of the optics was increased in order to stay below the critical angle for TIR (fig. 5.10e)).
The remaining parameters for the optimization are the system dimensions, the cone angle of the axicon and the shape of the focusing surface. The dimensions of the entire optics result from the specifications and the available materials. These are limited to materials which can be machined by diamond micromachining. There are only few materials both machinable and optically transparent at the working wavelength. Glasses are brittle materials and not well suited for milling of optical surfaces. The milling tool tends to chip off the surface rather than producing a defined shape. Non-Iron metals have good machining properties but obviously are not transparent. For reflective freeform optics they are the materials of choice.
In the department of Technische Optik a commonly used polymer is optical grade Polymethylmethacrylate (PMMA, Cadillac Plastics Type G222).
It is sensible to check the suitability of the material at an early stage of the design process. Plastics are used in many optical applications [212, 213] but the optical properties of plastics differ from glass in several aspects. Polymers are known to show stress birefringence, index inhomogeneities and a large thermal expansion coefficient. The optical grade PMMA is cast (instead of extruded) and cooled down slowly to room temperature. This procedure minimizes thermal stress and therefore inherent inhomogeneities and birefringence.
The thermal expansion coefficient α of PMMA is about one order of magnitude higher than the one of glass. In our example, the material data sheet states an α of $7 \cdot 10^{-5}$/K at room temperature. The length of the final design is 60 mm which means that a temperature change of 1 K results in a length variation of 4.2 µm. The temperature during the milling was kept constant at 24.3 °C. Typically, the temperature in the lab, is between 20 and 22 °C. The thermal expansion can be assumed to be isotropic. In the case of the monolithic trapping system it is legitimate to speak of a thermally compensated optical system.- When the temperature changes, the material shrinks at an equal percentage in

all dimensions. Thus, the optical performance is not affected. The expected effect would be a decrease of the working distance by the same percentage and can be neglected for a temperature difference of 2 to 4 °C.
PMMA is highly transparent in the NIR. Nevertheless, the issues of material homogeneity and birefringence mentioned above have to be kept in mind during design, experiment and the discussion of the results. To avoid stress-induced birefringence, the trapping module was glued into a brass ring which was screwed in a 5-axis positioning unit (Newport LP-1A)
The large working distance sets a lower limit for the system diameter. A suitable diameter of the PMMA blank was found to be 30 mm. This is a standard diameter of PMMA rods and offers compatibility with the standard mounting units.

Optimization and simulation The parameter variations discussed above have been simulated in the design loop (ZEMAX - ASAP - MATLAB). In the optimization of the final version of the trapping system, the focus could be reduced to a diffraction limited spot. The best results were reached when the surface line of the focusing surface was described by an even polynomial of the 16th order. This task would be very difficult if traditional fabrication was applied. However, it becomes easy to accomplish with ultraprecision micromilling since the polynomial can be programmed in the machine control. The accuracy of the reproduction of the shape is limited by the machine's positioning accuracy.
Alter the optimization in ZEMAX, the models of the trapping optics were transferred into an ASAP model. For the description of the optical system the same parameters as in the ZEMAX model were used. Therefore, no information is lost in this step. The light source was modeled as a Gaussian Beam with a beam waist of 2.5 mm (which equals a divergence of 0.14 mrad). Since we simulate the systems in the wave optics mode we are able to analyze interference effects in the ray optics model. A cross-section of the focus of the trapping optics is shown in fig. 5.11.

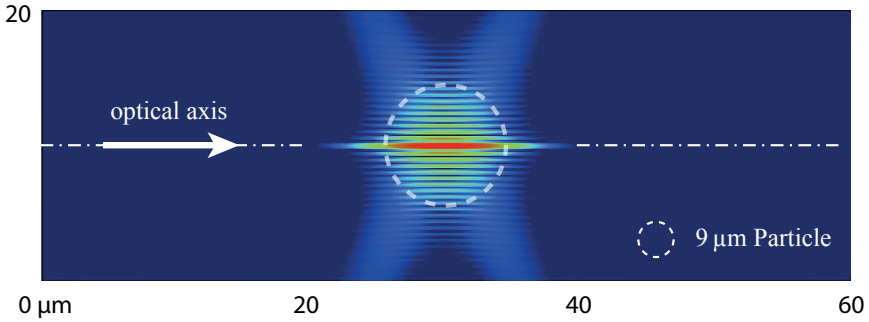

fig. 5.11: Detail of the focal area in ASAP

The simulation predicts a Bessel-beam-like interference pattern in the focus. To check if this result is plausible, the distribution has been examined for contradictions with fundamental physical principles. The distance between the interference rings is slightly above 500 nm. This is about half of the wavelength of the working beam, which can be expected from an interference pattern of two counterpropagating waves. The ring illumination is focused with an NA of 0.05. Theoretically, this results in a spot diameter of 20 µm. This value is approximately the axial extension of the simulated focus in ASAP. A measurement is necessary to confirm the calculation experimentally. This proof could not be collected as no detector with a sufficient lateral resolution is available (Nyquist-Shannon sampling theorem). Overall, the focal area can be described as a compressed Bessel beam.

The last surface of the system is a plane which is perpendicular to the optical axis. This shape has been selected for two main reasons. Firstly, during fabrication, the surface can be used as a reference plane. Secondly, this last surface of the optics serves as an alignment reference for the fluidic chip in the experiment. In combination with spacers, a highly parallel alignment is achieved.
The final design is shown in fig. 5.12

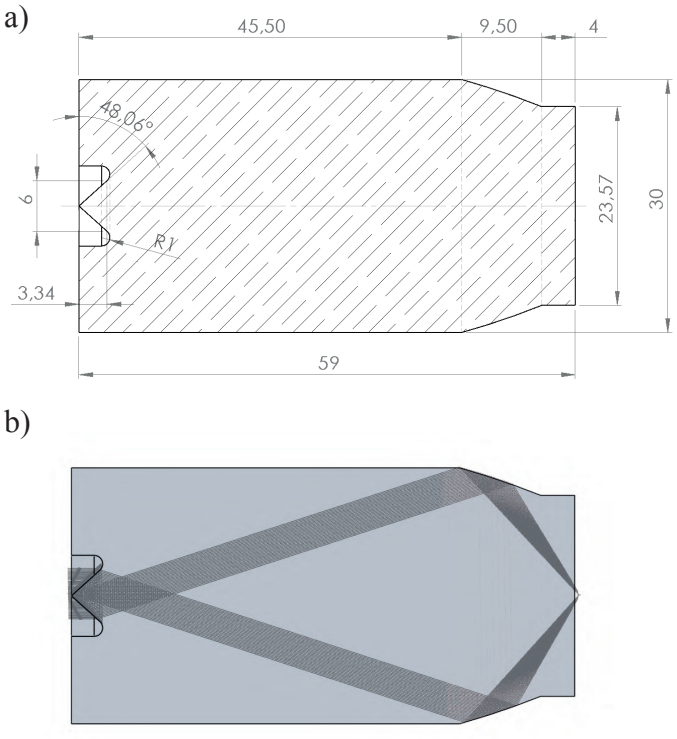

fig. 5.12: Final design of the trapping module; a) CAD drawing b) beam path in the system (fluidic chip is not shown)

The cone angle of this configuration is 48°, the length of the optics is 59 mm.

5.2.2 Feasibility study and tolerancing

So far, ideal cases have been assumed. The performance of the optics in the actual experiment needs to be predicted as well. In section 4.1 the performance of a standard trapping system is described which sets a reference for the new design. The presented system is an experimental optical setup. Therefore, it also needs to be evaluated if the tolerances for the optics are within feasible limits and trapping is still achieved, in the presence of fabrication errors. The power efficiency of the standard system was estimated at 34% (chapter 4 table 4.4). In the integrated design there are only two surfaces which results in a system transmission of 92%. The focus of the standard setup is a focused Gaussian beam - usually with a diffraction limited spot. As shown in the previous section, the focus of our design is a compressed Bessel beam. The extended focal area leads to a lower mean gradient and consequently to decreased forces. However, the center of the illumination cone is dark which reduces the axial scattering force. To receive an overall comparison of the performance of both setups, the new design has been compared with a Gaussian test pattern in the force calculation tool (fig. 5.13). The simulation promises a three times higher axial trapping force for the large working distance module. This theoretical value will not be reached in practice due to misalignments, fabrication errors and scattering at the surfaces of the optics.

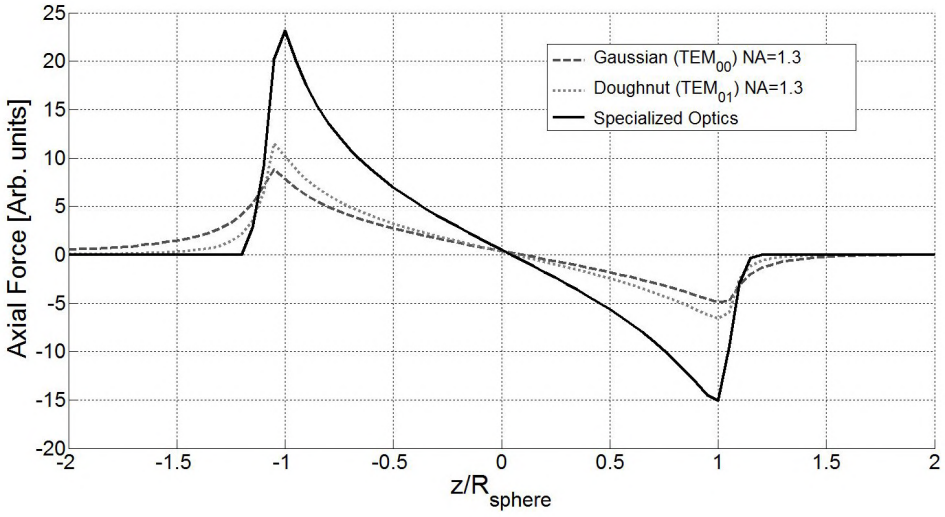

fig. 5.13: Potential forces in new design

The fabrication was identified as the critical issue for the feasibility. Here, the work piece has to be manually turned upside down in order to be able to machine

both optical surfaces. This introduces lateral shifts and tilts of the axicon and the focusing surface with respect to each other. Since the surfaces themselves are machined with the precision of the machine's positioning accuracy (0.5 µm according to Kugler), the manual turning is identified as the critical step.

For the tolerancing, the advantage of the parametric model in ASAP is evident. The variation to the system can be easily applied by directly changing the relevant parameters in the ASAP Code.
The following figures (fig. 5.14 and fig. 5.15) depict the effects of lateral shifts and tilts of axicon w. r. t. focusing surface.

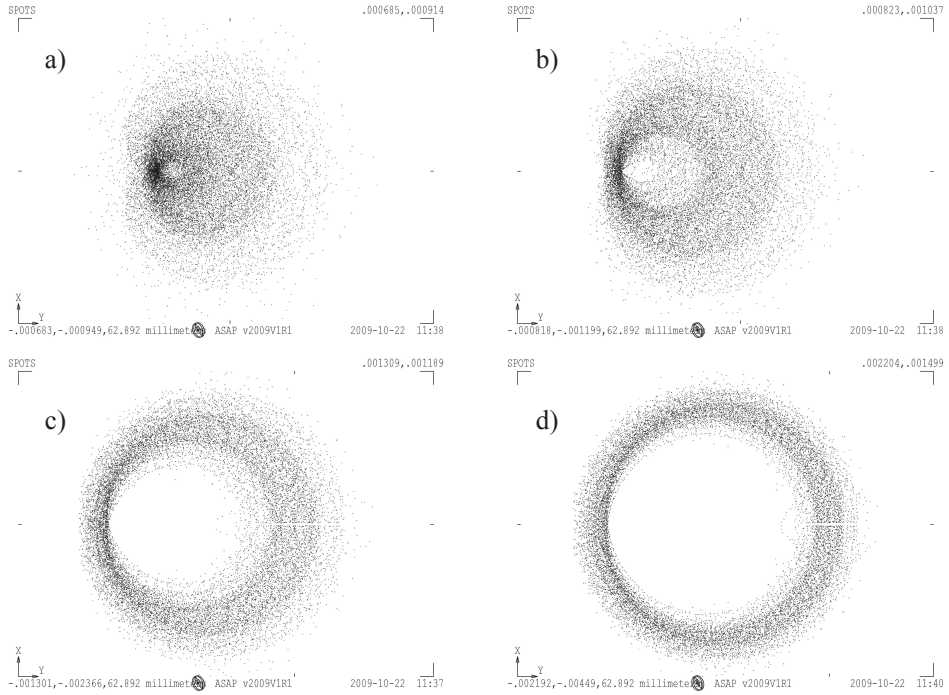

fig. 5.14: Influence of offsets of the axicon surface and the focusing ring on the quality of the focus; a) 1 µm b) 2 µm c) 5 µm d) 10 µm

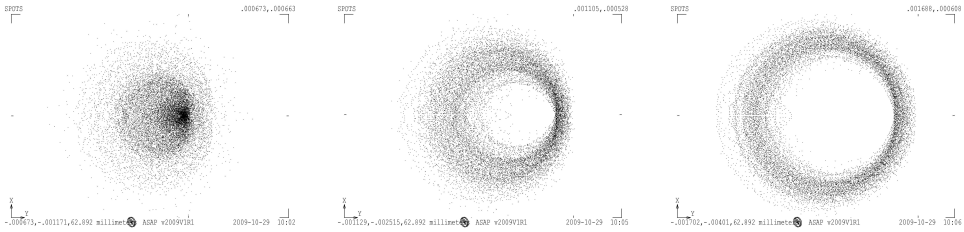

fig. 5.15: Influence of tilts of the axicon w. r. t. the focusing surface on the quality of the focus and the trapping force; a) 1' b) 5' c) 10'

The requirements for alignment of the optics in the experiment are realistic. The critical measure is the lateral displacement of the first and second surface which must be kept below 5 µm. According to the specialist in charge of the ultraprecision milling, the requirements are challenging but feasible.

5.2.3 Fabrication

Before returning to the specialized trapping system, we would like to provide a short introduction to the used technology. The selected fabrication method for the prototype is ultraprecision micromilling. The department of Technische Optik is in charge of a Kugler Microgantry Nano5x machining center (see fig. 5.16) which incorporates four machining modes. Besides micromilling the machining center can be used for flycutting, picosecond laser ablation and interference lithography. Since all machining processes are performed in the coordinate system of the machine, the precise fabrication of hybrid freeform optical elements is possible as well [179].

fig. 5.16: Image of the machining center Kugler Microgantry Nano5x; Source: KUGLER

The limiting factors for optics fabrication are the working space of the machine, the available tool geometries and the stiffness of the machine. The maximum working space of the machine is a cube of 10 cm edge length. The smallest milling tools available on the market have diameters of 5 µm (supplier: PMT Performance Micro Tools). Usually, the tools have spherical or cylindrical shapes.
The high speed spindle of the machining center operates at speeds up to 100.000 revolutions per minute. The chips in high precision milling are only of the thickness of one µm. The necessary stiffness is facilitated by the machine's granite

gantry frame. In order to achieve such results with a milling process, the machining environment has to be controlled. The pressure supply of the air bearings is stabilized in order to reduce the impact of pressure deviations of the central air supply. The temperature in the machine environment is stabilized. Furthermore, the working spindle itself has a compensation for the growth due to friction-induced temperature variations.
Currently, surface roughnesses of 10 nm (R_z) and shape accuracies of less than 1 µm are realized with ultraprecision (UP) milling at TU Ilmenau [185]. To achieve these values, a suitable fabrication strategy needs to be chosen. This applies especially in the last steps of surface finishing, when the actual path of the milling tool determines the final shape as well as the roughness. In these last machining cycles the thickness of the chip can be as low as 1 µm.
The lens data from the simulation was translated into machine code of the CNC milling machine. Using the available basic functions, the axicon and the polynomial description of the focusing surface can be programmed without loss of precision.
To guarantee the required alignment precision of the axicon and the focusing surface, the blank and its position were measured before and after flipping it. The probe for coordinate measurements is attached to the tool head and linked to the coordinate system of the machine (see fig. 5.17). Before flipping the cylinder, the top surface was machined to form a plane which is perpendicular to the rotational axis of the cylinder.

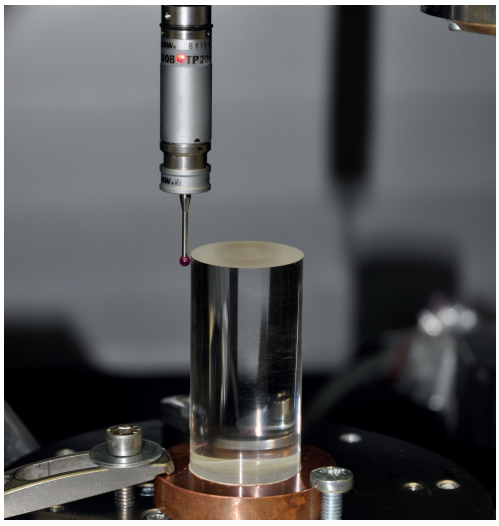

fig. 5.17: Calibration of the PMMA cylinder in the ultraprecision machining center; the cylinder is placed on top of a copper plate which serves as a reference plane; the measuring probe records the orientation and position of the cylinder's surface; Source: S. Stoebenau, TU Ilmenau

With tool diameters of 1 mm and less, the chip volume of the UP milling is very low. Therefore, the blank was coarsely preprocessed to get close to the final shape. For this task, a standard milling machine was used. The pre-machining leaves a material offset of several 100 µm for the UP milling. In a number of machining cycles the final shape is approached.
A final shape conserving polishing step was applied to further decrease the surface roughness. The prototype is shown in fig. 5.18.

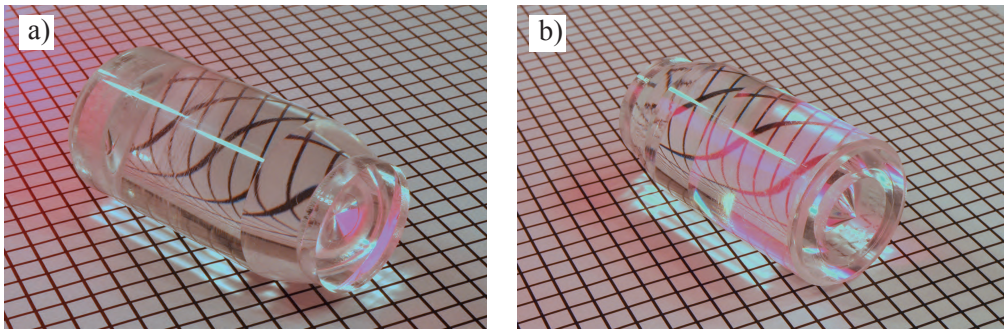

fig. 5.18: The completed prototype a) view of the focusing ring b) axicon side

The characterization of the fabrication quality proved to be challenging. The angles of the optical surfaces of the system are extreme for optical profiling e. g. interferometric measurements. To at least get an impression of the surfaces, two measurements were made:

1. white light interference microscopy of the axicon tip (fig. 5.19)
   The angle of 48° of the cone makes optical measurements of the surface difficult. Using a white light interference microscope the tip of the axicon could be characterized. As can be seen in 5.19a) only in the rounded center of the tip, data could be collected (red zone).

   The quality of the axicon tip is comparable to commercially available axicons with angles of up to 20°.

2. scan of the surface line of the focusing surface (fig. 5.20)
   This measurement has been realized with the autofocus sensor of a nanomeasuring machine.

   The visible groove on the focusing surface is 700 nm and 600 nm wide. The surface scan shows a structure which is mainly caused by tool marks of the milling process. Since the optics was polished and used experimentally before the measurement, there are scratches in other directions as well.

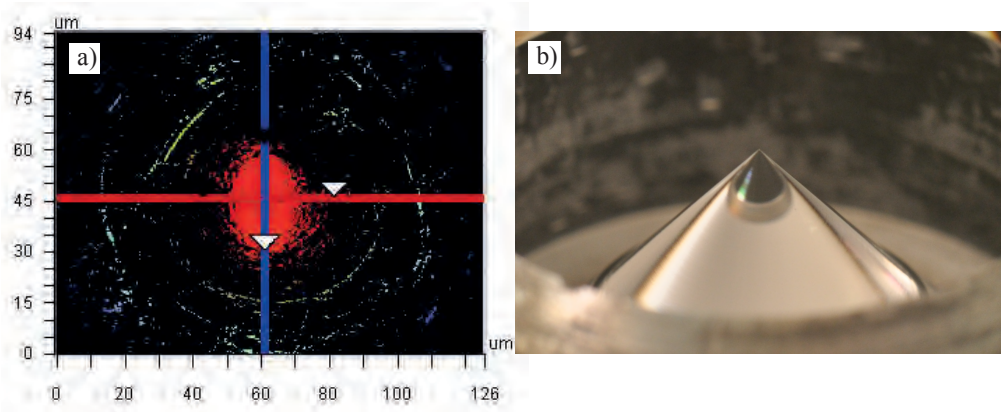

fig. 5.19: Characterization of the axicon surface; a) WLI measurement of the axicon center; Source: S. Stoebenau, TU Ilmenau b) photograph of the conic surface; Source: R. Mastylo, TU Ilmenau

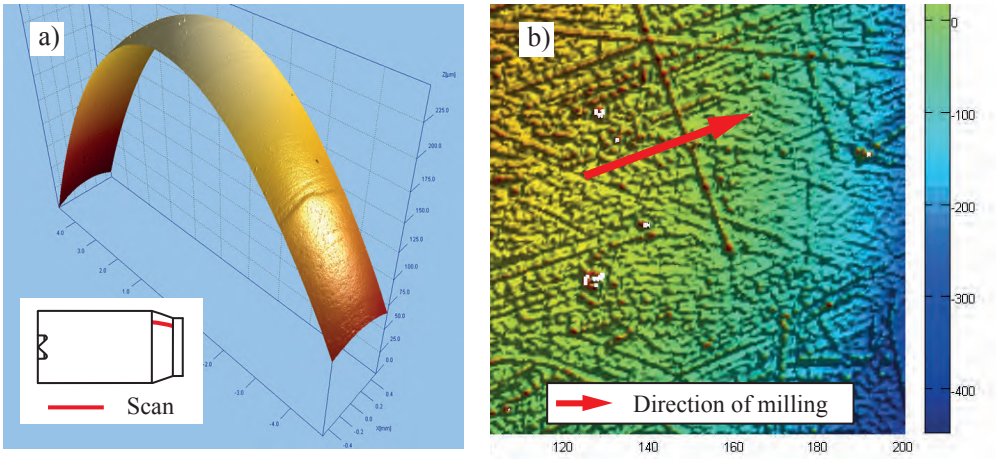

fig. 5.20: Characterization of the focusing surface; a) line scan b) surface scan

5.2.4 Experimental characterization

The data for the conclusive evaluation of the quality of the design and the fabrication needed to be collected experimentally. The experimental setup was much less complex compared to other setups (fig. 5.21). The collimated laser source (Nd-YAG; M=1.05; 1070 nm, IPG Photonics) was aligned parallel to an optical rail. For the observation of the trapping experiment a camera (uEye UI-1540SE-M, IDS) was mounted on a xyz-stage and then aligned with the optical axis of the laser. When moving the camera along the rail, the laser spot stays stationary in the image. This property can be used for the final alignment of the trapping optics.

The trapping optics was mounted in a Newport LP-1A 5-axis positioning unit. The alignment of the optics with the laser and the camera is achieved reliably in two steps:

1. It proved to be most purposeful to remove the tilt first. A cover slip is wrung onto the front flat of the trapping optics (axicon side). A 0.1 mm aperture is placed about 60 cm in front of the trapping optics, which produces a narrow beam. The reflex of the laser is then used to correct the tilts of the system w.r.t. the optical axis. Using this method, an angular deviation of less than 2 angular minutes can be reached.

2. The transverse correction is performed in the second step. The camera was combined with an achromatic lens (focal length of 60 mm) which allows the observation of the axicon through the trapping optics. Scattering due to tool marks and impurities of the material are used to assess the symmetry of the incidence of the laser beam. Shifting the trapping module laterally until the scattered light is symmetrical is a fast method to center the trapping optics on the optical axis. When the alignment is correct, the symmetry remains when the object plane is scanned through the optics along the z-axis.

The fluidic system consists of the glass substrate with a thickness of 530 µm, glass spacers with thickness of 170 µm and a second substrate on top. This sandwich is positioned in contact with the final plane surface of the trapping optics. Spacers made of 50 µm thick foil of biaxially-oriented polyethylene terephthalate (BoPET, Mylar) ensure a highly parallel alignment of the fluid channel and the optics. The assembly can be seen in image 5.21. The gap between the optics and the glass slide is immersed with water. Since the optical axis in the experiment is parallel to the optical table, the glass sandwich is oriented vertically. This is important to note because usually the test chambers are aligned horizontally and gravity acts in the direction of the laser. In the presented setup, gravity causes a steady movement of particles across the observation plane.

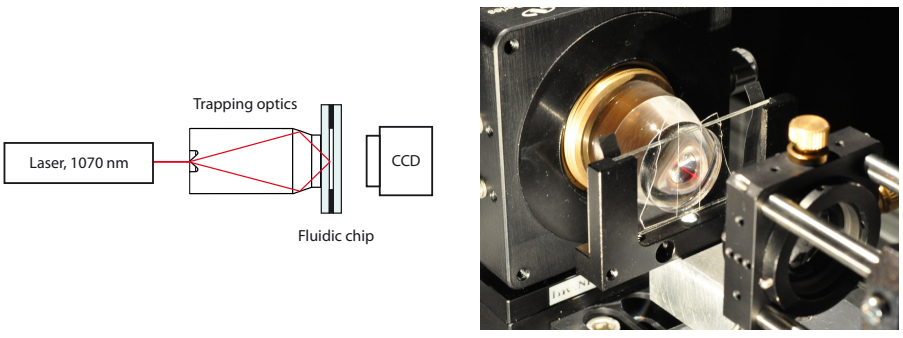

fig. 5.21: Trapping optics in Experiment

The direct assessment of the focusing properties of the optics by observing it with the camera is challenging from the imaging point of view. Since the light is leaving the trapping optics at angles which correspond to apertures between 1 and 1.3, only immersion objectives are suitable for the collection of the direct light. It was attempted to capture an image of the channel with a 1.3 100x Nikon objective. Since the depth of field of this objective is below 0.5 µm and the working distance is 200 µm only, the observation in this configuration is difficult. The calculated depth of focus in ASAP is more than 20 µm. Thus, it cannot be determined if the observation is focused in the right plane. Nevertheless, it can be seen, that the prototype optics does not produce a perfect circular pattern. A simpler way of observing the focus of the system is the use of a scattering fluid (e. g. diluted milk). To get a good axial resolution with this method, the scattering layer needed to be as thin as possible. To this end, we exchanged the spacer between the trapping optics and the fluidic system with a cover glass with a thickness of 90 µm (Thickness #00). As the spacer for the layer of scattering fluid a 36 µm Mylar foil was used. Fig. 5.22 shows the spot recorded with this method. The diameter of the spot has a full width at half maximum (FWHM) of approx. 10 µm.

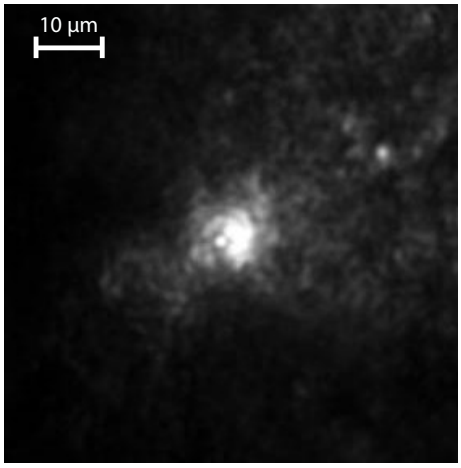

fig. 5.22: Focus of trapping module recorded in diluted milk

Since the spot diameter calculated in ASAP is 5.0 µm, the trapping forces were expected to be smaller than in the simulation.
The trapping experiments have been performed with silica spheres of different diameters. The suspensions with the particles were filled in the fluid channel. Due to gravitation, the particles were moving along the channel. Using this setup, we successfully trapped spheres with diameters of 9 µm and 4.5 µm.

By scanning through the channel we could prove that the particles are indeed trapped three-dimensionally. By reducing the laser power gradually until the particles fall out of the trap, we could measure the lateral trapping forces which are acting against gravity. The results were 4.9 pN (@ 250 mW) for the 9 µm and 0.25 pN (@ 180 mW) for the 4.5 µm spheres.

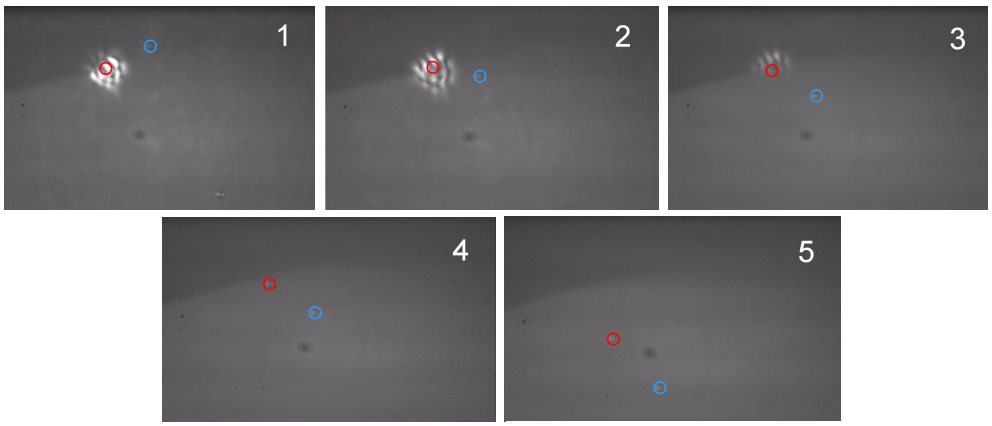

fig. 5.23: Trapping sequence of 9 µm silica spheres; the particles move from top to bottom. In 1-3 the red particle is trapped, after the release in image 4, the particle continues to drop down.

It was not possible to trap 1.5 µm microspheres in 3D. These smaller particles were aligned along a line, which suggests that a substructure is present in the focus. The simulation of the focus in ASAP (fig. 5.11) also suggests that the focal area for 1.5 µm spheres does not appear as a focus but resembles more a Bessel beam trap.

5.3 Summary

We demonstrated the potential of specialized designs by optimizing a conventional oil immersion objective. By applying minor modifications the trapping force of the sample objective could be improved significantly. The application of AR-coatings that are designed for the trapping wavelength increases the transmittance and the trapping forces per unit of laser power without any change to the system geometry. By changing one lens only, the working point of the system can be set to a location off the surface of the cover glass. Using water as immersion fluid leads to an invariance of the trapping performance to changes in the axial position of the trap in the channel.
With the example of a specialized integrated trapping module we have demonstrated the opportunities of the design process suggested in this thesis. The task of optical tweezing at a working distance of 650 µm was achieved by designing the entire optical system according to the specifications.
The simplicity of the self-contained monolithic optics and the possibility of replicating the optics by precision injection molding are promising factors for a future development of low-cost trapping systems for a larger group of users.

6 Design study for an integrated system for trapping in air

After the successful experiment presented in the previous section, the next step towards an optical nanotool for the use in the nanopositioning machine is the prototyping of a trapping system for particle trapping in air optics. In this chapter, studies for such a specialized optics are presented. In contrast to the first system, the specification of the second system includes the possibility of integrating an observation or presence monitoring respectively.
With the first system a monolithic trapping optics could be demonstrated successfully. For the combined task of trapping and monitoring, a modular optics approach appears to be preferable. Having the ability to align the separate components keeps more options for experiments.

6.1 Concepts for trapping optics

The selection of the general system configuration is again divided into two functional units. Similar to the trapping optics designed in the previous chapter, the first unit provides a ring illumination. In order to maximize the available space for the monitoring system, a configuration is chosen that was introduced by Ding [209]. In this publication an optical system is presented whichconsists of an axicon telesope and a microscope objective.
For the application in the NPM, most of the design specifications which have been introduced for the first trapping module apply for this setup as well. The available space for the entire system is again in the range of a typical microscope objective. Therefore, the focusing needs to be performed by an optimized element instead of an objective. The working distance of this system can be chosen freely. Since no glass or fluid layers have to be passed, the working distance can be as low as few microns.

The main difference in the design of the trapping beam results from the different ratio of refractive indices. For a particle with a refractive index of 1.58 retracting axial forces are generated by rays incident at angles larger than 36°. In water the same particle will experience retracting forces starting from 20° (fig. 6.1).

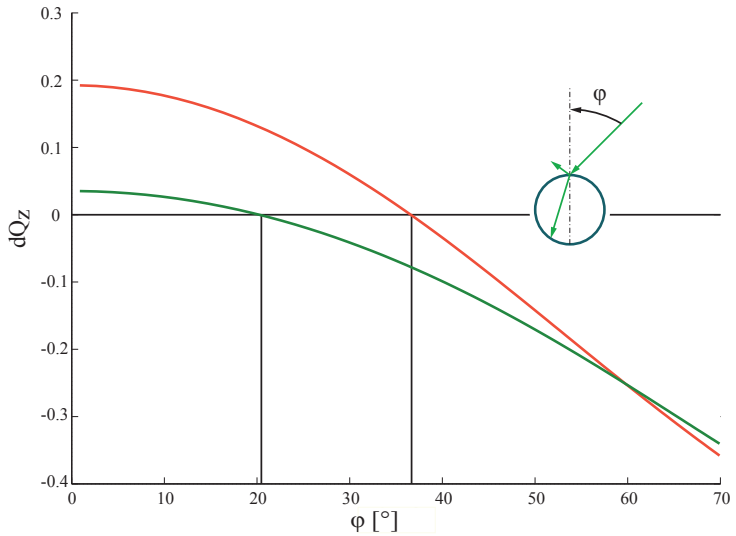

fig. 6.1: Efficiency curves for trapping a bead with refractive index of 1.58; red curve: bead in air, green curve: bead in water

The reason for this difference is mainly due to the difference in the reflection coefficient. For the bead in air the reflectivity for small angles is 5 times higher than for the bead in water. Consequently, the force in the direction of propagation is higher for the particle in air.

6.1.1 Illumination section

As mentioned in the previous section, an axicon telescope is chosen as illumination optics. This type of configuration creates a cylindrical beam with a dark center.
The telescope can be implemented with either a refractive or a reflective setup (fig. 6.2). The mirror telescope can be realized in a smaller space because the optical path is folded. The reflective optics can be expected to be more sensitive to alignment errors. A tilt of one mirror results in a tilt angle of the reflected beam which is double the initial error. A refractive telescope will require a longer optical setup. A benefit can be derived from this configuration when the desired diameter of the trapping beam can be fixed. In this case, the telescope

can be fabricated as a single element in the milling machine. When the blank is mounted on a rotational axis of the Kugler 5-axis machine, both sides can be fabricated without having to unmount the lens.

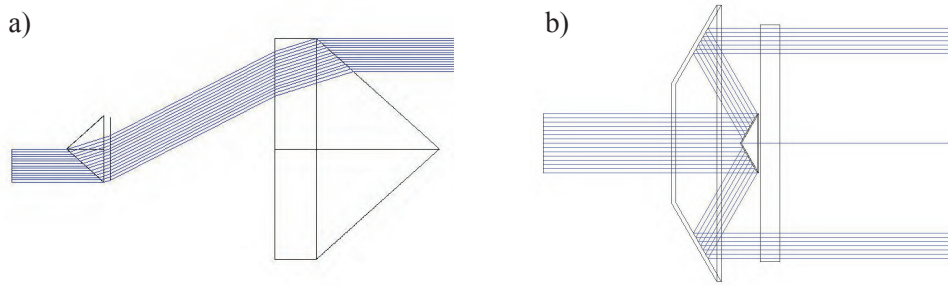

fig. 6.2: Optics for ring illuminations; a) refractive b) reflective

6.1.2 Focusing element

For the focusing unit two basic configurations are possible as well (fig. 6.3). Here, a purely reflective and a catadioptric element can be designed. The reflective element is a parabolic mirror. This surface shape focuses parallel rays at one point on the optical axis. This property is used in illumination optics for spotlights where the light source is located in the focal point of the paraboloid. The catadioptric setup is similar to the focusing ring of the trapping module tested in the previous chapter. The beam enters the element and is reflected by the first focusing surface. In the system shown in fig. 6.3b the beam leaves the material and is focused on the axis. The surface at the material-air interface has been set to be perpendicular to the center ray. This preserves symmetry but is not mandatory.

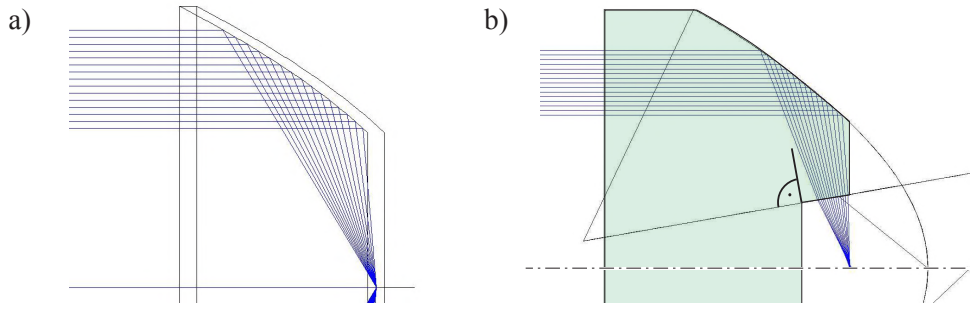

fig. 6.3: Focusing optics for trapping in air; a) reflective b) catadioptric

6.2 Integrated observation

As an additional feature for the following generations of trapping modules, an optical observation system has to be integrated into the module. Hence, a way of integrating an imaging system has to be found. When one of the configurations of the trapping tool as presented in 5.2 and 6 is chosen, there are several options one can think of to realize such an imaging task:

- Sharing the optical path of the trapping beam and the observation beam. The optical path for the trapping laser is already present in the system and optimized to high performance. However, this configuration is limited. In order to seperate the information from the observation, a beamsplitter such as a dichroic mirror is needed. This additional component in the trapping beam is a possible source for aberrations. If dichroic mirrors are used, the illumination and the observation need to have two different wavelengths, which is similar to optical setups used in flourescence microscopy. To effectively employ flourescence, a short wavelength source is needed for the excitation of the sample. Typically, NIR-lasers are used in case of optical trapping as these do not damage biological specimen. In the case of the optical nanotool, this restriction is unnecessary. In fact, shorter wavelengths have been shown to produce larger forces [214]. A last issue that has to be kept in mind is that only monitoring of the presence of particles and no actual imaging is required. The trapping optics is only designed to focus the laser to a single spot. When the observation shares the same path, the imaging properties will be identical.

- An ultracompact camera can be attached directly on top of the surface of the focusing unit. In recent years, the progress in microfabrication led to the miniaturization of camera modules. Currently, the smallest available camera modules are less than one cubic centimeter in size. These camera modules are used in endoscopes, for instance. The trapping module does not have to perform rapid movements and is mounted in a very stiff mechanical frame. Thus, the additional mass of a miniaturized camera is not an essential criterion for this solution. The imaging onto the camera chip could be achieved by using microlens arrays as suggested for compound eye cameras [215, 216].
  An open issue in this setup is the transfer of the images to an exterior display or storage device. Connections via cable would disturb the symmetry of the trapping beam by obscuring parts of the beam. Therefore, a wireless solution would be preferred. Then, obviously, the power supply has

to be integrated with the camera as well. A publication by Park in 2006 shows a wireless camera which would be small enough to be integrated in the available space [217].
Since the camera needs to be fitted into the trapping optics, this technical solution would result in a rather high level of engineering and development.

- The ultraprecision fabrication used for the prototype system in the previous section can be programmed to fabricate arbitrary shapes. Thus, it is possible to design and fabricate an imaging system which uses the center of the trapping optics and focuses the imaging beam outside of the actual trapping optics(see fig. 6.4). Since only few optical surfaces are available to perform the imaging task, the NA of the imaging is limited.

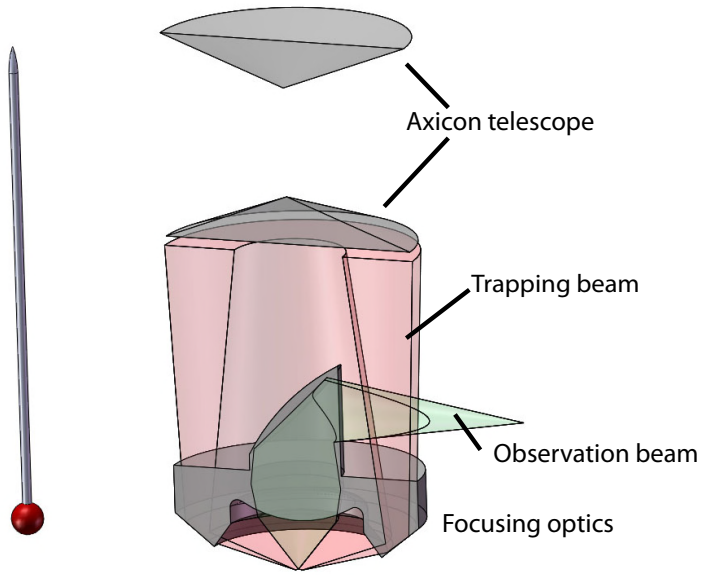

fig. 6.4: Concept study for an integrated observation

If only the presence of a particle in the trap needs to be monitored, simpler photodiode-based solutions are more suitable.

6.3 Summary

The experience from the previous experiment was transferred to concepts for trapping in air. In this case, a modular system is suggested instead of a monolithic system. This reduces the alignment effort during fabrication and increases the flexibility of the system. The space for the future integration of an imaging unit is reserved.

Optics for trapping in air need to be adjusted for the different relative refractive indices n_{rel}. While trapping water droplets in air (n_{rel}=1.33) is similar to trapping polystyrene (PS) beads in water (n_{rel}=1.19), the relative index for PS spheres in air, for instance, is 20% higher (n_{rel}=1.58). As a result, the reflected part of the beam is significantly higher and the paths of the beams are different. Similar to the system development shown in chapter 5 the final selection of a system configuration has to be closely coordinated with the fabrication.

7 Conclusion

In the introduction, two research questions were raised which challenge the potential of classical lens design for the optimization of existing optics and the creation of new trapping systems. Both questions can be answered in the affirmative.

We showed in which ways classical lens design can be employed to improve the performance in existing microscope-based setups. To this end, we simulated a real microscope objective and modified it according to the specification of an optical tweezing system. We found that by minor adjustments, only the trapping forces in a fluidic channel can be increased significantly over an extended field of view. When optimized AR-coatings are used, the transmission of the optics can be increased to values over 90%. This is an increase of 25% compared to the uncoated system and - according to [79] - up to twice the transmission of objectives currently used in optical trapping.

As proof for the presented design concept, we designed, fabricated and tested a trapping module with a working distance of 650 µm. The demonstration of 3D optical trapping at this extreme working distance serves as a first example for the increased freedom in design and application that is possible with modern lens design and ultraprecision machining of freeform surfaces. Furthermore, this demonstration sets a new record for the working distance of single beam gradient traps.

The successful combination of modern lens design software and a force calculation tool offers a useful tool for optics designers. Our system model includes physical effects such as Fresnel losses, dispersion and diffraction patterns of coherent beams. The parametric modeling of optical systems in the design process allows the variation of mechanical values during tolerancing instead of manually selecting the suitable parameters for aberrations, for instance.

While the presented work forms a solid basis for a holistic design of new trapping setups, there are - of course - further aspects that are worth looking into. Momentarily, the iterative optimization of forces has to be performed manually. An automatic optimization routine will increase the usability of the design process. The ray optics approach we use is limited to the simulation of particles larger than the wavelength. Using wave optics options in ray tracing software does add more realistic details to the simulation but cannot change the ray optics nature of the light-matter interaction. For future developments as a nanotool in the NPM a design routine is required, which is valid for nanoparticles as well. A possible approach would be to synthesize a wavefront from the ray data and to simulate the interaction in an EM simulation.
In this thesis several topics for further research projects are mentioned. The optimization potential of microscope objectives we suggested in chapter 5 needs to be confirmed experimentally.
We proposed the replication of the monolithic trapping module by precision injection molding in order to produce low-cost optical trapping systems. The realization of this idea represents a challenge for fabrication technology.
By using a holistic design as we suggest in 3.3 we envision more specific setups and a larger variety for applications in the industrial environment. Design for cost and design for manufacturing respectively are approaches that will gain significance if innovative products and solutions for lower budgets have to be developed.

Bibliography

[1] S. Sinzinger, M. Amberg, A. Oeder, D. Hein, C. Kremin, M. Hoffmann, J. Metze, and A. a. Grodrian, Integrated micro-opto-fluidic systems for optical manipulation of cell cultures, in *Optical Manipulation by nonlinear nanophotonics*, pages 33–34, Münster, 2008. 1.1

[2] H. Haferkorn, *Optik - physikalisch-technische Grundlagen und Anwendungen*, Wiley-VCH, Weinheim, 4., bearb. und erw. aufl edition, 2003. 1.1, 5.2.1

[3] E. F. Nichols and G. F. Hull, The pressure due to radiation, Astrophys. J. **17**(5), 315–351 (1903). 1.2

[4] S. Arrhenius, *Das Werden der Welten*, Leipzig Akademische Verlagsgesellschaft, Leipzig, 1907. 1.2

[5] J. C. Maxwell and J. J. Thompson, *A treatise on electricity and magnetism Vol 2*, Claredon Press, London, 1873. 1.2

[6] A. Bartoli, Il calorico ragiante e il secondo principio die thermodynamica, Nuovo Cimento **15**, 196202 (1876). 1.2

[7] P. Lebedev, Untersuchungen über die Druckkräfte des Lichtes, Annalen der Physik **311**(11), 433–458 (1901). 1.2

[8] G. Mie, Beiträge zur Optik trüber Medien, speziell kolloidaler Metallösungen, Annalen der Physik **4**(25), 379–445 (1908). 1.2, 2.2.3

[9] P. Debye, Der Lichtdruck auf Kugeln von beliebigem Material, Ann. Phys. **335**(11), 57–136 (1909). 1.2

[10] S. Ray, A note on the pressure of radiation on transparent dielectrics, Phys. Rev. **19**(5), 467–469 (1922). 1.2

[11] F. Ehrenhaft, Die Photophorese, Ann. d. Phys. **361**(10), 81132 (1918). 1.2

[12] R. Frisch, Experimenteller Nachweis des Einsteinschen Strahlungsrückstoßes, Zeitschrift f. Phys. **86**(1-2), 42–48 (1933). 1.2

[13] A. Ashkin, Acceleration and trapping of particles by radiation pressure, Phys. Rev. Lett. **24**(4), 156–158 (1970). 1.2, 3.1.1

[14] G. Roosen and C. Imbert, Optical levitation by means of two horizontal laser beams: a theoretical and experimental study, Phys. Lett. **59A**(1), 6–8 (1976). 1.2, 3.1.1

[15] G. Roosen, A theoretical and experimental study of the stable equilibrium postions of spheres levitated by two horizontal laser beams, Opt. Comm. **21**(1), 189–194 (1977). 1.2

[16] G. Roosen, B. F. d. Saint Louvent, and S. Slansky, Étude de la pression de radiation exercé sur une sphere creuse transparente par un faisceau cylindrique, Opt. Comm. **24**(1), 116–120 (1978). 1.2

[17] J. S. Kim and S. S. Lee, Scattering of laser beams and the optical potential well for a homogeneous sphere, J. Opt. Soc. Am. **73**(3), 303–312 (1983). 1.2

[18] A. Ashkin, Stable radiation-pressure particle traps using alternating light beams, Opt. Lett. **9**(10), 454–456 (1984). 1.2

[19] A. Ashkin, J. M. Dziedzic, J. E. Bjorkholm, and S. Chu, Observation of a single-beam gradient force optical trap for dielectric particles, Opt. Lett. **11**(5), 288–290 (1986). 1.2, 2.1.1, 2.1.4, 3.2.1

[20] A. Ashkin, J. M. Dziedic, and T. Yamane, Optical trapping and manipulation of single living cells using infra-red laser beams, Nature **330**, 769–771 (1987). 1.3

[21] A. Ashkin and J. M. Dziedzic, Optcal Trapping and Manipulation of Viruses and Bacteria, Science **235**(23544795), 1517–20 (1987). 1.3

[22] W. H. Wright, G. J. Sonek, Y. Tadir, and M. W. Berns, Laser Trapping in Cell Biology, IEEE J. Quantum Electron. **26**(12), 2148–2157 (1990). 1.3, 2.1.3

[23] G. Volpe, G. P. Singh, and D. Petrov, Dynamics of a growing cell in an optical trap, Appl. Phys. Lett. **88**(231106) (2006). 1.3

[24] M. Gu, S. Kuriakose, and X. Gan, A single beam near-field laser trap for optical stretching, folding and rotation of erythrocytes, Opt. Epxress **15**(3), 1369–1375 (2007). 1.3, 2.2.3, 3.1.1

[25] S. C. Grover, A. G. Skirach, R. C. Gauthier, and C. P. Grover, Automated single-cell sorting system based on optical trapping, J. Biomed. Opt. **6**(1), 14–22 (2001). 1.3

[26] D. J. Arndt-Jovin and T. M. Jovin, Automated cell sorting with flow systems, Ann. Rev. Biophys. Bioeng. **7**, 527–558 (1978). 1.3

[27] M. P. MacDonald, G. C. Spalding, and K. Dholakia, Microfluidic sorting in an optical lattice, Nature **426**(6965), 421 (2003). 1.3

[28] Y. Y. Sun, X.-C. Yuan, L. S. Ong, and J. Bu, Large-scale optical traps on a chip for optical sorting, Appl. Phys. Lett. **90**, 03110 (2007). 1.3

[29] J. Guck, R. Ananthakrishnan, H. Mahmood, T. J. Moon, C. C. Cunningham, and J. Käs, The Optical Stretcher: A Novel Laser Tool to Micromanipulate Cells, Biophys. J. **81**, 767–784 (2001). 1.3, 3.3.2

[30] J. Guck, R. Ananthakrishnan, T. J. Moon, C. C. Cunningham, and J. Käs, Optical Deformability of Soft Biological Dielectrics, Phys. Rev. Lett. **84**(23), 5451–5454 (2000). 1.3

[31] R. Ananthakrishnan, J. Guck, F. Wottawah, S. Schickinger, B. Lincoln, M. Romeyke, and J. Käs, Modelling the structural response of an eukaryotic cell in the optical stretcher, Current Science **88**(9), 1434–1440 (2005). 1.3

[32] A. Clement-Sengewald, K. Schütze, A. Ashkin, G. A. Palma, G. Kerlen, and G. Brem, Fertilization of bovine oocytes induced solely with combined laser microbeam and optical tweezers, J. Assist. Reprod. Genet. **13**(3), 259–265 (1996). 1.3

[33] A. Rohrbach, Stiffness of Optical Traps: Quantitative Agreement between Experiment and Electromagnetic Theory, Phys. Rev. Lett **95**, 168102 (2005). 1.3, 2.2.2, 4.3.4, 5.1.2

[34] H. Kress, E. H. K. Stelzer, D. Holzer, F. Buss, G. Griffiths, and A. Rohrbach, Filopodia act as phagocytic tentacles and pull with discrete steps and a load-dependent velocity, Proceedings of the National Academy of Sciences **104**(28), 11633–11638, posted–at = 2011–01–22 18:29:59 (jul 2007). 1.3

[35] E.-L. Florin, A. Pralle, J. Hörber, and E. Stelzer, Photonic Force Microscope Based on Optical Tweezers and Two-Photon Excitation for Biological Applications, J. Struct. Biol. **119**, 202–211 (1997). 1.3

[36] A. Rohrbach, C. Tischer, D. Neumayer, E.-L. Florin, and E. Stelzer, Trapping and tracking a local probe with a photonic force microscope, Rev. Sci. Instr. **75**(6), 2197–2210 (2004). 1.3, 3.2.1, 3.3.2

[37] W. Singer, S. Bernet, N. Hecker, and M. Ritsch-Marte, Three-dimensional force calibration of optical tweezers, J. Mod. Opt. **47**(14/15), 2921–2931 (2000). 1.3

[38] H. Felgner, O. Müller, and M. Schliwa, Calibration of light forces in optical tweezers, Appl. Opt. **34**(6), 977–982 (1995). 1.3

[39] N. B. Viana, M. S. Rocha, O. N. Mesquita, A. Mazolli, P. A. Maia Neto, and H. M. Nussenzveig, Towards absolute calibration of optical tweezers, Phys. Rev. E **75**(2), 021914 (2008). 1.3, 2.1.4, 2.2.2

[40] A. Ashkin, Trapping of Atoms by Resonance Radiation Pressure, Phys. Rev. Lett. **40**(12), 729–731 (1978). 1.3

[41] S. Chu, Laser Manipulation of Atoms and Particles, Science **253**(5022), 861 – 866 (1991). 1.3, 2.1

[42] S. Chu, l. Hollberg, J. E. Bjorkholm, and A. Ashkin, Three-Dimensional Viscous Confinement and Cooling of Atoms by Resonance Radiation Pressure, Phys. Rev. Lett. **55**(1), 48–51 (1985). 1.3

[43] E. L. Raab, M. Prentiss, A. Cable, S. Chu, and D. E. Pritchard, Trapping of Neutral Sodium Atoms with Radiation Pressure, Phys. Rev. Lett. **59**(23), 26312634 (1987). 1.3

[44] L. Sacconi, G. Romano, R. Ballerini, M. Capitanio, M. De Pas, and M. Giuntini, Three-dimensional magneto-optic trap for micro-object manipulation, Opt. Lett. **26**(17), 1359–1361 (2001). 1.3

[45] R. Ghadiri, M. Surbek, and O. A. Esen, Cemal, Optically based Manufacturing with Polymer Particles, Phys. Procedia **5**, 4751 (2010). 1.3

[46] A. Ostendorf, I. Ksouri, A. Aumann, and R. Ghadiri, Assembling and Manipulating with Light - Optical micro-machining tool for manufacturing and manipulation of arbitrary particles, Optik Photonik **7**(4), 44–47 (2012). 1.3

[47] J. Glückstad, A. Banas, S. Tauro, and D. Palima, BioPhotonics Workstation: a university tech transfer challenge, in *Proc. SPIE 8097 / Optical Trapping and Optical Micromanipulation VIII*, page 809714, San Diego, Sept. 2011 2011. 1.3

[48] M. M. Burns, J.-M. Fournier, and J. A. Golovchenko, Optical Binding, Phys. Rev. Lett **63**(12) (1989). 1.3

[49] O. Brzobohaty, T. Cizmar, V. Karasek, M. Siler, K. Dholakia, and P. Zemanek, Experimental and theoretical determination of optical binding forces, Opt. Express **18**(24), 25389–25402 (2010). 1.3

[50] J.-M. Fournier, J. Rohner, P. Jacquot, R. Johann, S. Mias, and R.-P. Salathé, Assembling mesoscopic particles by various optical schemes, in *Trapping and Optical Micromanipulation II/ San Diego /Proc. SPIE 5930*, number 59300Y, 2005. 1.3

[51] A. Labeyrie, M. Guillon, and J.-M. Fournier, Optics of "Laser Trapped Mirrors" for large telescopes and hypertelescopes in space, Proc. SPIE **5899** (2005). 1.3

[52] W. H. Wright, G. J. Sonek, and M. W. Berns, Radiation trapping forces on microspheres with optical tweezers, Appl. Phys. Lett. **63**(6), 715–717 (1993). 2.1, 4.3.1, 4.3.4

[53] W. H. Wright, G. J. Sonek, and M. W. Berns, Parametric study of the forces on microspheres held by optical tweezers, Appl. Opt. **33**(9), 1735–1748 (1994). 2.1, 2.2.4

[54] A. Ashkin and J. P. Gordon, Stability of radiation-pressure particle traps: an optical Earnshaw theorem, Opt. Lett. **8**(10), 511–513 (1983). 2.1.1

[55] G. Roosen and S. Slansky, Influence of the beam divergence on the exerted force on a sphere by a laser beam and required conditions for stable optical levitation, Opt. Comm. **29**(3), 341–346 (1979). 2.1.1, 2.1.3

[56] K. T. Gahagan and G. A. Swartzlander Jr, Optical vortex trapping of particles, Opt. Lett. **21**(11), 827–829 (1996). 2.1.1

[57] K. T. Gahagan and G. A. Swartzlander Jr, Trapping of low-index microparticles in an optical vortex, J. Opt. Soc. Am. B **15**(2) (1998). 2.1.1

[58] L.-G. Wang, C.-L. Zhao, L.-Q. Wang, X.-H. Lu, and S.-Y. Zhu, Effect of spatial coherence on radiation forces acting on a Rayleigh dielectric sphere, Opt. Lett. **32**(11), 1393–1395 (2007). 2.1.2

[59] C. Zhao, Y. Cai, X. Lu, and H. T. Eyyuboglu, Radiation force of coherent and partially coherent flat-topped beams on a Rayleigh particle, Opt. Express **17**(3), 1753–1765 (2009). 2.1.2

[60] P. Li, K. Shi, and Z. Liu, Manipulation and spectroscopy of a single particle by use of white-light optical tweezers, Opt. Lett. **30**(2), 156–158 (2005). 2.1.2, 3.1.2

[61] C. López-Mariscal, J. C. Gutiérrez-Vega, M. D., and K. Dholakia, Laserless Optical Trapping, in *FIO 2007*, 2007. 2.1.2, 3.1.2

[62] A. Ashkin, Forces of a single-beam gradient laser trap on a dielectric sphere in the ray optics regime, Biophys. J. **61**(2), 569–582 (1992). 2.1.3, 3.1.1, 3.1.2, 4.3.1, 4.3.4

[63] R. Gussgard, T. Lindmo, and I. Brevik, Calculation of the trapping force in a strongly focused laser beam, J. Opt. Soc. Am. A **9**(10), 1922–1980 (1992). 2.1.3

[64] S. B. Kim and S. S. Kim, Radiation forces on spheres in loosely focused Gaussian beam: ray-optics regime, J. Opt. Soc. Am. B **23**(5), 897–903 (2006). 2.1.3

[65] J. A. Lock, Calculation of the radiation trapping force for laser tweezers by use of generalized LorenzMie theory - I. Localized model description of an on-axis tightly focused laser beam with spherical aberration, Appl. Opt. **43**(12), 2532–2544 (2004). 2.1.4, 2.2.2, 3.1.1

[66] J. A. Lock, Calculation of the radiation trapping force for laser tweezers by use of generalized LorenzMie theory - II. On-axis trapping force, Appl. Opt. **43**(12), 2545–2554 (2004). 2.1.4

[67] K. F. Ren, G. Gréhan, and G. Gouesbet, Prediction of reverse radiation pressure by generalized LorenzMie theory, Appl. Opt. **35**(15), 2702–2710 (1996). 2.2.1

[68] G. X. Ganic, Djenan and M. Gu, Exact radiation trapping force calculation based on vectorial diffraction theory, Opt. Express **12**(12), 2670–2675 (2004). 2.2.1, 4.3.1

[69] P. Török, P. Varga, and G. R. Booker, Electromagnetic diffraction of light focused through a planar interface between materials of mismatched refractive indices: structure of the electromagnetic field. I, J. Opt. Soc. Am. A **12**(10), 2136–2144 (1995). 2.2.1

[70] S. Nemoto and H. Togo, Axial force acting on a dielectric sphere in a focused laser beam, Appl. Opt. **37**(27), 6386–6394 (1998). 2.2.1

[71] R. S. Dutra, N. B. Viana, P. A. Maia Neto, and H. M. Nussenzveig, Polarization effects in optical tweezers, J. Opt. A: Pure Appl. Opt. **9**(2007), 221–227 (2007). 2.2.1

[72] T. Wohland, A. Rosin, and E. H. K. Stelzer, Theoretical Determination of the Influence of the Polarization on forces Exerted by Optical Tweezers, Optik **102**(4), 181–190 (1996). 2.2.1

[73] H. Kawauchi, K. Yonezawa, Y. Kozawa, and S. Sato, Calculation of optical trapping forces on a dielectric sphere in the ray optics regime produced by a radially polarized laser beam, Opt. Lett. **32**(13), 1839–1841 (2007). 2.2.1

[74] T. A. Nieminen, N. R. Heckenberg, and H. Rubinsztein-Dunlop, Forces in optical tweezers with radially and azimuthally polarized trapping beams, Opt. Lett. **33**(2), 122–124 (2008). 2.2.1

[75] M. Gu, P. C. Ke, and X. S. Gan, Trapping force by a high numerical-aperture microscope objective obeying the sine condition, Rev. Sci. Instrum. **68**(10), 3666–3668 (1997). 2.2.2

[76] A. Rohrbach and E. Stelzer, Optical trapping of dielectric particles in arbitrary fields, J. Opt. Soc. Am. A **18**(9), 839–853 (2001). 2.2.2, 2.2.2

[77] S. Zwick, T. Haist, Y. Miyamoto, L. He, M. Warber, A. Hermerschmidt, and W. Osten, Holographic twin traps, J. Opt. A: Pure Appl. Opt. **11**, 034011 (2009). 2.2.2, 3.1.3, 4.2

[78] N. B. Viana, M. S. Rocha, O. N. Mesquita, A. Mazolli, and P. A. Maia Neto, Characterization of objective transmittance for optical tweezers, Appl. Opt. **45**(18), 4263–4269 (2006). 2.2.2, 5.1.2

[79] K. C. Neuman and S. M. Block, Optical trapping, Rev. Sci. Instr. **75**(9), 2787–2809 (2004). 2.2.2, 5.1, 5.1.2, 5.1.2, 7

[80] A. Rohrbach and E. H. K. Stelzer, Trapping forces, force constants, and potential depths for dielectric spheres in the presence of spherical aberrations, Appl. Opt. **41**(13), 2494–2507 (2002). 2.2.2, 3.1.1

[81] K. C. Vermeulen, G. J. L. Wuite, J. M. Stienen, and C. F. Schmidt, Optical trap stiffness in the presence and absence of spherical aberrations, Appl. Opt. **45**(8), 1812–1819 (2006). 2.2.2, 5.1

[82] K.-B. Im, H.-I. Kim, I.-J. Joo, C.-H. Oh, S.-H. Song, P.-S. Kim, and P. Byong-Chon, Optical trapping forces by a focused beam through two media with different refractive indices, Opt. Comm. **226**(2003), 25–31 (2003). 2.2.2, 3.1.1

[83] E. Fällman and O. Axner, Influence of a glasswater interface on the on-axis trapping of micrometer-sized spherical objects by optical tweezers, Appl. Opt. **42**(19), 3915–3926 (2003). 2.2.2, 3.1.1

[84] Y. Roichman, A. Waldron, E. Gardel, and D. G. Grier, Optical traps with geometric aberrations, Appl. Opt. **45**(15), 3425–3429 (2006). 2.2.2, 3.1.1, 3.1.2, 5.1

[85] K. D. Wulff, D. G. Cole, R. L. Clarc, R. DiLeonardo, C. J. Leach, Jonathan, G. Gibson, and M. J. Padgett, Aberration correction in holographic optical tweezers, Opt. Express **14**(9), 4170–4175 (2006). 2.2.2, 2.2.4, 3.1.2, 5.1.4

[86] C. López-Quesada, J. Andilla, and E. Martín-Badosa, Correction of aberration in holographic optical tweezers using a ShackHartmann sensor, Appl. Opt. **48**(6), 1084–1090 (2009). 2.2.2, 3.1.2, 5.1.4

[87] J. A. Lock, S. Y. Wrbanek, and K. E. Weiland, Scattering of a tightly focused beam by an optically trapped particle, Appl. Opt- **45**(15), 3634–3645 (2006). 2.2.2

[88] T. A. Nieminen, H. Rubinsztein-Dunlop, and N. R. Heckenberg, Calculation and optical measurement of laser trapping forces on non-spherical particles, J. Quant. Spectrosc. Radiat. Transfer **70**(4-6), 627–637 (2001). 2.2.3

[89] L. Chang, Yi-Ren: Hsu and S. Chi, Optical trapping of a spherically symmetric sphere in the ray-optics regime: a model for optical tweezers upon cells, Appl. Opt. **45**(16), 3885–3892 (2006). 2.2.3

[90] R. C. Gauthier, Laser-trapping properties of dual-component spheres, Appl. Opt. **41**(33), 7135–7144 (2002). 2.2.3

[91] R. C. Gauthier, Theoretical investigation of the optical trapping force and torque on cylindrical micro-objects, J. Opt. Soc. Am. A **14**(12), 3323–3333 (1997). 2.2.3

[92] R. C. Gauthier, Trapping model for the low-index ring-shaped micro-object in a focused, lowest-order Gaussian laser-beam profile, J. Opt. Soc. Am.A **14**(4), 782–789 (1997). 2.2.3, 4.3.1, 4.3.1

[93] R. C. Gauthier and A. Frangioudakis, Theoretical investigation of the optical trapping properties of a micro-optic cubic glass structure, Appl. Opt. **39**(18), 3060–.3070 (2000). 2.2.3

[94] S. C. Grover, R. C. Gauthier, and A. E. Skirtach, Analysis of the behaviour of erythrocytes in an optical trapping system, Opt. Expr. **7**(13), 533–539 (2000). 2.2.3

[95] E. Higurashi, H. Ukita, H. Tanaka, and O. Ohguchi, Optically induced rotation of anisotropic micro-objects fabricated by surface micromachining, Appl. Phys. Lett **64**(17), 2209–2210 (1994). 2.2.3

[96] J. Käs, Forces on Small Spheres in a One-Beam Gradient Trap - Universität Leipzig - Biophysics Lab Course, Technical report, 2005. 2.2.3

[97] K. Svoboda and S. M. Block, Optical trapping of metallic Rayleigh particles, Opt. Lett. **19**(13), 930–932 (1994). 2.2.3

[98] A. Ashkin, *Optical trapping and manipulation of neutral particles using lasers - a reprint volume with commentaries*, World Scientific, New Jersey, NJ [u.a.], 2006. 3, 3.1.1

[99] A. Constable, J. Kim, J. Mervis, F. Zarinetchi, and M. Prentiss, Demonstration of a-fiber-optical light-force trap, Opt. Lett. **18**(21), 1867–1869 (1993). 3.1.1, 3.1.1

[100] R. C. Gauthier and S. Wallace, Optical levitation of spheres: analytical development and numerical computations of the force equations, J. Opt. Soc. Am. B **12**(9), 1680–1686 (1995). 3.1.1, 4.2, 4.3

[101] R. C. Gauthier and A. Frangioudakis, Optical levitation particle delivery system for a dual beam fiber optic trap, Appl. Opt. **39**(1), 26–33 (2000). 3.1.1

[102] F. Merenda, J. Rohner, J.-M. Fournier, and R.-P. Salathé, Miniaturized high-NA focusing-mirror multiple optical tweezers, Opt. Express **15**(10), 6075–6086 (2007). 3.1.1, 3.3.2

[103] E. Sidick, S. D. Collins, and K. André, Trapping forces in a multiple-beam fiber-optic trap, Appl. Opt. **36**(25), 6423–6433 (1997). 3.1.1

[104] D. Rudd, C. López-Mariscal, M. Summers, M. Shahvisi, J. C. Gutiérrez-Vega, and D. McGloin, Fiber based optical trapping of aerosols, Opt. Express **16**(19), 14550–14560 (2008). 3.1.1

[105] J. Hu, Zhaohui: Wang and J. Liang, Manipulation and arrangement of biological and dielectric particles by a lensed fiber probe, Opt. Express **12**(17), 4123–4128 (2004). 3.1.1

[106] K. Taguchi and N. Watanabe, Single-beam optical fiber trap, J. Phys **61**, 1137–1141 (2007). 3.1.1, 3.3.2

[107] Z. Liu, C. Guo, J. yang, and Y. Libo, Tapered fiber optical tweezers for microscopic particle trapping: fabrication and application, Opt. Express **14**(25), 12510–12516 (2006). 3.1.1, 3.3.2

[108] M. Ohtsu, K. Kobayashi, H. Ito, and G.-H. Lee, Nanofabrication and Atom Manipulation by Optical Near-Field and Relevant Quantum Optical Theory, **88**(9), 1499–1504 (2000). 3.1.1

[109] S. Cabrini, C. Liberale, D. Cojoc, A. Carpentiero, M. Prasciolu, S. Mora, V. Begiorgio, F. De Angelis, and E. Di Fabrizio, Axicon lens on optical fiber forming optical tweezers, made by focused ion beam milling, Mircoel. Eng. **83**, 804–807 (2006). 3.1.1

[110] R. S. Taylor and C. Hnatovsky, Particle trapping in 3-D using a single fiber probe with an annular light distribution, Opt. Express **11**(21), 2775–2782 (2003). 3.1.1, 3.3.2

[111] C. Liberale, P. Minzioni, F. Bragheri, F. De Angelis, E. Di Fabrizio, and I. Cristiani, Miniaturized all-fibre probe for three-dimensional optical trapping and manipulation, Nature Photon. **1**(12), 723–727 (2007). 3.1.1

[112] F. Bragheri, P. Minzioni, C. Liberale, E. Di Fabrizio, and I. Christiani, Design and optimization of a reflection-based fiber-optic tweezers, Opt. Express **16**(22), 17647–17653 (2008). 3.1.1

[113] G. Thalhammer, R. Steiger, M. Meinschad, M. Hill, S. Bernet, and M. Ritsch-Marte, Combined acoustic and optical trapping, Biomed. Opt. Express **2**(10), 2859–2870 (2011). 3.1.1

[114] P. Y. Chiou, A. T. Ohta, and M. C. Wu, Massively parallel manipulation of single cells and microparticles using optical images, Nature **436**, 370–372 (21 July 2005 2005). 3.1.1

[115] M. Esseling, S. Glasener, F. Volonteri, and C. Denz, Opto-electric particle manipulation on a bismuth silicon oxide crystal, Appl. Phys. Lett. **100**(16), 161903 (2012). 3.1.1

[116] S. Kuriakose, D. Morrish, X. Gan, J. W. M. Chon, K. Dholakia, and M. Gu, Near-field optical trapping with an ultrashort pulsed laser beam, Appl. Phys. Lett. **92**, 081108 (2008). 3.1.1

[117] R. F. Marchington, M. Mazilu, S. Kuriakose, V. Garcés-Chávez, P. J. Reece, T. F. Krauss, M. Gu, and K. Dholakia, Optical deflection and sorting of microparticles in a near-field optical geometry, Opt. Express **16**(6), 3712–3726 (2008). 3.1.1

[118] M. Siler, T. Cizmar, M. Sery, and P. Zemanek, Optical forces generated by evanescent standing waves and their usage for sub-micron particle delivery, Appl. Phys. B **84**, 157–165 (2006). 3.1.1

[119] T. Cizmar, M. Siler, M. Sery, P. Zemanek, G.-C. Veneranda, and K. Dholakia, Optical sorting and detection of sub-micron objects in a motional standing wave, Phys. Rev. B **74**(035105), 1–6 (2006). 3.1.1

[120] S. Kühn, P. Measor, H. Schmidt, E. J. Lunt, and A. R. Hawkins, Two-beam optical trap in a waveguide, in *FiO 2007*, edited by OSA, page PDP B7, San Jose, 16.09.2007 2007. 3.1.1, 3.9

[121] P. Measor, S. Kühn, E. J. Lunt, B. S. Phillips, A. R. Hawkins, and H. Schmidt, Multimode mitgration in an optofluidic chip for particle manipulation and sensing, Opt. Express **17**(26), 24342–24348 (2009). 3.1.1

[122] B. J. Roxworthy and K. C. Toussaint, Efficient plasmonic trapping using bowtie nanoantennas, in *FiO 2011*, edited by OSA, San Jose, 2011. 3.1.1

[123] B. J. Roxworthy, K. D. Ko, A. Kumar, K. H. Fung, G. L. Liu, N. Fang, and K. C. Toussaint, Bowtie Nanoantennas for Plasmonic Optical Trapping, in *OTA*, edited by OSA, 04/11/2011 2011. 3.1.1

[124] J.-H. Kang, K. Kim, H.-S. Ee, Y.-H. Lee, T.-Y. Yoon, M.-K. Seo, and H.-G. Park, Low-power nano-optical vortex trapping via plasmonic diabolo nanoantennas, Nature Comm. **2**(582) (2011). 3.1.1, 3.9

[125] A. E. Siegman, Defining, measuring, and optimizing laser beam quality, in *Laser resonators and coherent optics: Modeling, technology, and applications*, Los Angeles, Jan. 18-20 1993. 3.1.2

[126] B. E. A. Saleh and M. C. Teich, *Fundamentals of photonics*, Wiley series in pure and applied optics, A Wiley-Interscience publication, Wiley, New York [u.a.], 1991. 3.1.2

[127] A. Ashkin, J. M. Dziedzic, and T. Yamane, Optical trapping and manipulation of single cells using infrared laser beams, Nature **330**(24), 769–771 (1987). 3.1.2

[128] G. J. Escadon, Y. Liu, and G. J. Sonek, Beam Magnification and the Efficiency of Optical Trapping with 790-nm AlGaAs Laser Diodes, IEEE Phot. Tech. Lett. **6**(5), 597–600 (1994). 3.1.2, 3.3.2

[129] T. C. Bakker Schut, E. F. Schipper, B. G. de Grooth, and J. Greve, Optical-trapping micromanipulation using 780-nm diode lasers, Opt. Lett. **18**(6), 447–449 (1993). 3.1.2

[130] R. A. Flynn, A. L. Birkbekc, M. Gross, M. Ozkan, B. Shao, M. M. Wang, and S. C. Esener, Parallel transport of biological cells using individually addressable VCSEL arrays as optical tweezers, Sensor Actuat B **87**, 239–243 (2002). 3.1.2, 3.1.3

[131] Y. Ogura, N. Shirai, and J. Tanida, Optical levitation and translation of a microscopic particle by use of multiple beams generated by vertical-cavity surface-emitting laser array sources, Appl. Opt. **41**(27), 5645–5654 (2002). 3.1.2

[132] A. Kroner, C. Schneck, F. Rinaldi, R. Rösch, and R. Michalzik, Application of vertical-cavity laser-based optical tweezers for particle manipulation in microfluidic channels, in *Proc. SPIE / Nanophotonics II*, pages 69881R–69881R–12, Strasbourg, 7 April 2008 2008. 3.1.2, 3.1.3

[133] P. Fischer, E. M. Wright, T. Brown, W. Sibett, J. E. Morris, C. López-Chávez, A. E. Carruthers, and K. Dholakia, *White Light Takes Shape*, December 2006 2006. 3.1.2

[134] P. Li, K. Shi, and Z. Liu, White Light Supercontinuum Optical Tweezer, in *CLEO 2005*, edited by OSA, page CFN1, Baltimore, 2005. 3.1.2

[135] M. Guillon, K. Dholakia, and D. McGloin, Optical trapping and spectral analysis of aerosols with a supercontiuum laser source, Opt. Express **16**(11), 7655–7664 (2008). 3.1.2

[136] J. E. Morris, A. E. Carruthers, M. Mazilu, P. J. Reece, T. Cizmar, P. Fischer, and K. Dholakia, Optical micromanipulation using supercontinuum Laguerre-Gaussian and Gaussian beams, Opt. Express **16**(14), 10117–10129 (2008). 3.1.2

[137] R. R. Alfano, *The Supercontinuum Laser Source - Fundamentals with Updated References*, Springer eBook Collection, Physics and Astronomy [Dig. Serial], Springer-11651 [Dig. Serial], Springer Science+Business Media, Inc, New York, NY, second edition edition, 2006. 3.1.2

[138] H. Urey, Spot size, depth-of-focus, and diffraction ring intensity formulas for truncated Gaussian beams, Appl. Opt. **43**(3), 620–625 (2004). 3.1.2

[139] T. Ota, T. Sugiura, S. Kawate, M. J. Booth, M. A. A. Neil, R. Juskaitis, and T. Wilson, Enhancement of Laser Trapping Force by Spherical Aberration Correction Using a Deformable Mirror, Jpn. J. Appl. Phys. **42**, 701–703 (2003). 3.1.2, 5.1

[140] E. Fällman and O. Axner, Design for fully steerable dual-trap optical tweezers, Appl. Opt. **36**(10), 2107–2113 (1997). 3.1.2, 3.1.3, 3.1.3

[141] E. Martín-Badosa, M. Montes-Usategui, A. Carnicer, J. Andilla, E. Pleguezuelos, and I. Juvells, Design strategies for optimizing holographic optical tweezers setups, J. Opt. A: Pure Appl. Opt. **9**, 267–277 (2007). 3.1.2

[142] H. He, N. R. Heckenberg, and H. Rubinsztein-Dunlop, Optical particle trapping with higher order doughnut beams produced using high efficiency computer generated holograms, J. Mod. Opt. **42**, 217–223 (1995). 3.1.2

[143] D. Ganic, X. Gan, and M. Gu, Optical trapping force with annular and doughnut laser beams based on vectorial diffraction, Opt. Express **13**(4), 1260–1265 (2005). 3.1.2

[144] D. Ganic, X. Gan, M. Gu, M. Hain, S. Somalingam, S. Stankovic, and T. Tschudi, Generation of doughnut laser beams by use of a liquid-crystal cell with a conversion efficiency near 100Opt. Lett. **27**(15), 1351–1354 (2002). 3.1.2

[145] D. W. Zhang and X.-C. Yuan, Optical doughnut for optical tweezers, Opt. Lett. **28**(9), 740–742 (2003). 3.1.2

[146] T. P. Meyrath, F. Schreck, J. L. Hanssen, C.-S. Chuu, and M. G. Raizen, A high frequency optical trap for atoms using Hermite-Gaussian beams, Opt. Express **13**(8), 2843–2851 (2005). 3.1.2

[147] M. Woerdemann, C. Alpmann, and C. Denz, Optical assembly of microparticles into highly ordered structures using InceGaussian beams, Appl. Phys. Lett **96**(111101), 1–3 (2011). 3.1.2

[148] J. Arlt, V. Garces-Chavez, W. Sibbett, and K. Dholakia, Optical micromanipulation using a Bessel light beam, Opt. Comm **197**, 239–245 (2001). 3.1.2

[149] F. O. Fahrbach, P. Simon, and A. Rohrbach, Microscopy with self-reconstructing beams, Nat. Phot. (2010). 3.1.2

[150] J. Durnin and J. J. Miceli, *Nondiffracting Beams*, 1987. 3.1.2

[151] C. López-Mariscal, J. C. Gutiérrez-Vega, G. Milne, and K. Dholakia, Orbital angular momentum transfer in helical Mathieu beams, Opt. Express **14**(9), 4182–4187 (2006). 3.1.2

[152] C. Alpmann, R. Bowman, M. Woerdemann, M. Padgett, and C. Denz, Mathieu beams as versatile light moulds for 3D micro particle assemblies, Opt. Express **18**(25), 26084–26091 (2010). 3.1.2

[153] Z. Zheng, B.-F. Zhang, H. Chen, J. Ding, and H.-T. Wang, Optical trapping with focused Airy beams, Appl. Opt. **50**(1), 43 (2011). 3.1.2

[154] J. Rohner, J.-M. Fournier, P. Jacquot, F. Merenda, and R. P. Salathé, Multiple Optical Trapping in High Gradient Interference Fringes, in *Proc. of the SPIE Vol. 6326*, edited by K. Dholakia and G. C. Spalding, 2006. 3.1.2

[155] D. G. Grier and Y. Roichman, Holographic optical trapping, Appl. Opt **45**, 880–887 (2006). 3.1.3

[156] Y. Sun, J. Bu, L. S. Ong, and X.-C. Yuan, Simultaneous optical trapping of microparticles in multiple planes by a modified self-imaging effect on a chip, Appl. Phys. Lett **91**(051101) (2007). 3.1.3

[157] C. Mennerat-Robilliard, D. Boiron, J.-M. Fournier, A. Aradian, and P. Horak, Cooling cesium atoms in a Talbot lattice, Europhys. Lett **44**(4), 442–448 (1998). 3.1.3

[158] M. Amberg, S. Stoebenau, and S. Sinzinger, Single-step replication of a highly integrated PDMS optofluidic analysis system, Appl. Opt. **49**(22), 4326–4330 (2010). 3.1.3, 3.3.2

[159] K. Visscher, S. P. Gross, and S. M. Block, Construction of Multiple-Beam Optical Traps with Nanometer-Resolution Position Sensing, Sel. Top. Quant. Elec. **2**(4), 1066–1076 (1996). 3.1.3

[160] G. J. Brouhard, H. T. Schek III, and A. J. Hunt, Advanced optical tweezers for the study of cellular and molecular biomechanics, Biomed. Eng. **50**(1), 121–125 (2003). 3.1.3

[161] K. Sasaki, M. Koshioka, H. Misawa, N. Kitamura, and H. Masuhara, Pattern formation and flow control of fine particles by laser scanning mircomanipulation, Opt. Lett. **16**(19), 1463–1465 (1991). 3.1.3

[162] U. Mirsaidov, W. Timp, K. Timp, M. Mir, P. Matsudaira, and G. Timp, Optimal optical trap for bacterial viability, Phys. Rev. E **78**, 021910 (2008). 3.1.3

[163] P. L. Biancaniello and J. C. Crocker, Line optical tweezers instrument for measuring nanoscale interactions and kinetics, Rev. Sci. Instr **77**(11), 113702–113702 (2006). 3.1.3

[164] D. Ruh, B. Tränkle, and A. Rohrbach, Fast parallel interferometric 3D tracking of numerous optically trapped particles and their hydrodynamic interaction, Opt. Express **19**(22), 21627–21642 (2011). 3.1.3

[165] M. Polin, K. Ladavac, S.-H. Lee, Y. Roichman, and D. G. Grier, Optimized holographic optical traps, Opt. Expr. **13**(15), 5831–5845 (2005). 3.1.3, 5.1.4

[166] A. Hermerschmidt, S. Krüger, T. Haist, S. Zwick, M. Warber, and W. Osten, Holographic optical tweezers with real-time hologram calculation using a phase-only modulating LCOS-based SLM at 1064 nm, in *Proc. SPIE 6905*, 2008. 3.1.3

[167] K. Ladavac and D. G. Grier, Microoptomechanical pumps assembled and driven by holographic optical vortex arrays, Opt. Express **12**(6), 1144–1149 (2004). 3.1.3

[168] P. J. Rodrigo, I. R. erch Nielsen, C. A. Alonzo, and J. Glückstad, GPC-based optical micromanipulation in 3D real-time using a single spatial light modulator, Opt. Express **14**, 13107–13112 (2006). 3.2.1

[169] M. J. Friese, A. G. Truscott, H. Rubinsztein-Dunlop, and N. R. Heckenberg, Three-dimensional imaging with optical tweezers, Appl. Opt. **38**(31), 6597–6603 (1999). 3.2.1

[170] C. Jensen-McMullin, H. P. Lee, and E. R. Lyons, Demonstration of trapping, motion control, sensing and fluorescence detection of polystyrene beads in a multi-fiber optical trap, Opt. Express **16**(7), 2634–2642 (2005). 3.2.1

[171] P. J. Rodrigo, I. R. Perch-Nielson, and J. Glückstad, Three-dimensional forces in GPC-based counterpropagating-beam traps, Opt. Express **14**(12), 5812–5822 (2006). 3.2.2

[172] S. Sinzinger and J. Jahns, *Microoptics*, Wiley-VCH, Weinheim, 2., rev. and enl. ed edition, 2003. 3.3.1, 3.3.1

[173] R. G. Hunsperger, *Integrated Optics - Theory and Technology*, Springer-Verlag, s.l., 6. aufl edition, 2009. 3.3.1

[174] M. Amberg and S. Sinzinger, Design Considerations for Efficient Planar Optical Systems, Opt. Comm. **267**, 74–78 (2006). 3.3.1

[175] S. Sinzinger, Microoptically integrated correlators for security applications, Opt. Comm. **290**, 69–74 (2002). 3.3.1

[176] K. Iga, M. Oikawa, S. Misawa, J. Banno, and Y. Kokubun, Stacked planar optics - An application of the planar microlens, Appl. Opt. **21**(19), 3456–3460 (1982). 3.3.1

[177] H. P. Herzig, *Micro-optics - elements, systems and applications*, Taylor und Francis, London [u.a.], 1997. 3.3.1

[178] M. Amberg, *Optische Mikrosysteme und Bauelemente für die Optofluidik*, PhD thesis, 2010. 3.3.1

[179] R. Kleindienst, R. Kampmann, S. Stoebenau, and S. Sinzinger, Hybrid optical (freeform) componentsfunctionalization of nonplanar optical surfaces by direct picosecond laser ablation, Appl. Opt. **50**(19), 3221–3228 (2012). 3.3.1, 5.2.3

[180] J. Jahns, H. Knuppertz, and M. Bohling, All-reflective planar-integrated free-space micro-optical femtosecond pulse shaper, Opt. Eng. **48**(12), 123001 (2009). 3.3.1

[181] S. P. Smith, S. R. Bhalotra, A. L. Brody, B. L. Brown, K. Boyda, Edward, and M. Prentiss, Inexpensive optical tweezers for undergraduate laboratories, Am J. Phys. **67**(1), 26–35 (1999). 3.3.2

[182] D. C. Appleyard, K. Y. Vandermeulen, H. Lee, and M. J. Lang, Optical trapping for undergraduates, Am. J. Phys. **75**(1), 5–14 (2007). 3.3.2

[183] M. Sery, Z. Lostak, M. Kalman, P. Jakl, and P. Zemanek, Compact laser tweezers, in *Proc. of SPIE Vol. 6609*, pages 66090N–1, 2007. 3.3.2

[184] Z. Ulanowski and I. K. Ludlow, Compact optical trapping microscope using a diode laser, Meas. Sci. Technol. **11**(12), 1778–1785 (2000). 3.3.2

[185] S. Stoebenau, M. Amberg, and S. Sinzinger, Micromilling for the fabrication of complex optical microsystems, in *Proc. of the 10th International Conference of the EUSPEN*, pages 412–415, Delft, May 31st - June 4th 2010. 3.3.2, 5.2.3

[186] E. Schonbrun, C. Rinzler, and K. B. Croizer, Microfabricated water immersion zone plate optical tweezer, Appl. Phys. Lett. **92**, 071112 (2008). 3.3.2

[187] E. Schonbrun and K. B. Crozier, Spring constant modulation in a zone plate tweezer using linear polarization, Opt. Lett. **33**(17), 2017–2019 (2008). 3.3.2

[188] A. R. Hawkins and H. Schmidt, *Handbook of optofluidics*, CRC Press, Boca Raton, Fla. [u.a.], 2010. 3.3.2

[189] D. Psaltis, S. R. Quake, and C. Yang, Developing optofluidic technology through the fusion of microfluidics and optics, Nature **442**(7101), 381–386 (2006). 3.3.2

[190] C. Monat, P. Domachuk, and B. J. Eggleton, Integrated optofluidics: A new river of light, Nature Photon. **1**(2), 106–114 (2007). 3.3.2

[191] A. H. J. Yang, S. D. Moore, B. S. Schmidt, M. Klug, M. Lipson, and D. Erickson, Optical manipulation of nanoparticles and biomolecules in sub-wavelength slot waveguides, Nature **457**(7225), 71 (2009). 3.3.2

[192] S. Mandal and D. Erickson, Optofluidic transport in liquid core waveguiding structures, Appl. Phys. Lett. **90**(18), 184103 (2007). 3.3.2

[193] S. J. Cran-McGreehin, K. Dholakia, and T. F. Krauss, Monolithic integration of microfluidic channels and semiconductor lasers, Opt. Express **14**(17), 7723–7729 (2006). 3.3.2

[194] S. J. Cran-McGreehin, T. F. Krauss, and K. Dholakia, Integrated monolithic optical manipulation, Lab on a Chip **6**, 11221124 (2006). 3.3.2, 3.9

[195] G. J. L. Wuite, R. J. Davenport, A. Rappaport, and C. Bustamente, An Integrated Laser Trap/Flow Control Video Microscope for the Study of Single Biomolecules, Biophys. J. **79**, 1155–1167 (2000). 3.3.2

[196] J. S. Dam, P. J. Rodrigo, I. R. Perch-Nielsen, C. A. Alonzo, and J. Glückstad, Computerized drag-and-drop alignment of GPC-based optical micromanipulation system, Opt. Express **15**(4), 1923–1931 (2007). 3.3.2

[197] K. C. Neuman, E. H. Chadd, G. F. Liou, K. Bergman, and S. M. Block, Characterization of Photodamage to Escherichia coli in Optical Traps, Biophys. J. **77**(5), 28562863 (1999). 4.1, 5.1.2

[198] l. Barroso Peña, B. Kemper, M. Woerdemann, A. Vollmer, S. Ketelhut, G. von Bally, and C. Denz, Optical tweezers induced photodamage in living cells quantified with digital holographic phase microscopy, in *Proc. SPIE*, pages 84270A–84270A–7, 2012. 4.1

[199] B. R. Corporation, Wave Optics in ASAP - Technial Guide, Technical report, 2008. 4.2

[200] T. A. Nieminen, V. L. Y. Loke, A. B. Stilgoe, G. Knöner, A. M. Brancyk, N. R. Heckenburg, and H. Rubinsztein-Dunlop, Optical tweezers computational toolbox, J. Opt. A: Pure Appl. Opt. **9**, 196–203 (2007). 4.3

[201] C. Bauer, *Untersuchung optimierter Lichtverteilungen fur optische Pinzetten*, PhD thesis, TU Ilmenau, Ilmenau, March 2009 2009. 4.3

[202] A. Oeder, S. Stoebenau, and S. Sinzinger, Optimized free-form optical trapping systems, Opt. Lett. **37**(2), 274–276 (2012). 5

[203] P. C. Ke and M. Gu, Characterization of trapping force in the presence of spherical aberration, J. Mod. Opt. **45**(10), 2159–2168 (1998). 5.1

[204] M. Laikin, *Lens design*, CRC Press, Boca Raton,FL [u.a], 4. ed edition, 2007. 5.1.1, 5.1, 5.1.4

[205] K. F. Palmer and D. Williams, Optical properties of water in the near infrared, J. Opt. Soc. Am. A **64**(8), 1107–1110 (1974). 5.1.1

[206] A. J. Parker and K. W. Raine, An investigation into the performance of microscope objectives with near infrared light, Meas. Sci. Technol. **2**, 159–163 (1991). 5.1.2

[207] K. Svoboda and S. M. Block, Biological applications of optical forces, Annu. Rev. Biophys. Biomol. Struct. **23**, 247–285 (1994). 5.1.2

[208] H. Haferkorn and W. Richter, *Synthese optischer Systeme*, Dt. Verl. der Wiss, Berlin, 1984. 5.2.1

[209] Z. Ding and G. Lai, Enhancement of axial optical trapping force using a pair of axicons, in *CLEO / Pacific Rim '99*, pages 369–370 vol. 2, Seoul, 1999. 5.2.1, 6.1

[210] M. Abramovitz and M. W. Davidson, *Darkfield Illumination*, 21.07.2012 2012. 5.2.1

[211] H. Wolter, Spiegelsysteme streifenden Einfalls als abbildende Optiken für Röntgenstrahlen, Ann. d. Phys. **445**(1-2), 94–114 (1952). 5.2.1

[212] M. Pfeffer, Optomechanical Aspects of Plastic Optics, in *DGaO-Proceedings*, 2005. 5.2.1

[213] J. D. Lytle, Specifying glass and plastic optics - what's the difference?, in *Proc of Spie Vol. 0181*, 1979. 5.2.1

[214] S. Sato and H. Inaba, Optical trapping and manipulation of microscopic particles and biological cells by laser beams, Opt. Quantum Electron. **28**, 1–16 (1996). 6.2

[215] J. Duparré, P. Dannberg, P. Schreiber, A. Bräuer, and A. Tünnermann, Thin compound-eye camera, Appl. Opt. **44**(15), 2949–2956 (2005). 6.2

[216] R. Horisaki, S. Irie, Y. Ogura, J. Tanida, Y. Nakao, T. Toyoda, and Y. Masaki, High-quality image acquisition using a compact compound-eye camera, in *Computational Optical Sensing and Imaging (COSI) 2007*, 2007. 6.2

[217] C. Park and P. H. Chou, eCAM: Ultra Compact, High Data-Rate Wireless Sensor Node with a Miniature Camera, in *ACM SenSys 2006*, pages 359–360, Boulder, 10/31/2006 2006. 6.2

Acknowledgement

Research sometimes seems like a long hike on a windy and partly obscure path. Hence, it is very important to have companions who accompany the traveler and assure him that the destination will be reached eventually. Having said this, I would like to acknowledge the people who walked with me on that path.
First of all I would like to thank my supervisor Prof. Stefan Sinzinger for giving me the opportunity to engage in the field of optical trapping. He encouraged me to follow the idea of specialized optics for optical tweezers and I highly appreciate his trust in me and the ambitious project of the monolithic trapping module.
The application of the design process was possible thanks to the contribution of Mr. Carl Bauer. He wrote the MATLAB code the force calculation software in his diploma thesis. I highly value Carl's critical thinking and the constructive discussions during the design of the prototype. I also thank Prof. Herbert Gross for consulting us in the first design stages of the prototype I presented in this thesis.
I am happy that I had the opportunity of many inspiring conversations and collaborations with my colleagues from the department of Technische Optik. In particular I would like to acknowledge the contributions the successful experimental work. Martin Amberg introduced me to the handling of optical trapping setups and shared his experience on optical trapping with me. Sebastian Stoebenau did an amazing job fabricating the trapping module and I would like to thank him for his commitment.
Even though they did not have a direct contributions to my research I would also thank the friends I had the pleasure of getting to know during my time in Ilmenau. Since they never failed to cheer me up, it is important to me to include them in this list. Especially I would like to mention the members of 5idelity, the university's chamber choir and orchestra, Second Unit Jazz, the VDI Student Chapter, the OSA Student Chapter Ilmenau and MINF.
I would also like to express my gratitude to my parents for supporting me throughout my time in Ilmenau.
Last but not least I would like to thank my wife Manuela for her patience and for the times she didn't ask me "When are you going to finish?", even when I left the

kids and household to her and locked myself up in the office during the last year.

Funding

The research presented in this thesis was funded by the Freistaat Thüringen in the project "Integrierte mikrooptische Pinzette" (FKZ: B 514-06006), by the German Research Association in the project B7 'Nanotools" within the CRC 622 for "Nanopositioning and- measuring machines" and by the German Federal Ministry of Education and Research (BMBF) in the project "Kompetenzdreieck Optische Mikrosysteme" (FKZ: 16SV5473).